HIGH χ BLOCK COPOLYMERS FOR SUB 20 nm PITCH PATTERNING: SYNTHESIS, SOLVENT ANNEALING, DIRECTED SELF ASSEMBLY, AND SELECTIVE BLOCK REMOVAL

A Dissertation
Presented to
The Academic Faculty

by

Nathan Dudney Jarnagin

In Partial Fulfillment
of the Requirements for the Degree
Doctor of Philosophy in the
School of Chemistry and Biochemistry

Georgia Institute of Technology
December 2013

HIGH χ BLOCK COPOLYMERS FOR SUB 20 nm PITCH PATTERNING: SYNTHESIS, SOLVENT ANNEALING, DIRECTED SELF ASSEMBLY, AND SELECTIVE BLOCK REMOVAL

Approved by:

Dr. Clifford L. Henderson, Co-advisor
School of Chemical and Biomolecular Engineering
Georgia Institute of Technology

Dr. John Reynolds
School of Chemistry and Biochemistry
Georgia Institute of Technology

Dr. Laren Tolbert, Co-advisor
School of Chemistry and Biochemistry
Georgia Institute of Technology

Dr. David Bucknall
Materials Science and Engineering
Georgia Institute of Technology

Dr. David Collard
School of Chemistry and Biochemistry
Georgia Institute of Technology

Date Approved: August 26, 2013

ACKNOWLEDGEMENTS

First, I would like to thank my co-advisor Dr. Clifford Henderson, who gave me the opportunity and motivation to succeed in this work. He consistently led our research team, and required our best efforts. The result was a tough yet fun environment, which I will definitely miss. I would also like to thank my other co-advisor, Dr. Laren Tolbert. He provided much of the organic synthesis expertise, and played a key role in the discussion and direction of this work. He also provided much needed encouragement. Other key team members were Dr. Jing Cheng, Dr. Wei-ming Yeh, Dr. Richard Lawson, Andrew Peters, and Dr. Pete Ludovice. I am extremely lucky to have worked with such a great group of people, and I appreciate the unique input from each of these team members. The work in this dissertation is a direct result of the combined efforts and discussion of the block copolymer team. I would also like to thank our collaborators at Intel for helpful discussion and financial support of this project.

No graduate experience can be successful without the support and assistance of colleagues and fellow students. This includes research scientists Dr. Janusz Kowalik and Dr. Kyril Solntsev, who provided both expertise and camaraderie within the Tolbert lab. I would like to also thank the other group members in both the Henderson Lab and Tolbert lab; this includes Juan Vargas, Verjine Khodaverdian, Brett Fellows, Chris Walker, Ameneh Chesmehkani, Jose Baltazar, Benjamin Nation, Brandon Sharp, and Caleb Breaux. Furthermore, I would like to thank Dr. Perry and the Perry group for both help and friendship during my time in their lab. I would also like to acknowledge several individuals at Tech who helped me on numerous occasions. This includes Eric Woods

from the Georgia Tech clean room, Richard Bedell from the chemistry electrical shop, and Arian Padron from chemistry IT support department. I would also like to thank Dr. David Collard, Dr. John Reynolds, and Dr. David Bucknall for serving on my committee and providing useful insight and support. I am also thankful for the support of Dr. Brian Cooper and Dr. Kenneth Gonsalves, two professors who provided mentorship during my education at UNC Charlotte.

Finally, I would like to mention my parents for their love, sacrifice, and support. This includes both the big and little things, from driving me to and from ball practice as a kid, to paying for my undergraduate education, and allowing me to pursue my interests. My education would not be possible without them.

TABLE OF CONTENTS

LIST OF TABLES

LIST OF FIGURES

LIST OF SYMBOLS AND ABBREVIATIONS

χ	Flory Huggins interaction parameter
^{1}H NMR	Proton-1 nuclear magnetic resonance
AFM	Atom force microscopy
ALD	Atomic layer deposition
AIBN	Azobisisobutyronitrile
CD	Critical dimension
BCP	Block copolymer
DCM	Dichloromethane
DSA	Directed self assembly
DSC	Differential scanning calorimetry
EUV	Extreme ultraviolet
FTIR	Fourier transform infrared spectroscopy
GPC	Gel permeation chromatography
IC	Integrated circuit
MIBK	Methyl isobutyl ketone
NRT	Normalized remaining thickness
PAB	Post apply bake
PAG	Photoacid generator
PAS	Poly(acetoxystyrene)
PEB	Post exposure bake
PGMEA	Propylene glycol monomethyl ether acetate
PGMA	Poly(glycidyl methacrylate)
PHOST	Poly(hydroxystyrene)

PS	Poly(styrene)
PMMA	Poly(methylmethacrylate)
PPDMSS	Poly(pentamethyldisilylstyrene)
PTMSS	Poly(trimethylsilylstyrene)
RAFT	Reversible addition/fragmentation chain transfer polymerization
RIE	Reactive ion etching
SEM	Scanning electron microscopy
TGA	Thermogravimetric analysis
TLC	Thin layer chromatography
UV	Ultraviolet
XPS	X-ray photoelectron spectroscopy
RIE	Reactive ion etching

SUMMARY

Traditional photolithographic techniques have facilitated the unprecedented improvement in computing power via the continued downward scaling of feature sizes associated with memory and logic devices. However, due to the issues associated with next generation photolithographic techniques, namely the cost and complexity of double patterning and the inefficient power source associated with extreme ultraviolet lithography (EUVL), industry is interested in alternative patterning technologies to enable the continuation of Moore's law and the fabrication of patterns with sub-20 nm pitch. Block copolymer (BCP) thin film patterns, generated using directed self-assembly (DSA) of diblock copolymers, have shown excellent promise as templates for semiconductor device manufacturing, since they have the potential to produce feature pitches and sizes well below 20 nm and 10 nm, respectively, using current 193 nm optical lithography.

While block copolymers could enable the extension of Moore's law via the formation of patterns at relevant nanometer length scales, this technology must address three key challenges. First, current materials do not provide sufficient thermodynamic driving force to achieve useful nanometer dimensions. Second, traditional polymerization techniques do not provide the precise control of molecular weight and low PDI required for DSA applications. Finally, these block copolymer materials must exhibit selective block removal via processes such as reactive ion etching allowing the transfer of the block copolymer pattern into the underlying substrate. **The goal of this**

work was to investigate a styrene based block copolymer system, namely PS-b-PHOST, that addresses these three challenges.

Currently, the most widely used block copolymer for DSA studies, poly(styrene)-b-poly(methylmethacrylate) (i.e. PS-b-PMMA), lacks the thermodynamic driving force necessary for phase separation at these smallest lengths scales. According to theory, phase separation of lamellar morphologies in diblock copolymers only occurs when χN>10.5, where χ is the Flory Huggins interaction parameter and N is the total degree of polymerization for the diblock copolymer. Since block domain sizes scale as $\sim N^{2/3}$ in the strong segregation limit (and more generally as N^{α} where $0.66 \leq \alpha \leq 1$), to achieve small feature sizes requires the use of shorter block chain lengths. In order to satisfy the requirement that χN>10.5 at the same time means that polymers with higher χ values must be used to achieve the smallest possible DSA feature sizes and pitches. In this work, the PMMA block from PS-b-PMMA was replaced with a block containing highly polar and hydrogen bonding functionality, poly(hydroxystyrene) or PHOST. PHOST was chosen since it is known to form extensive hydrogen bond networks from earlier resist material studies, a fact which results in an increase in χ due to this increased enthalpic interaction for PHOST as compared to PMMA.

Targeted polymer molecular weights and low polydispersities were required for directed self assembly patterning since the pitch and morphology of the BCP is dependent on the characteristic length scale (or degree of polymerization) of each block on the polymer chain. In this work, nitroxide mediated polymerization (NMP) techniques were utilized to produce the diblock copolymers reported here. NMP provided good molecular weight control and low PDI without the use of metallic reagents that can

contaminate the polymer samples and cause contamination problems in subsequent processing of block copolymers in clean room facilities. Block copolymers synthesized with the universal nitroxide initiator exhibited improved PDI in comparison with block copolymers synthesized with the traditional TEMPO initiator. Here, PS-b-PHOST polymers were synthesized with a range of molecular weights (M_n=5000-30000 g/mol and PDI=1.2) with symmetric volume fraction between the block which enabled lamellar morphology. Also, a series of random copolymers, poly(styrene)-r-poly(hydroxystyrene)-r-poly(glycidylmethacrylate) or PS-r-PHOST-r-PGMA, were synthesized as potential neutral underlayer substrates for the PS-b-PHOST system.

Phase separation via solvent annealing of low molecular weight PS-b-PHOST, with symmetrical volume fraction between the blocks, on neutral underlayer substrates provided thin film vertical lamellae with 13 nm pitch. These results illustrated the improved resolution of PS-b-PHOST compared with the current industry standard of PS-b-PMMA (with 20 nm pitch). Also, the directed self assembly of lamellar patterns via graphoepitaxy was demonstrated. Here, lithographically patterned SU-8 lines on the neutral underlayer provided guiding walls for physical alignment. The BCP was spin coated and solvent annealed on these substrates resulting in directed self assembly of PS-b-PHOST with 18 nm pitch within the trench.

For semiconductor device manufacturing, selective block removal of the BCP pattern is required, in which one of the blocks is selectively etched away, leaving the other block to serve as an etch resistant mask for pattern transfer to the underlying substrate. While PS-b-PHOST exhibited favorable thermodynamic properties providing phase separation of patterns with sub 20 nm pitch, this material exhibited no practical

etch contrast. Hence, this material required some modification to allow selective block removal. Here, an area selective atomic layer deposition (ASALD) and etch technique was investigated which provided selective block removal of PHOST-b-PS block copolymer patterns which initially exhibited no inherent etch contrast. Layer by layer titanium oxide (TiO_2) growth (0.4 Å/cycle) occurred in the PHOST domain during exposure to ALD precursors (tetrakis(dimethylamido titanium(IV)) and water) while no oxide growth occurred on the PS domain. Scanning electron microscopy (SEM) showed that upon subsequent oxygen plasma etching, the PS domain is removed leaving a high fidelity etch relief pattern of the original block copolymer template.

While this novel ASALD and etch method effectively provided selective block removal of PS-b-PHOST patterns, the ALD process adds additional complexity and processing steps to the fabrication process. An alternative approach is to utilize a styrene derivative with a chemical functionality which exhibits high etch resistance in comparison with the PHOST block. Here, polystyrene with trimethylsilyl functionality was used, which was readily converted to silicon oxide upon oxygen plasma etching, where SiO_2 exhibited high etch resistance and high thermal and mechanical stability in comparison with PHOST.

In this study, nitroxide mediated polymerization was used to prepare PTMSS homopolymer materials, and PTMSS-b-PHOST block copolymer materials (M_n=17300-26800 g/mol, and PDI of 1.2) with roughly 50/50 volume fraction allowing formation of lamellae structures (pitch=32-40 nm). Solvent annealing conditions were explored and optimized (including underlayer composition and solvent choice). Etch resistance of homopolymer films composed of TMS styrene and other relevant materials were

explored. The film thickness loss of PTMSS homopolymer films rapidly plateaued as a function of etch time (with about 10 nm film thickness loss), indicating conversion of the TMS group to the etch resistant silicon dioxide functionality. PTMSS-b-PHOST phase separated patterns were also exposed to oxygen plasma allowing selective block removal of the PS domain as indicated by SEM cross section analysis.

CHAPTER 1

INTRODUCTION: THE EXTENSION OF MOORE'S LAW THROUGH THE DIRECTED SELF ASSEMBLY OF BLOCK COPOLYMERS

1.1 The Integrated Circuit and Photolithography

1.1.1 Moore's Law

Integrated circuit (IC) based microelectronic devices are a ubiquitous technology that pervades all aspects of life including communication, transportation, manufacturing, and computing. In 1959, Bob Noyce and Jack Kirby were credited for inventing the silicon integrated circuit allowing electronic logic/memory devices to be printed on a silicon chip. Since all the circuitry and components of the device are fabricated on a monolithic piece of silicon, the entire device can be fabricated simultaneously through a series of processing steps, thereby eliminating the cost and inefficiency of hand wiring the large number of individual components. So, simply by printing smaller features on the chip, more transistors can be crammed onto the chip while the cost of processing the wafer remains the same, thereby dramatically reducing cost per transistor. In fact, the IC industry has doubled the number of transistors per chip approximately every 18-24 months, thus cutting the cost per transistor in half at each device generation while the

computing power grows exponentially. This trend is commonly known as Moore's law, and is represented graphically in Figure 1.1 [1-3]. Following Intel's road map, the recent technology nodes are 65 nm in 2005, 45 nm in 2007, 32 nm in 2009 and 22 nm in 2011 (Figure 1.2) [4]. Here, the nodes represent the half pitch of the densest features on the chip. The pitch is defined as the center to center distance between two adjacent lines.

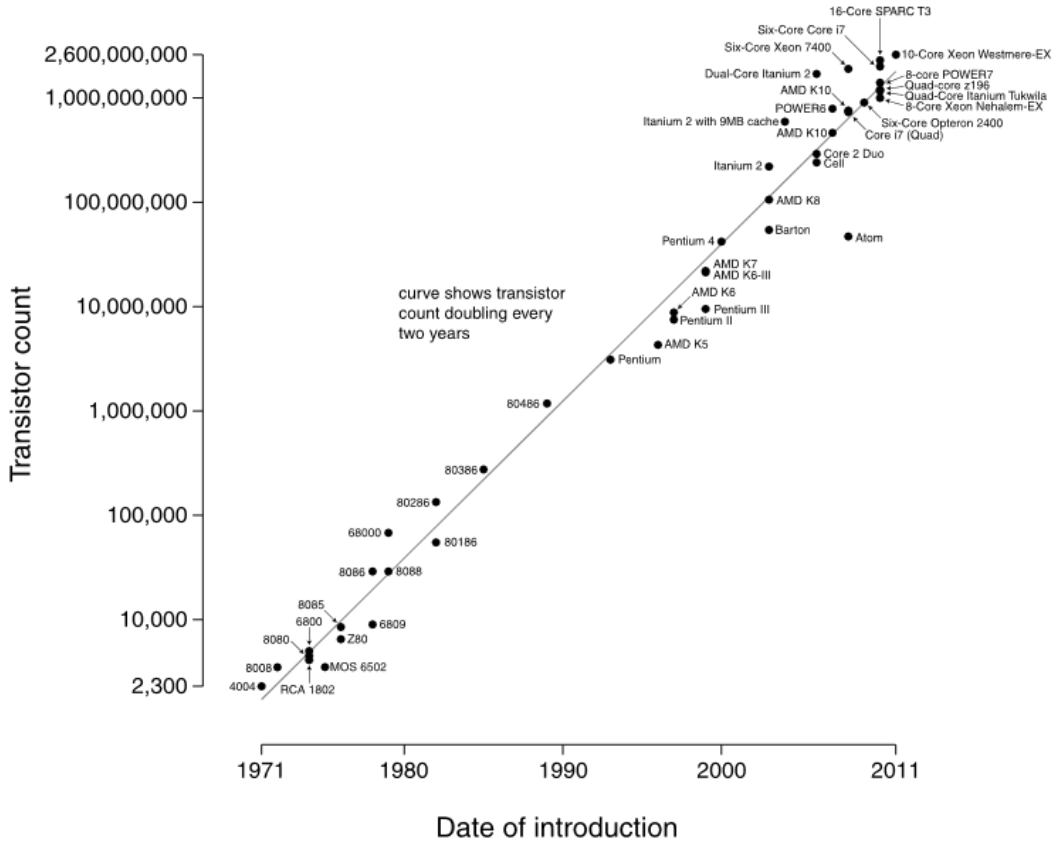

Figure 1.1 Microprocessor transistor count and Moore's Law (1971-2011)[2].

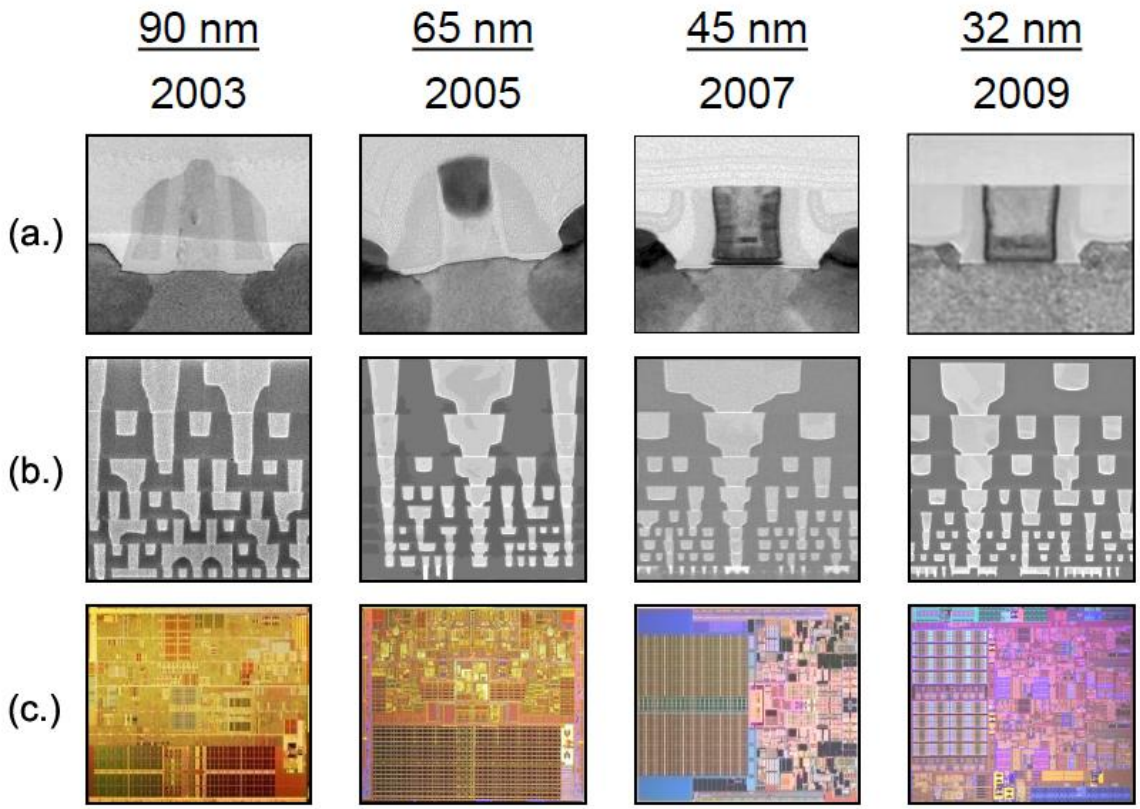

Figure 1.2 Recent microprocessor technology nodes: (a.) TEM cross section view of the transistor, (b.) SEM cross section view of the processor, (c.) top down view of the processor[4].

1.1.2 Projection Optical Lithography

Projection optical lithography is the standard process used to print relief patterns on the semiconductor device during integrated circuit fabrication. An overview of this photolithographic process is shown in Figure 1.3, where a predetermined pattern on a photomask is imaged onto the photoresist coated wafer. The photomask is typically a quartz surface with a chrome material on top which defines the master pattern. Here, the substrate is a thin film of functional electronic material on a silicon substrate, with a light sensitive material (known as a photoresist) on top of the sample. The sample is

illuminated, and the mask is used to selectively allow specific areas of the substrate to be exposed. A photochemical reaction takes place in the exposed regions of the photoresist dramatically altering the solubility of the exposed regions. The sample is then immersed in a developing solution which either removes the exposed regions or unexposed regions, thereby transferring the pattern on the mask into the resist layer. In positive tone resists, the exposed areas are removed, while in negative resists, the unexposed regions are removed. The resulting relief pattern functions as a etch mask allowing pattern transfer to the underlying substrate through etch processing. Repeating this process through multiple layers allows fabrication of the complete integrated semiconductor device.

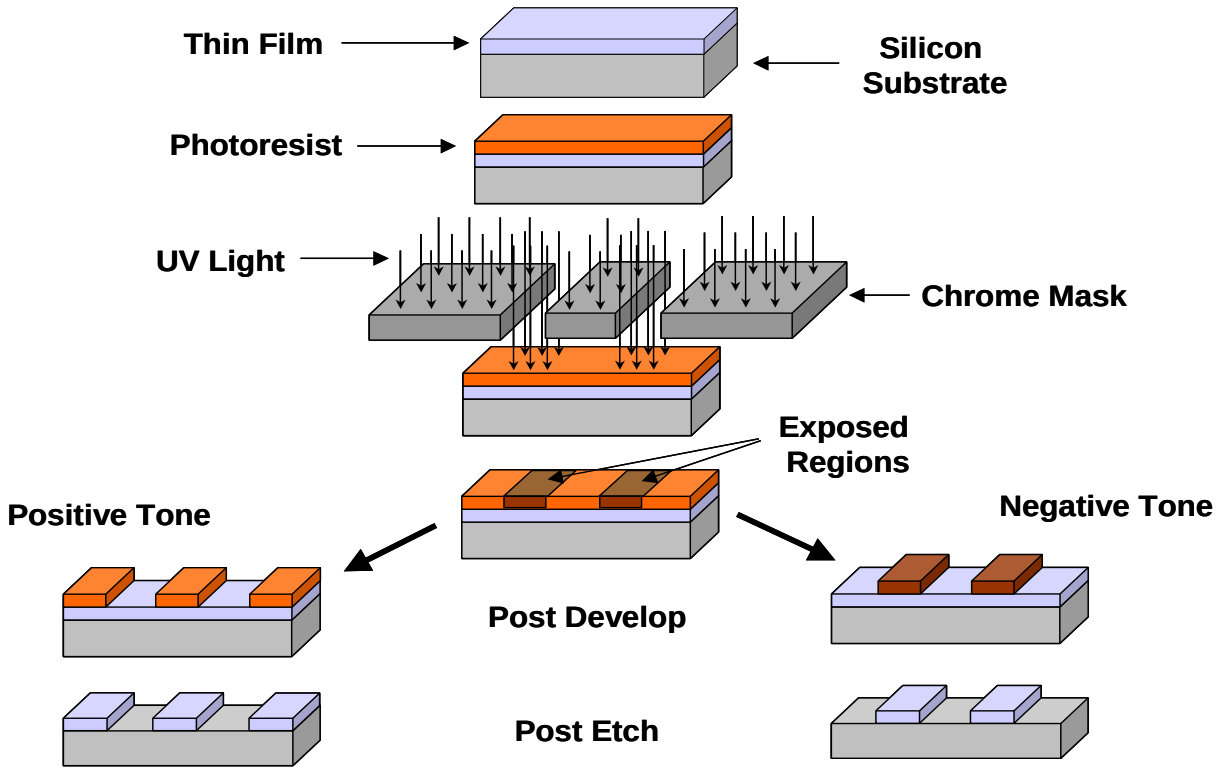

Figure 1.3. General overview of the photolithography process.

1.1.3 Trends in Projection Optical Lithography

Original optical lithographic systems employed contact printing, in which the mask is brought into close proximity with the wafer, and then optically aligned with the previous patterns on the wafer. Next, the mask is pressed onto the wafer surface and the mask/wafer assembly is flood exposed to provide the relief pattern[5]. Unfortunately, the mask and wafer are in direct contact, which reduces mask lifetimes, and results in high defect density. This technique evolved into projection lithography, which avoids direct contact of the mask and wafer. In this technique, the mask image is projected onto the wafer surface via a refractive optical system. The essential components of projection optical lithography are represented in Figure 1.4[6].

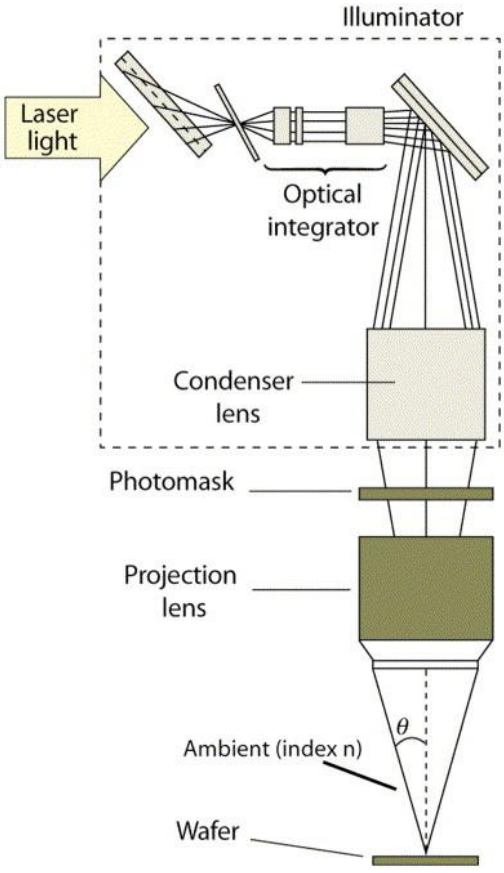

Figure 1.4 The essential components of the projection optical lithography system[6].

Projection optical lithography is the standard process used by the semiconductor industry for over three decades, allowing the dramatic reduction in feature size by a factor of 30. However, challenges due to the wavelike nature of light limit the extension of projection optical lithography toward higher resolution. As the pitch approaches the wavelength of the exposure system, the wave-like nature of light fundamentally limits the fidelity of the resulting pattern. Here, the diffraction of light reduces contrast between nominally dark and bright areas of the densely packed patterns. In fact, principles of optics dictate that the contrast becomes zero when the pitch equals one half the wavelength. This fundamental limit to the resolution of the optical exposure tools is described by the Rayleigh relationship (Equation 1.1), where HP is the half pitch of the printed feature, λ is the exposure wavelength. ($NA=n\sin\theta$) represents the numerical aperture, where n is the refractive index of the medium above the photoresist, and θ is the half angle of the converging beam on the sample The dimensionless scaling parameter (k_1) is determined by the performance of the imaging optics, photomask, and photoresist. Table 1.1 summarizes recent trends in optical lithography in reference to the parameters associated with the Rayleigh equation and the resulting minimum pitch and half pitch[7]. The following section discusses these trends in detail, as well as alternative technologies to extend optical lithography.

$$HP = \frac{k_1\lambda}{n\sin\theta} = \frac{k_1\lambda}{NA} \tag{1.1}$$

Table 1.1 Recent trends in photolithography in reference to relevant optical parameters.

λ (nm)	365	248	193	193*i*	13.5
k_1	0.5	0.4	0.3	0.3	0.4
NA	0.6	0.9	0.9	1.2	0.35
R(nm)	304	110	64	48	15
Pitch(nm)	608	220	129	97	30

1.1.4 k_1 parameter

According to equation one, a decrease in k_1 corresponds to decreasing pitch. As mentioned above, the fundamental limit for one to one line /space patterns is k_1=0.25. Current k_1 values approach 0.3, yet further improvements in k_1 would result in a relatively small gain in resolution, with the risk of reduced process control and diminished yield[7]. It should be noted, that when the pitch is relaxed, k_1<<0.25 is possible since the resolution is no longer limited by the diffraction of light by densely spaced patterns on the photomask; instead it is dependent on the processing conditions of the sample. In fact, isolates transistor gates as small as 9 nm have been fabricated with a wavelength of 248 nm[8].

1.1.5 Wavelength

Following the Rayleigh lens equation, decreasing the wavelength provided the historic decrease in feature size (Table 1.1). Until the late 1980's, ultraviolet (UV) lithography was performed with high-pressure mercury (Hg) discharge lamps. Specific

wavelengths of 436 nm (G line) and 365 nm (I line) were selected from the discharge arc by means of filters (Figure 1.5)[5]. Excimer lasers are an efficient source of deep ultraviolet (DUV) radiation, and have since replaced mercury lamps as the primary exposure tool for industrial production. These lasers function by the excitation of monomeric noble gases, which form a short lived excited dimer. Relaxation of this dimer back to the dissociated ground state results in the emission of DUV light. The two key DUV wavelengths are 248 nm produced by a KrF eximer laser, and 193 nm produced by an ArF eximer laser. The F_2 laser operating at 157 nm offers a 19% advance relative to ArF, and in 2002 it appeared that this technology would replace 193 nm imaging. However, due to the lack of appropriate lens materials (including a suitable replacement for quartz), this technology was dropped from the industry road map[9].

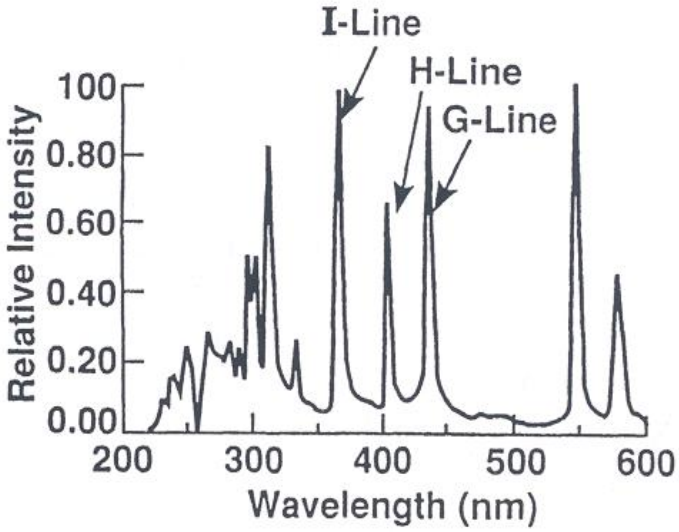

Figure 1.5 Spectrum of a Hg discharge lamp[5].

1.1.6 Numerical Aperture and 193 nm Immersion Lithography

An alternative route to improving resolution is to increase the numerical aperture. Here, a high index fluid is introduced between the last optical element of the exposure system and the photoresist, increasing the *NA* in Equation 1.1. At 193 nm, the refractive index for high purity water is 1.44, resulting in a maximum theoretical *NA* of 1.44. In practice, the numerical aperture increases from 0.86 for dry 193 nm exposure systems to 1.2 for 193 nm immersion exposure systems, resulting in an ~30% reduction in pitch (Table 1.1) [7].

1.1.7 Next Generation Optical Lithography: EUVL

Extreme ultraviolet lithography (EUVL) is a strong contender for industrial production of next generation IC devices[10]. This approach follows the same principles as conventional lithography except it utilizes a wavelength of 13.5 nm. Following Rayleigh's equation (with λ=13.5 nm, and *NA*=0.35) provides a pitch of 30 nm for this system. While the small wavelength may allow improved resolution, it also introduces several problems[11]. First, the absorbance of this short wavelength light is extremely strong regardless of the material. Hence, all reflective optics must be used in a near vacuum environment. These mirrors utilize alternating layers of silicon and molydenum to improve reflectivity, yet transmission is still limited to about 70 percent per optical element. Hence, an extremely high power EUV source is necessary to account for the power loss in this optical system. These issues have stalled industrial implementation of

this technology, motivating industry to utilize and investigate alternative lithographic approaches.

1.1.8 Next Generation Optical Lithography: Double Patterning

Due to the delay in readiness of EUV lithography, double patterning is the current technology used to extend 193 nm immersion techniques to the 32 nm node, 22 nm node, and potentially beyond. While, many variations of this approach exist (each with its own process related challenges), a representative double patterning example is represented in Figure 1.6 [12]. The key to this approach is that it combines two separately lithographed patterns resulting in a final overlaid arrangement with half the pitch of each original pattern. For example, 193 nm immersion exposure that provides 60 nm pitch can be printed twice to reduce the pitch to 30 nm. Due to its \relatively straightforward implementation, without the need for additional infrastructure, double patterning has been used at the 45 nm, 32 nm, and 22 nm node, and may be used for the 15 nm node as well. The primary drawback of double patterning is the increased number of steps used to process each wafer, which raises the production cost of each chip. Also, serious design issues and overlay challenges exist for the 22 nm node and below[13].

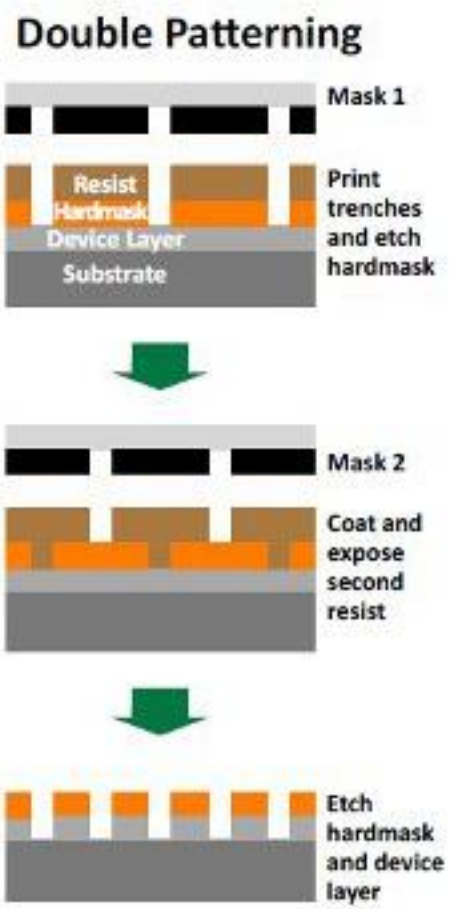

Figure 1.6 Double patterning option utilizing litho/etch/litho/etch process with two separate exposure steps[12].

1.2 Directed Self Assembly of Block Copolymers

Given the uncertain future of EUVL, and the increased processing cost of double patterning, the semiconductor industry is investigating alternative lithographic techniques. Even if one assumes the eventual implementation of EUVL, which could provide 30 nm pitch, double patterning only reduces this pitch by half to 15 nm. To maintain Moore's law into the next decade and beyond, novel patterning techniques are required.

One potential alternative that has grabbed industry attention is directed self assembly (DSA) of block copolymers. The key results that garnered industry interest are that block copolymers routinely phase separate with pitch less than 30 nm; also these BCP materials have been patterned into a variety of relevant geometries[14-17]. The next section will review the basic properties of directed self assembled block copolymer materials, and introduce several material and processing challenges associated with implementing this technology.

1.2.1 Integration of Traditional Optical Lithography with the Directed Self Assembly of Block Copolymers

Directed self assembly of block copolymers utilizes a primary lithographic pattern to guide the alignment of the block copolymer material (Figure 1.7)[16, 18-20]. Here, the BCP is spin coated onto a substrate with a set of primary guiding patterns written at a relaxed pitch. Then, the BCP is allowed to phase separate and to align according to the primary guiding pattern. Next, one of the BCP domains is selectively removed to generate the relief pattern that can be transferred into the underlying silicon substrate through etch processing. The result is pitch subdivision of the original primary lithographic pattern by the secondary block copolymer pattern resulting in a dramatic reduction in the critical dimension and the pitch. Figure 1.8 represents a practical example of directed self assembly utilizing a trench fabricated by traditional lithographic techniques to guide the aligned BCP. Details of the alignment process will be discussed in Chapter 3. The next section reviews the conditions required for phase separation, and describes the structure of the phase separated result.

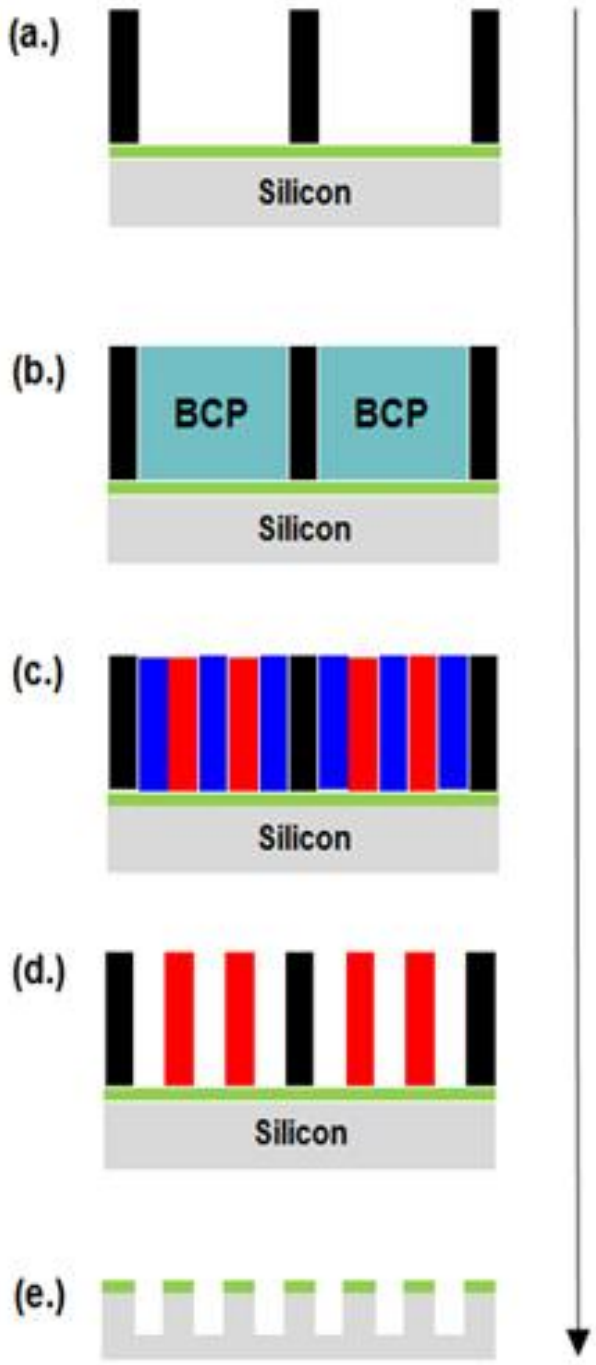

Figure 1.7 Profile view of the directed self assembly process: (a.) fabrication of the primary pattern on top of a conducting layer (green) on a silicon substrate; (b.) spin coat of the BCP; (c.) phase separation of the BCP; (d.) Selective removal of one of the BCP domains; (e.) transfer of BCP relief pattern into the underlying substrate through etch processing.

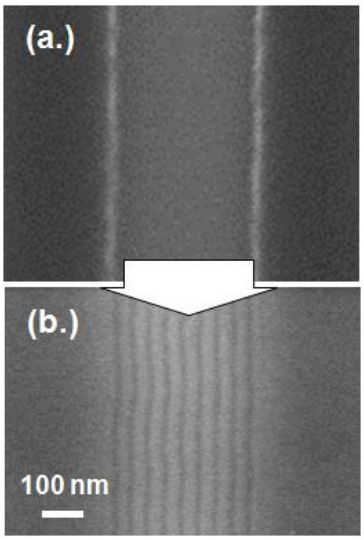

Figure 1.8 Directed self assembly of block copolymer materials: (a.) Trench fabricated through electron beam lithography, (b.) alignment of BCP within the trench resulting in pitch subdivision.

1.2.2 Phase Behavior of a Binary Mixture

A binary mixture is a system with two different chemical species. If the mixture is uniform all components are intermixed on a molecular scale. An example of a binary mixture is a blend of low molecular weight poly(styrene) and poly(butadiene)[21, 22]. However, given appropriate thermodynamic conditions, the homopolymer mix will phase separate into two distinct phases (regions with different compositions). A relevant example is poly(styrene) and poly(methylmethacrylate)[23]. Here, the two phases will separate in an arrangement which reduces the surface area between the two domains (Figure 1.9). However, the polymer mixture is viscous (even above the glass transition temperature) such that the phase separated homopolymer mixture does not necessarily reach the equilibrated phase separated state. If the two distinct polymer blocks were covalently tethered to form a block copolymer, phase separation can still occur. However, the length scale of the phase separated regions would now depend on the length scale (i.e. degree of polymerization) of the block copolymer (Figure 1.9). As

mentioned previously, the length scale of this phase separated result is often less than 30 nm pitch, hence the semiconductor industry is interested in utilizing this technology for production of integrated semiconductor devices with feature sizes of 30 nm pitch and below.

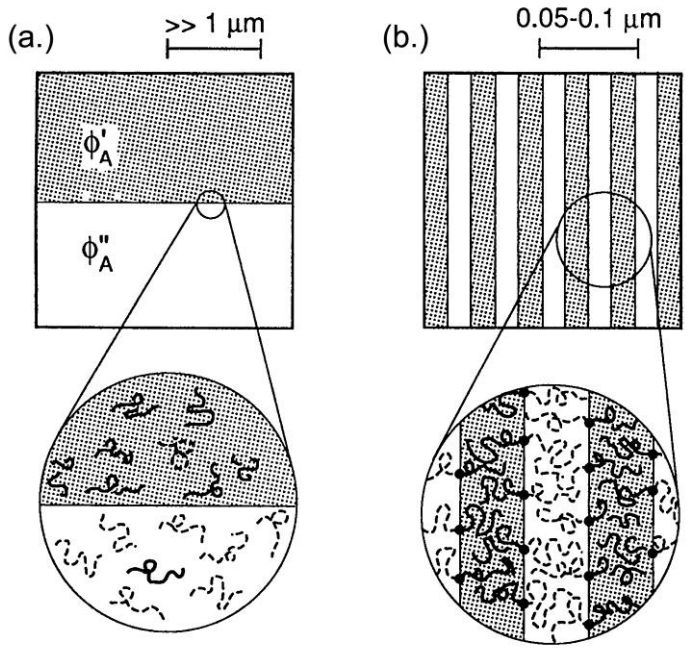

Figure 1.9 Representative phase behavior of a thermodynamically incompatible polymer-polymer system: (a.) macrophase behavior of a linear homopolymer mix, and (b.) microphase behavior of a block copolymer with a covalent link between the domains[24].

1.2.3 Thermodynamics of Phase Separation

The change in free energy of mixing (ΔG_m) associated with the polymer chains is described by Flory-Huggins theory (Equation 1.2)[22, 24]. This approach utilizes a simplified lattice model which assumes components are incompressible and mix at constant volume, and utilizes a mean field between approach which ignores correlations

along the chain. The first two terms on the right hand side in this equation account for the entropy of mixing (ΔS_m) and include the number of segments per chain for both polymer components (N_A and N_B) and include the volume fraction of each block (ϕ). The third term represents the enthalpy of mixing (ΔH_m) and includes the Flory-Huggins interaction parameter (χ)

$$\frac{\Delta G_m}{k_B T} = \frac{\phi_A}{N_A} ln(\phi_{B)} + \frac{\phi_B}{N_B} ln(\phi_A) + \chi \phi_A \phi_B \quad (1.2)$$

1.2.4 Entropy Component

Mixing naturally increases the randomness of the system, hence the entropy term is always positive and promotes mixing. Yet, when compared with the mixing of small molecules (N=1), connecting the monomers into chains (N>>1) drastically reduces the number of possible states in the mixed system, hence entropy of mixing is relatively small. In fact, the entropy of mixing for a polymer solution is roughly half that of the regular solution (Figure 1.10)[22].

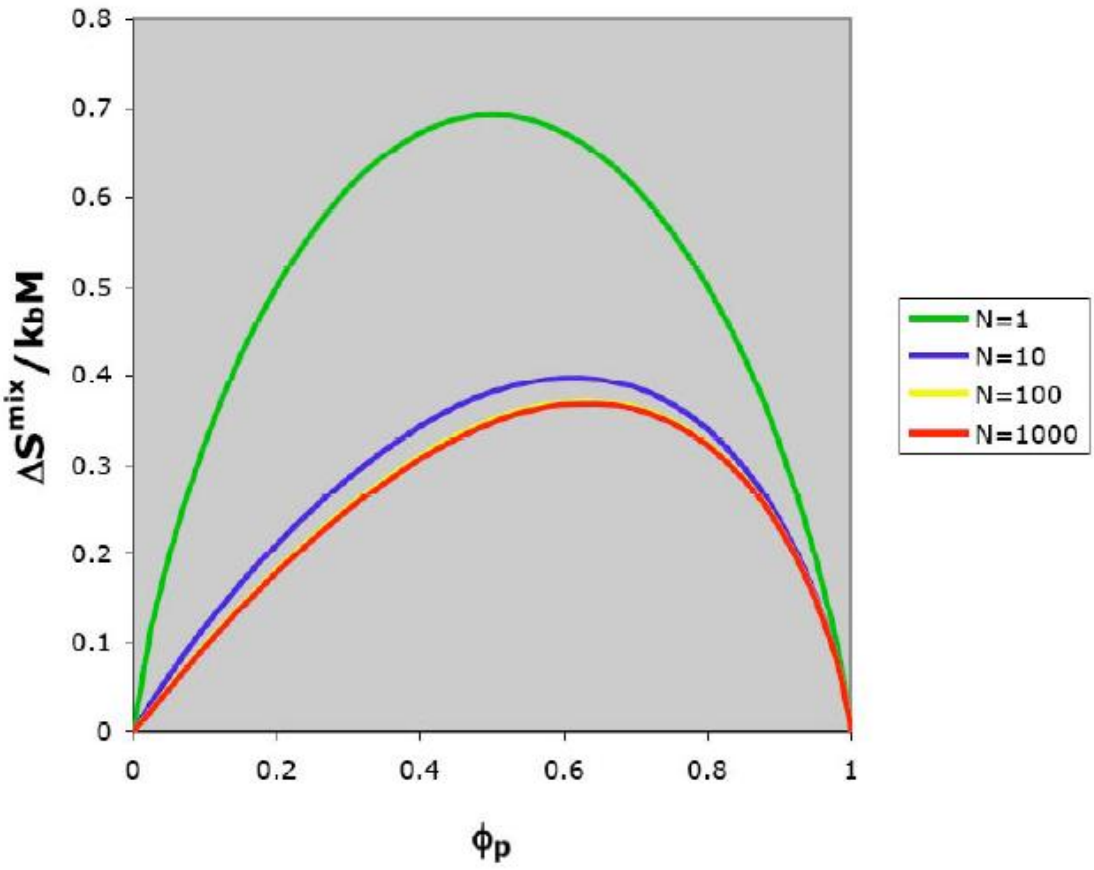

Figure 1.10 Entropy of mixing for an ideal homopolymer mix The top curve represents a mixture with $N = N_A = N_B = 1$. The bottom curved represents a mixture with $N = N_A = N_B = 1000$[15].

1.2.5 Enthalpy of Mixing

Due to the small contribution of entropy to the free energy of mixing, mixing is primarily driven by enthalpic interactions. The choice of a particular pair of monomers establishes the magnitude and sign of the enthalpy of mixing, which can be approximated by the Flory-Huggins interaction parameter χ (Equation 1.3) [22]. Here, χ is a dimensionless parameter which measures the strength of pair wise interaction energies (ϵ) between the species in the mixture compared with the same species in their pure

component states. If there is a net attraction between species (χ<0), a single phase mixture is favored. Usually, there is a net repulsion between species (they like themselves better than they like each other) and the Flory-Huggins interaction parameter is positive (χ>0).

$$\chi = k_B T \left[\epsilon_{AB} - \frac{1}{2}(\epsilon_{AA} - \epsilon_{BB}) \right] \tag{1.3}$$

1.2.6 Composition Profile, Segregation Strength, and Free Energy of Mixing

As discussed above, free energy of mixing scales with N^{-1} and χ, hence the product χN dictates the strength of segregation between the domains (Figure 1.11). If χN<10, the A-B interactions are sufficiently weak that the individual copolymers remain largely unperturbed, and the ordered composition profile is approximately sinusoidal. This regime is referred to as the weak segregation limit and the periodic length scales as $D \sim a N^{1/2}$ [25]. As χN>>10, a narrow interface immerges with an interfacial width of $\sim a N^{-1/2}$ [23], resulting in well separated micro-domains of almost pure A and pure B. Here, the system minimizes the total area of this interface between domain A and domain B, through extended and perturbed chain configurations. The resulting micro-domain sizes scale as $D \sim a \chi^{1/6} N^{2/3}$ [26].

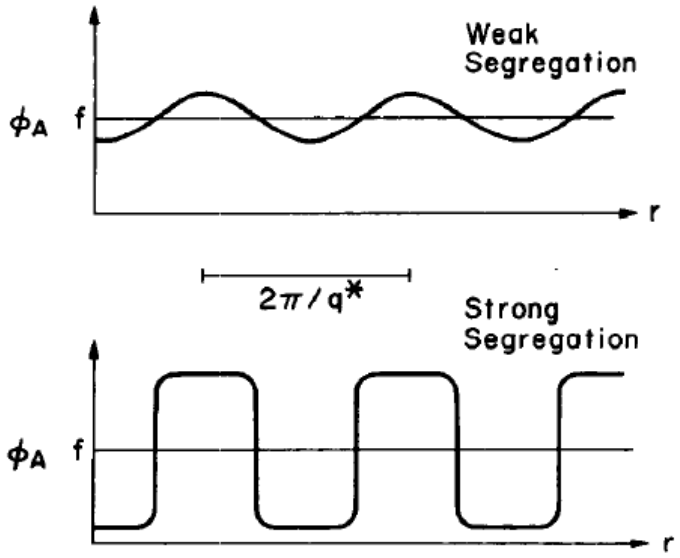

Figure 1.11 One-dimensional compositional profile characterizing the weak and strong segregation limits. ϕ_A represents the local volume fraction of the A-block, while *f* represents the stoichiometric volume fraction of the A-block[27].

1.2.7 Phase Morphology

For diblock copolymers, the phase morphology is dependent on the product of χN, and also on the overall volume fraction of the A component resulting in a rich phase diagram with several thermodynamically stable morphologies (Figure 1.12)[25-27]. For χN<10.5, only a disordered phase is observed. At larger values of χN above the order disorder transition (ODT), seven microphase structures are predicted. The lamellar phase is stable for all nearly symmetrical diblocks. A gyroid or hexagonally packed cylinder phase is stable for diblock with intermediate symmetry. Excessively asymmetric volume fraction results in body centered cubic (bbc) morphology with the minor phase comprising the cylinder domain.

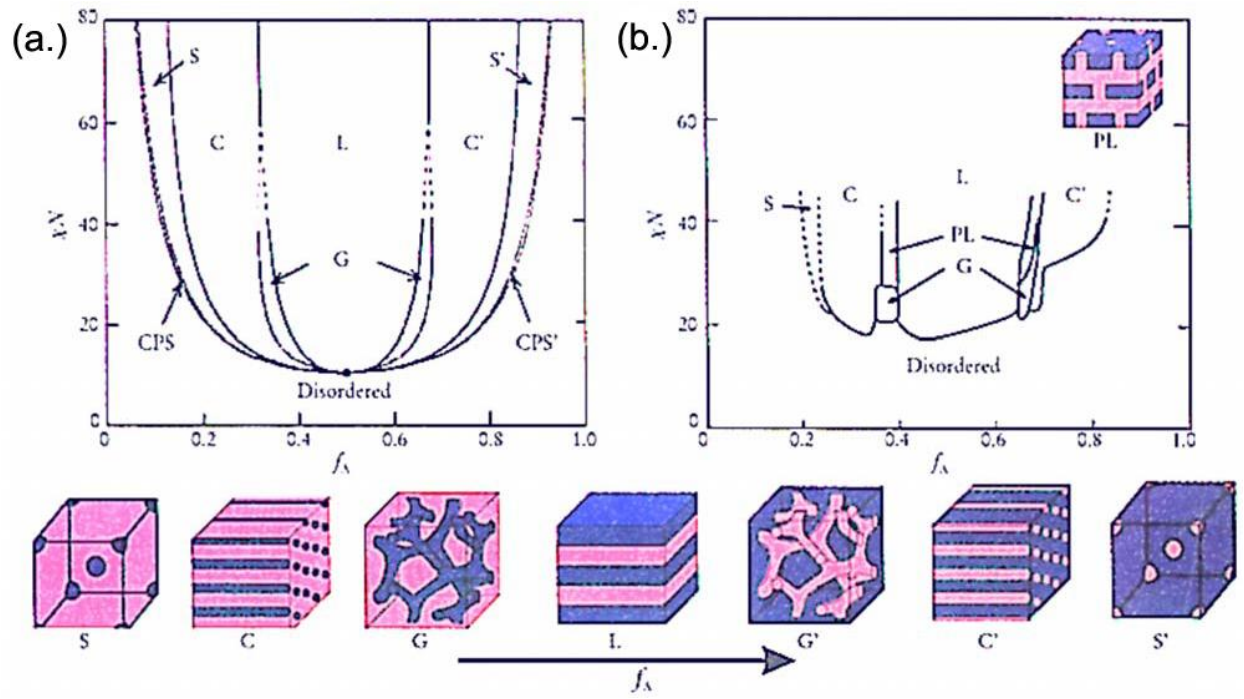

Figure 1.12 Phase diagram for AB diblock copolymers. (a.) Equilibrium morphology as predicted by self consistent mean field theory. (b.) experimental phase diagram of poly(styrene)-b-poly(isoprene)[10].

1.3 Toward Next Generation Block Copolymer Patterning: Key Challenges and the Introduction of a High χ BCP System

Block copolymer (BCP) thin film patterns, generated using directed self-assembly (DSA) of diblock copolymers, have shown excellent promise as templates for semiconductor device manufacturing since they routinely exhibit pitch of 30 nm, and they have the potential to produce features with pitches well below 20 nm[28]. For example, a primary lithographic pattern produced from current lithographic techniques could be used to guide the self assembly of block copolymers with very small pitch resulting in pitch subdivision of the original primary pattern. **While this technique readily facilitates the directed self assembly of BCP with pitch above 20 nm, several challenges are associated with pushing the resolution to 20 nm and below.** These

challenges include the following: demonstration of high χ systems which provide sub 20 nm patterning, synthesis of BCP with controlled molecular weight and low PDI, and selective block removal to generate the relief etch mask. This section will discuss these three challenges and present a block copolymer system, poly(styrene)-block-poly(hydroxystyrene) (PS-b-PHOST), which addresses these issues leading to the directed self assembly of block copolymer patterns with sub 20 nm pitch.

1.3.1 High χ Systems Enabling High Resolution

As discussed above, the propensity of the blocks to phase separate depends on the thermodynamic driving forces which are characterized by the Flory Huggins interaction parameter (χ). When the enthalpic energy gains produced by phase separation of the blocks are sufficiently large as to overcome the entropic driving force to mix the blocks, micro-phase separation occurs that can give rise to a large number of interesting nanostructured phases that depend on the relative volume fractions of the two blocks. The condition at which such micro-phase separation occurs is characterized by Equation 1.4, where χ is the Flory Huggins interaction parameter, and N is the degree of polymerization. For block copolymers with compositions near 50:50 volume fraction of the two blocks, lamellar phase separated patterns form. The pitch of such lamellar patterns in the strong segregation regime is proportional to the statistical segment length (a), Flory Huggins interaction parameter (χ), and the degree of polymerization (N) as shown in Equation 1.5. Since the length scale of these structures is proportional to the degree of polymerization of the blocks, relatively large increases in χ must be achieved to offset reductions in N.

$$\chi N > 10.5 \tag{1.4}$$

$$D \sim a\chi^{1/6}N^{2/3} \tag{1.5}$$

Currently the most widely studied block copolymer (BCP) for thin film DSA applications is poly(styrene)-block-poly(methylmethacrylate) or PS-b-PMMA. PS-b-PMMA possess an extremely modest χ value of approximately 0.04, which translates into a minimum practical DSA pitch for such materials on the order of 20 nm[23]. If the χ could be increased by an order of magnitude, the minimum pitch could be reduced to 10 nm and below (Table 1.2).

Table 1.2 Pitch scaling trends (χ and the associated minimum pitch) for diblock copolymer phase separation in the strong segregation regime.

χ	**Minimum Pitch**
0.04 (PS-b-PMMA)	**20 nm**
0.2	**9 nm**
0.5	**6 nm**
1.0	**4 nm**

Production of diblock copolymers with higher χ values can be achieved by incorporating polymer blocks that have stronger interactions between monomers of the same type and which have interactions that are orthogonal in nature to the types of interactions between monomers of the second block type. One example is the use of a polymer block that exhibits hydrogen bonding interactions in conjunction with a polymer block that interacts primarily though quadrupolar interactions. In this work, the PMMA

block from PS-b-PMMA has been replaced with a block containing highly polar and hydrogen bonding functionality, poly(hydroxystyrene) or PHOST (Figure 1.13). PHOST is chosen since it is known to form extensive hydrogen bond networks from earlier resist material studies, a fact which should result in an increase in χ due to this increased enthalpic interaction for PHOST as compared to PMMA[29].

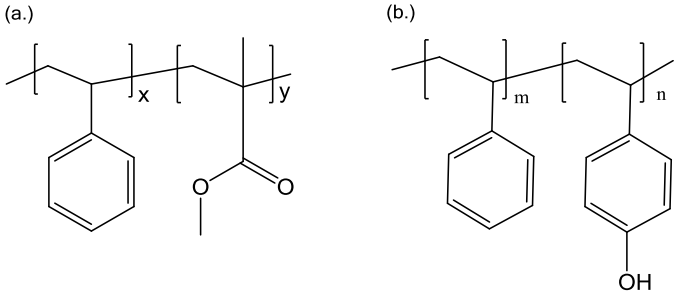

Figure 1.13 (a.) poly(styrene)-b-poly(methylmethacrylate) or PS-b-PMMA, (b.) poly(styrene)-b-poly(hydroxystyrene) or PS-b-PHOST.

1.3.2 Controlled Synthesis of Block Copolymers with Targeted Molecular Weight and Low PDI

For semiconductor device manufacturing using traditional photolithography, the dimensions of the lithographic patterns are primarily determined by the photomask and the manufacturing process conditions. With the integration of directed self assembly of block copolymers with traditional photolithography, the resulting pattern is now also critically dependent on the molecular structure of the block copolymer material. As mentioned above, the phase morphology, domain length scale, and interfacial width are proportional to the degree of polymerization of the block copolymer. Furthermore, the polydispersity of the polymer also affects the pitch and interfacial width between the domains. See Chapter 2 for further discussion.

While traditional radical chain growth polymerization has been successfully performed for decades, this techniques does not provide the control necessary for targeted molecular weights and low PDI. In fact, free radical polymerization with azoisobutyronitrile (AIBN) initiator generally results in PDI of approximately 1.5-2.5. An alternative technique is "living" polymerization which enables control over molecular weight and molecular weight distribution with PDI approaching 1.0. Here, the occurrence of premature termination is limited, and molecular weight increases with time until the monomer is consumed or the reaction is intentionally terminated. In the mid 1990's, these living polymerization techniques were initially developed and have branched out into three related techniques[30-33]:

-Atom Transfer Radical Polymerization (ATRP)

-Reversible Addition/Fragmentation Chain Transfer Polymerization (RAFT)

-Nitroxide Mediated Polymerization (NMP)

In this work, nitroxide mediated polymerization is utilized to produce the PS-b-PHOST material, since this method provides good molecular weight control and low PDI for styrene based polymers[31, 34]. Furthermore, this method avoids the use of metallic reagents that can contaminate the polymer samples and cause contamination problems in subsequent processing in clean room facilities. Details of this techniques are discussed in Chapter 2.

1.3.3 Selective Block Removal

Selective block removal of the BCP pattern is required in order to generate the etch relief image for pattern transfer into the underlying substrate. Here, high etch contrast is utilized between the domains to remove one of the blocks with etch processing[16, 35, 36]. Etch contrast primarily relies on atomic composition, and PS and

PHOST both have similar chemical compositions, hence this material exhibits no appreciable etch contrast[37].

An additional processing step after phase separation could be utilized to provide sufficient etch contrast between the blocks. In fact, several processes have been reported that selectively functionalize one of the blocks with high etch resistance functionality[38, 39]. The primary drawback of these approaches is that the reactant infiltrates the PHOST and functionalizes the entire volume of the domain, resulting in an increase in the effective volume, thereby distorting the original pattern. See Chapter 4 for full discussion of these techniques.

An alternative to infiltrating the polymer material is to utilize the OH functionality already present on the surface of the PHOST as a selective substrate for atomic layer deposition (ALD). Here, ALD precursors react directly with the surface of the PHOST domain growing an etch resistant oxide layer on top of the PHOST domain, while the PS domain remains inert to ALD growth. The characteristic feature of ALD is alternate dosing of reactants onto the substrate, in which only a chemisorbed monolayer of one precursor is retained on the substrate with each dose. This monolayer can then react with the other precursor upon subsequent dosing. Hence, when the reaction cycle is repeated, a solid film is deposited on the substrate, layer by layer. Here, the precursor doesn't swell the block, but the outer surface of the PHOST domain is functionalized with the oxide, and the oxide can continue to grow on this surface. Therefore, an etch resistant oxide layer is formed on the surface of the PHOST domain, while the PS domain is easily removed via oxygen plasma etching. In this work, an area selective atomic layer deposition (ASALD) and etch process is presented which provides selective block removal of poly(hydroxystyrene)-b-poly(styrene) (PHOST-b-PS) block copolymer patterns which initially exhibited no inherent etch contrast. This process (summarized in Figure 1.14) is discussed in Chapter 5.

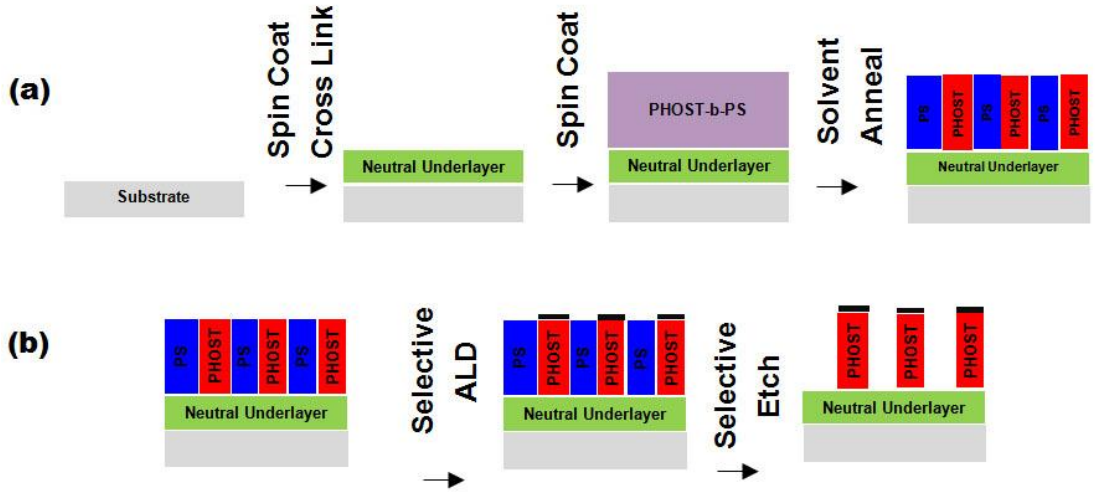

Figure 1.14 Selective block removal process flow: (a.) spin coating and cross-linking neutral underlayer, spin coating of PS-b-PHOST, and solvent annealing to provide vertical lamellar fingerprint patterns; (b.) area selective ALD and etch resulting in a relief image of the original block copolymer pattern.

1.4 References

1. Moore, G. *Electronics Magazine* **1965,** 38, (8).

2. Chacos, B. Breaking Moore's Law: How chipmakers are pushing PCs to blistering new levels. http://www.pcworld.com/article/2033671/breaking-moores-law-how-chipmakers-are-pushing-pcs-to-blistering-new-levels.html.

3. Borodovsky, Y. **2006**, 615301-615301.

4. Bohr, M. Intel's Revolutionary 22 nm Transistor Technology. http://download.intel.com/newsroom/kits/22nm/pdfs/22nm-Details_Presentation.pdf

5. L. F. Thompson C. G. Wilson, M. J. B., *The Introduction to Microlithography*. American Chemical Society: Washington, D. C., 1994.

6. Rothschild, M. *MRS Bulletin* **2005,** 30, 942-946.

7. Brunner, T. A. *J Vac Sci Technol B* **2003,** 21, (6), 2632-2637.

8. Fritze, M. C., C.K. ; Astolfi, D.K. ; Yost, D.R. ; Burns, J.A. ; Chang-Lee Chen ; Gouker, P.M. ; Suntharalingam, V. ; Wyatt, P.W. ; Keast, C.L. . *Circuits and Devices Magazine, IEEE* **2003,** 19, (1), 43-47.

9. Lapedus, M. Intel drops 157-nm tools from lithography roadmap. http://www.eetimes.com/electronics-news/4092441/Intel-drops-157-nm-tools-from-lithography-roadmap (4/25/2013).

10. Wagner, C.; Harned, N. *Nat Photonics* **2010,** 4, (1), 24-26.

11. Ito, T.; Okazaki, S. *Nature* **2000,** 406, (6799), 1027-1031.

12. LaPedus, M. Lithography Vendors Expand Immersion Roadmaps. http://semimd.com/blog/2012/01/25/lithography-vendors-expand-immersion-roadmaps/

13. Zimmerman, P. Double patterning lithography: double the trouble or double the fun? http://spie.org/x35993.xml

14. Kim, H. C.; Hinsberg, W. D. *J Vac Sci Technol A* **2008,** 26, (6), 1369-1382.

15. Kim, H. C.; Park, S. M.; Hinsberg, W. D. *Chem Rev* **2010,** 110, (1), 146-177.

16. Jung, Y. S.; Ross, C. A. *Nano Lett* **2007,** 7, (7), 2046-2050.

17. Bang, J.; Jeong, U.; Ryu, D. Y.; Russell, T. P.; Hawker, C. J. *Adv Mater* **2009,** 21, (47), 4769-4792.

18. Cheng, J. Y.; Rettner, C. T.; Sanders, D. P.; Kim, H. C.; Hinsberg, W. D. *Adv Mater* **2008,** 20, (16), 3155-3158.

19. Cheng, J. Y.; Mayes, A. M.; Ross, C. A. *Nat Mater* **2004,** 3, (11), 823-828.

20. Chai, J.; Buriak, J. M. *ACS Nano* **2008,** 2, (3), 489-501.

21. Roe, R. J.; Zin, W. C. *Macromolecules* **1980,** 13, (5), 1221-1228.

22. Rubinstein, M., *Polymer Physics*. Oxford University Press: Oxford, New York, 2003.

23. Russell, T. P.; Hjelm, R. P.; Seeger, P. A. *Macromolecules* **1990,** 23, (3), 890-893.

24. Bates, F. S. *Science* **1991,** 251, (4996), 898-905.

25. Leibler, L. *Macromolecules* **1980,** 13, (6), 1602-1617.

26. Khandpur, A. K.; Forster, S.; Bates, F. S.; Hamley, I. W.; Ryan, A. J.; Bras, W.; Almdal, K.; Mortensen, K. *Macromolecules* **1995,** 28, (26), 8796-8806.

27. Bates, F. S.; Fredrickson, G. H. *Phys Today* **1999,** 52, (2), 32-38.

28. Herr, D. J. C. *J Mater Res* **2011,** 26, (2), 122-139.

29. Quinn, J. D.; Register, R. A. *Journal of Polymer Science: Part B: Polymer Physics* **2009,** 47, 2106-2113.

30. Matyjaszewski, K.; Xia, J. H. *Chem Rev* **2001,** 101, (9), 2921-2990.

31. Hawker, C. J.; Bosman, A. W.; Harth, E. *Chem Rev* **2001,** 101, (12), 3661-3688.

32. Chiefari, J.; Chong, Y. K.; Ercole, F.; Krstina, J.; Jeffery, J.; Le, T. P. T.; Mayadunne, R. T. A.; Meijs, G. F.; Moad, C. L.; Moad, G.; Rizzardo, E.; Thang, S. H. *Macromolecules* **1998,** 31, (16), 5559-5562.

33. Braunecker, W. A.; Matyjaszewski, K. *Prog Polym Sci* **2007,** 32, (1), 93-146.

34. Barclay, G. G.; Hawker, C. J.; Ito, H.; Orellana, A.; Malenfant, P. R. L.; Sinta, R. F. *Macromolecules* **1998,** 31, (4), 1024-1031.

35. Cushen, J. D.; Otsuka, I.; Bates, C. M.; Halila, S.; Fort, S.; Rochas, C.; Easley, J. A.; Rausch, E. L.; Thio, A.; Borsali, R.; Willson, C. G.; Ellison, C. J. *ACS Nano* **2012,** 6, (4), 3424-3433.

36. Hirai, T.; Leolukman, M.; Liu, C. C.; Han, E.; Kim, Y. J.; Ishida, Y.; Hayakawa, T.; Kakimoto, M.; Nealey, P. F.; Gopalan, P. *Adv Mater* **2009,** 21, (43), 4334.

37. Watanabe, F.; Ohnishi, Y. *J Vac Sci Technol B* **1986,** 4, (1), 422-425.

38. Peng, Q.; Tseng, Y. C.; Darling, S. B.; Elam, J. W. *ACS Nano* **2011,** 5, (6), 4600-4606.

39. Peng, Q.; Tseng, Y. C.; Darling, S. B.; Elam, J. W. *Adv Mater* **2010,** 22, (45), 5129.

CHAPTER 2

SYNTHESIS AND CHARACTERIZATION OF PS-b-PHOST BLOCK COPOLYMER AND PS-r-PHOST-r-PGMA RANDOM COPOLYMER AS A NEUTRAL UNDERLAYER FOR THE PS-b-PHOST SYSTEM

Targeted polymer molecular weights and low polydispersities are required for directed self assembly patterning, since the pitch and morphology of the BCP are dependent on the characteristic length scale (or degree of polymerization) of each block on the polymer chain. Nitroxide mediated polymerization (NMP) provides controlled molecular weight and low polydispersity for styrene based systems. In this work, NMP techniques were utilized to produce the diblock copolymers reported here. NMP provided good molecular weight control and low PDI without the use of metallic reagents that can contaminate the polymer samples and cause contamination problems in subsequent processing of block copolymers in clean room facilities. Block copolymers synthesized with the universal nitroxide initiator exhibited improved PDI in comparison with block copolymers synthesized with the traditional TEMPO initiator. Here, PS-b-PHOST polymers were synthesized with a range of molecular weights (M_n=8500-30000 g/mol) with low PDI approaching 1.2. Also, a series of random copolymers were synthesized as potential neutral underlayer substrates for the PS-b-PHOST system.

2.1 Introduction

Diblock copolymers are a specific class of copolymer materials where the different monomers are not randomly distributed, but are grouped into discrete homogeneous sections (or blocks). Conceptually, block copolymers can be thought of as homo-polymers linked end-to-end via a covalent bond. These materials are generally synthesized via chain polymerization reactions, where synthesis of the first homogenous block serves as the initiator for polymerization of the second block. Here, when the polymerization of monomer A is complete, monomer B is added to the reaction mix resulting in a polymer with a long block of A repeat units, followed by a long block of B repeat units. One can continue the sequential propagation by addition of a third monomer, or the reaction can be intentionally terminated[1].

The key to chain polymerization of block copolymers is the elimination of unwanted termination reactions allowing sequential addition of different monomers, and targeted molecular weights with low polydispersities. Targeted molecular weights are required since the pitch and morphology of the BCP is dependent on the length scale (or degree of polymerization) of each block on the polymer chain[2]. Polydispersity also critically influences the block copolymer self assembly. As polydispersity increases, both the domain spacing and the interfacial thickness increase, and phase transitions may be introduced[3-6].

2.1.1 Conventional Radical Techniques

Chain polymerization reactions have been successfully performed for decades with conventional radical techniques generating many important polymers for a wide

variety of applications. However, these conventional techniques exhibit a wide range of termination reactions resulting in poor molecular weight control and high polydispersity (with a theoretical lower PDI limit of 1.5 for traditional radical approaches)[7]. Typical termination reactions in chain polymerization include combination and disproportionation (Figure 2.1)[8]. Combination reactions includes the direct annihilation of two radical centers in a bimolecular reaction. Disproportionation results when a hydrogen radical that is beta to one radical center is transferred to another radical. Due to the presence of excessive termination events, traditional radical chain polymerization is not a viable approach for preparation of diblock copolymers, and industry has since focused on alternative living radical techniques.

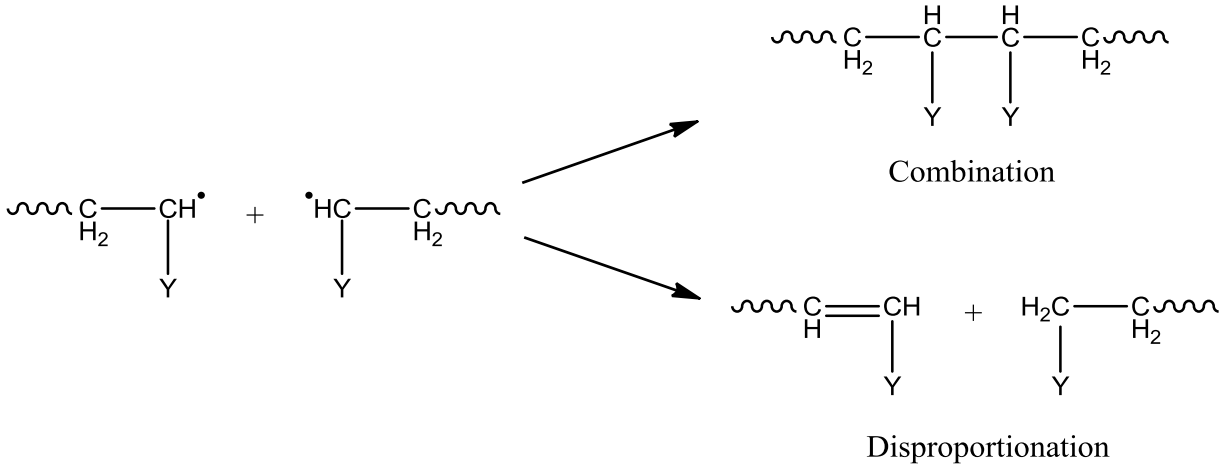

Figure 2.1. Two principal termination reactions that may occur in free radical polymerization are combination and disproportionation.

2.1.2 Living Polymerizations

Living polymerizations are defined as systems where irreversible terminations and transfers are efficiently suppressed, allowing synthesis of block copolymers via sequential addition of monomers[9]. Living radical polymerizations utilize a dormant state of the propagating radical species, thereby minimizing the likelihood of two propagating radicals irreversibly reacting in a termination event. The generalized scheme of living radical polymerizations is represented in Figure 2.2. Here, the initiator undergoes homolytic bond cleavage to produce one reactive radical and one stable radical. The reactive radicals quickly initiate polymerization, while the stable radicals are too stable to initiate polymerization[1]. An appropriate equilibrium constant for the propagating species and dormant species is required to achieve living characteristics[10]. Here, the equilibrium constant should not be too low that the propagation does not proceed at a reasonable rate. Yet, it should not be too high that normal bimolecular termination reactions become significant. Furthermore, the initiator should decompose rapidly insuring all the propagating radical chains grow for approximately the same time.

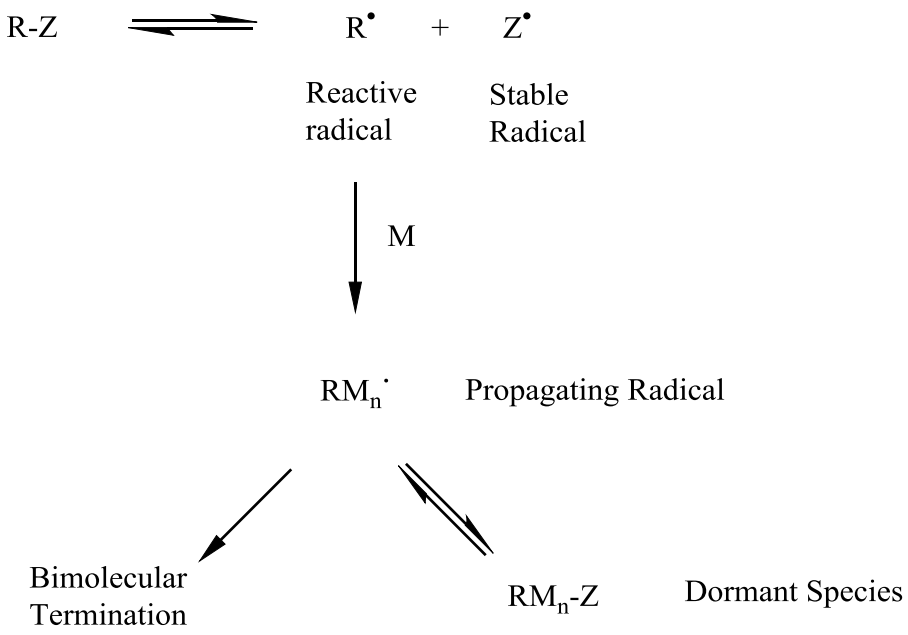

Figure 2.2. Reaction scheme for living radical polymerization.

2.1.3 Concentration of the Propagating Radical and Stable Radical

As expected, the concentration of the propagating radical and stable radical are equal at the start of the polymerization. Yet, there is a rapid and drastic change in the concentration[11]. Here, the propagating radical can react with the stable radical and itself, and any occurrence of self termination of the propagating radical will result in a relative increase of the stable radical. So as time develops, this stable radical increases, and the relative amount of propagating radical decreases, and the self termination becomes less favored. Overall, the concentration of the stable radical is about four orders of magnitude greater than the concentration of the propagating radical.

2.1.4 Concentration of the Dormant Species

The stable radical species serves as a "controlling agent" because it can sufficiently couple with the propagating radical to convert it to the dormant non-propagating species. The dormant species is in equilibrium with the propagating radical and equilibrium favors the dormant species by several orders of magnitude. The concentration of the propagating species is 10^{-7}-10^{-8} M, while the concentration of the dormant species is 10^{-1}-10^{-3} M (about six orders of magnitude difference)[1]. The overall result of the equilibrium between the dormant and propagating chain is suppression of bimolecular termination and controlled chain growth.

2.1.5 Types of Controlled Radical Polymerizations

Living radical systems, also referred to as controlled radical systems, were pioneered in the 1990's and have since branched off into three related approaches: atom transfer radical polymerization (ATRP), reversible addition/fragmentation chain transfer polymerization (RAFT), and nitroxide mediated polymerization (NMP)[12-16]. Figure 2.3 illustrates the trend in annual citation count for these controlled radical polymerizations techniques[17]. Table 2.1 summarizes the benefits and limitations of these techniques.

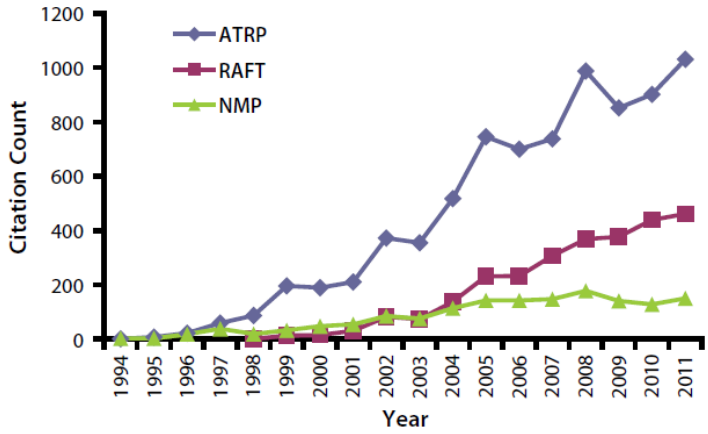

Figure 2.3 Scifinder search results as of 2011 for ATRP, RAFT, and NMP technologies.

Table 2.1 Primary benefits and limitations of ATRP, RAFT, and NMP.

	ATRP	RAFT	NMP
Primary Benefits	• Versatile • Ability to tailor catalyst to specific needs	• Versatile • No use of transition metals	• No use of transition metals • Low potential for odor and discoloration
Primary Limitations	• Use of transition metals • many variables affecting polymer characteristics	• High potential for odor and discoloration	• Least versatile

2.1.6 Poly(styrene)-b-Poly(hydroxystyrene) (PS-b-PHOST) via Nitroxide Mediated Polymerization

While other living radical techniques have greater popularity and more citations, nitroxide mediated polymerization was used in this study to synthesize PS-b-PHOST. While not as versatile toward acrylate systems, NMP has proven to be highly compatible with a range of functionalized styrene systems, hence it was an obvious candidate[13, 18]. Furthermore, NMP avoids transition metals that can contaminate the polymer samples and cause contamination problems with subsequent processing in clean room facilities. Also, NMP is noted for its simplicity: the polymerization is thermally initiated without the need for an external radical source. Purification involves simple precipitation and filtration due to the absence of a metal catalyst.

2.1.7 NMP Mechanism

The mechanism for nitroxide mediated polymerization is represented in Figure 2.4. Here, the thermally promoted homolysis of the nitroxide initiator generates the propagating radical and the stable nitroxide radical. Propagation proceeds by reaction with the monomer to produce the polymer chains. Reversible termination events between the nitroxide and the propagating radical serve to decrease the availability of the reactive radical species, thereby providing control over polymerization.

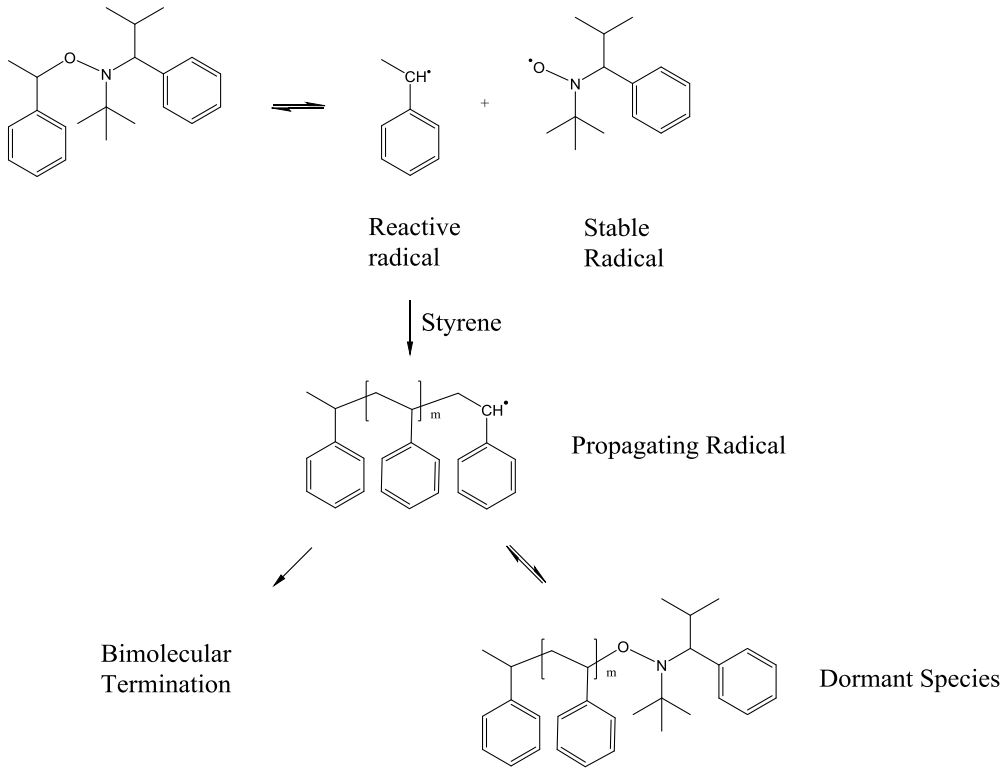

Figure 2.4. Overall mechanism for nitroxide mediated polymerization, illustrated with universal alkoxyamine initiator and styrene monomer.

Choosing the appropriate alkoxyamine is key to tuning the radical concentration and reactivity allowing controlled polymerization and low PDI. Initial NMP efforts relied on TEMPO as the mediating radical which had limited use within styrene based systems[19]. Recently, a universal nitroxide mediated initiator was demonstrated which allowed controlled polymerization of a wide variety of styrene systems, and also acrylate systems as well[20]. In this work, both TEMPO radical and the universal radical systems were investigated toward the polymerization of PS-b-PHOST (Figure 2.5). Such methods were used since they can provide for good molecular weight control and low PDI without the use of metallic reagents that can contaminate the polymer samples.

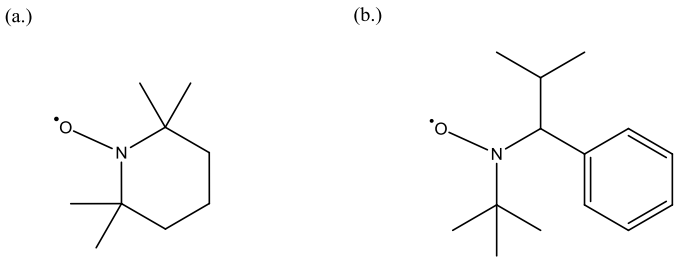

Figure 2.5 Stable nitroxide radicals useful in controlled living polymerizations (a.) TEMPO radical (2,2,6,6-tetramethylpiperidin-1-yl)oxidanyl, (b.) Universal NMP initiator (2,2,5-trimethyl-4-phenyl-3-azahexane-3-nitroxide).

2.1.8 Neutral Underlayer

When a BCP is confined to a thin film, the morphology is also critically dependent on the energetics at the block copolymer/substrate interface[21-23]. In order to form vertical lamellae, the underlayer must be approximately neutral with respect to its interactions with each block of the BCP. This avoids preferential wetting of either block with the substrate, a situation that results in lamellae oriented parallel to the substrate surface. Polymer mats, which are thin film cross-linked polymer networks, are commonly used as one method to control the interfacial interactions and wetting behavior of the BCP substrate. By adjusting the monomer composition and cross-link density, the chemical composition of the surface can be modified to be neutral with respect to each block of the BCP. Here, a series of random copolymers composed of styrene, acetoxystyrene, and glycidyl methacrylate were prepared via conventional radical polymerization. The relative molar ratios of styrene and hydroxystyrene were varied to tune the surface energy of the material, while incorporation of glycidyl methacrylate enabled cross-linking upon UV exposure. The surface energy of the underlayer was

evaluated with contact angle analysis. PS-b-PHOST was then spin coated and annealed on this neutral underlayer which resulted in vertical lamellar morphology (see Chapter 3 for processing details and discussion).

2.2 Experimental Section

2.2.1 Materials and Methods

All reagents were purchased from Sigma Aldrich or Acros Organics unless otherwise noted. Inhibitor was removed with a glass column containing neutral alumina oxide from the monomers immediately before polymerization. All other reagents were used as received. ^{1}H-NMR spectra were obtained using a Varian Mercury Vx 400 MHz spectrometer. All spectra were referenced to the residual solvent proton signal. Fourier transform infrared (FTIR) spectra from bulk samples (KBr pellet) were obtained using a Bruker Vertex 80v in transmission mode. Gel-permeation chromatography (GPC) analysis was carried out using a Waters 1515 isocratic pump coupled to a Waters 2489 UV detector with THF as the eluant. All GPC measurements were carried out at a flow rate of 0.3 mL/min and 35º C, and calibrated using narrow molecular weight polystyrene standards. Film thicknesses were measured using a Woollam M-2000V ellipsometer over a wavelength range of 350 nm to 1000 nm. Patterned samples were imaged using a Carl Zeiss Ultra60 SEM with 2 keV acceleration voltage.

2.2.2 Poly(acetoxystyrene) (PAS) Macro-initiator

A mixture of acetoxystyrene (2.30 g, 14.2 mmol, 200 equiv), universal NMP initiator (23 mg, 0.07 mmol, 1 equivalent), and nitroxide radical (2,2,5-trimethyl-4-phenyl-3-azahexane-3-nitroxide) (1mg, 0.004 mmol, 0.05 equiv) was added to a glass ampoule equipped with a magnetic stir bar (Figure 2.6)[20]. The reaction mixture was degassed through three freeze pump thaw cycles and sealed under vacuum. The mixture was warmed to room temperature, stirred for 10 min, and immersed into a pre-heated oil bath at 125 ˚C. After 12 hours, the reaction was quenched by quick immersion in liquid nitrogen. The viscous reaction mixture was dissolved in THF, precipitated in methanol at 0 ˚C, filtered, and dried under vacuum to yield a colorless powder. (0.43 g, 19% yield) M_n=8100 g/mol, PDI 1.18.

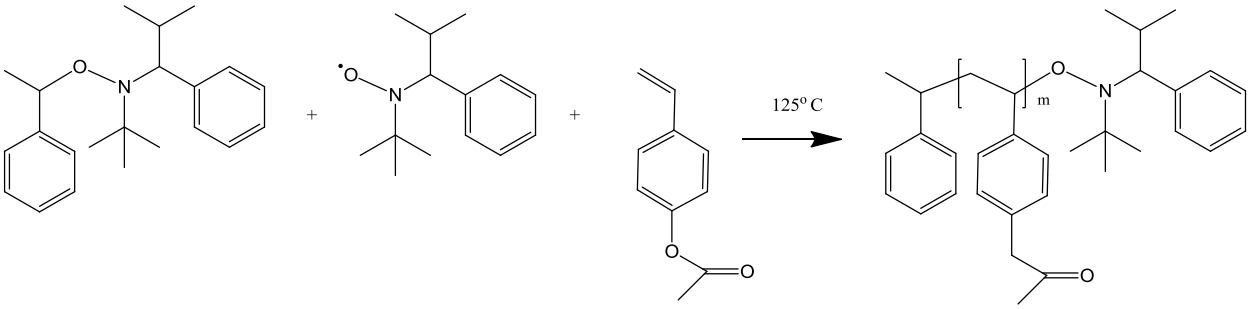

Figure 2.6 Nitroxide mediated polymerization of PAS macro-initiator.

2.2.3 Poly(styrene)-b-Poly(hydroxystyrene) (PS-b-PHOST)

A mixture of styrene (0.52 g, 5.0 mmol, 400 equiv), and PAS macro-initiator (0.10 g, 0.01 mmol, 1 equivalent) was added to a glass ampoule equipped with a magnetic stir bar (Figure 2.7)[20]. The reaction mixture was degassed through three freeze pump thaw cycles and sealed under vacuum. The mixture was warmed to room temperature, stirred for 10 min, and immersed in a pre-heated oil bath at 125 ˚C. After 12 hours, the reaction was quenched by quick immersion in liquid nitrogen. The viscous reaction mixture was dissolved in THF, precipitated in methanol at 0 ˚C, filtered, and dried under vacuum to yield a white powder. (0.13 g, 20% yield). PS-b-PAS (6800-b-8100g/mol), M_n=14900 g/mol , PDI=1.20.

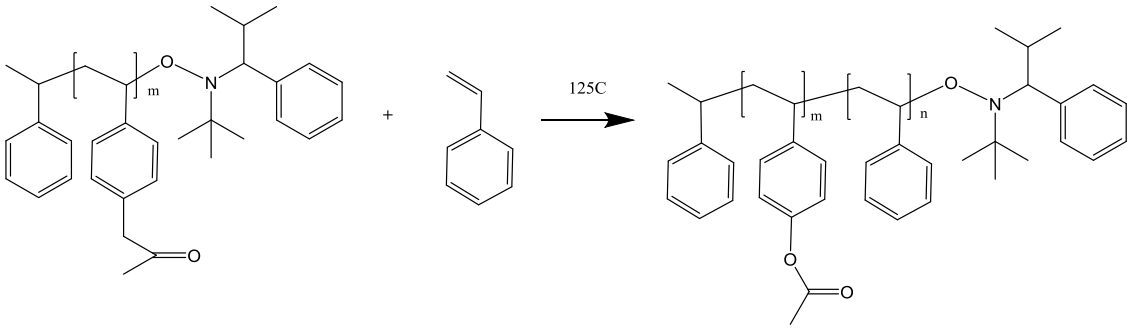

Figure 2.7 Nitroxide mediated polymerization of PS-b-PAS using PAS macro-initiator.

Removal of the acetyl protecting group from the PAS block was accomplished via hydrazinolysis, (with hydrazine hydrate in about 2:1 ratio by weight of the PAS block) (Figure 2.8) [24]. PS-b-PAS (6800-b- 8100g/mol) (0.13 g) was added to dioxane (1.3 mL) and hydrazine hydrate (0.14 g) and stirred for 6 hours under nitrogen. The resulting mixture was added to a large excess of 5% aqueous hydrochloric acid and stirred for

several hours. The PS-b-PHOST product was washed with deionized water and isolated by centrifugation, followed by drying under vacuum at room temperature overnight, providing PS-b-PHOST(6800-6000 g/mol) with M_n of 12800 g/mol assuming full deprotection, and PDI of 1.2. The polymer was characterized by NMR, and FT-IR analysis.

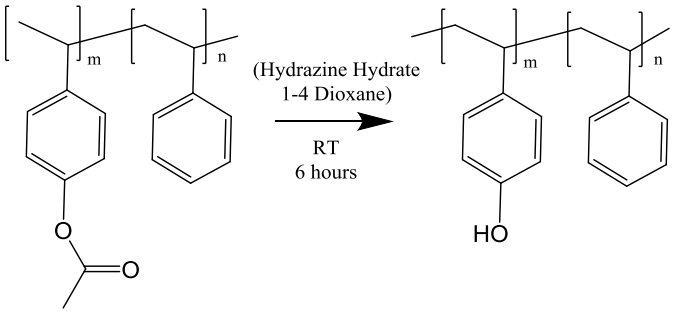

Figure 2.8 Deprotection of acetoxystyrene using hydrazinolysis.

2.2.4 Poly(styrene)-r-poly(hydroxystyrene)-r- poly(glycidylmethacrylate) (PS79-r-PHOST19-r-PGMEA5), Neutral Cross- linked Underlayer

A mixture of styrene (1.40 g, 13.4 mmol, 80 equiv), 4-acetoxystyrene (0.136 g, 0.84 mmol, 5 equiv), glycidyl methacrylate (0.358 g, 2.52 mmol, 15 equiv), and azobisisobutyronitrile (0.050 g, 0.30 mmol, 1.8 equiv) was added to a glass ampoule equipped with a magnetic stir bar (Figure 2.9). The reaction mixture was degassed through three freeze pump thaw cycles and sealed under vacuum. The mixture was warmed to room temperature, stirred for 10 min, and immersed in a pre-heated oil bath at

65 ºC. After 14 hours, the reaction was quenched by quick immersion in liquid nitrogen. The viscous reaction mixture was dissolved in THF, precipitated in methanol at 0 ºC, filtered, and dried under vacuum to yield a white powder (1.27 g, 64% yield). M_n=14900 g/mol, PDI=1.64. The molar composition of PS-r-PAS-r-PGMA was determined to be 65, 21, and 14 percent respectively via ^{1}H-NMR analysis. Finally, the acetoxystyrene was deprotected via hydrazinolysis. *^{1}H-NMR data used in calculating molar composition: ^{1}H NMR (300MHz, Acetone-d, ppm) δ 7.25-6.16 (aromatic region), 4.10-3.02 (COO-CH$_2$ on glycidyl functional group), 2.47-2.10 (acetoxy group).*

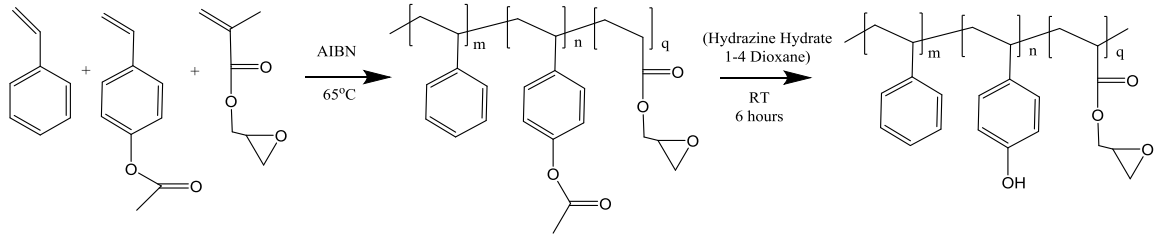

Figure 2.9. Synthesis of PS-r-PAS-r-PGMA using traditional radical polymerization with AIBN initiator followed by deprotection of acetoxystyrene using hydrazinolysis to yield PS-r-PHOST-r-PGMA.

Neutral cross-linked underlayer films were made by spin casting in PGMA with commercial TPS-N1 photoacid generator (5 wt% of polymer) followed by baking at 120º C for 2 min to remove the casting solvent, which resulted in 20 nm films as measured by spectroscopic ellipsometry. Films were cross linked via deep ultraviolet exposure (Oriel Instruments 500W Hg-Xe arc lamp with a 248 nm band-pass filter) followed by post

exposure bake at 120º C for 120 s and sonication for 10 min in PGMEA to remove uncross-linked polymer (normalized remaining thickness was 0.92).

2.3 Results and Discussion

2.3.1 Solution Polymerization Using TEMPO Initiator

Initial synthesis investigation of PS and PAS utilized solution polymerization with TEMPO initiator. Here, acetoxystyrene, a protected form of poly(hydroxystyrene), was used since phenols are known to interfere with radical based polymerization reactions. Solution polymerization was convenient because it allowed periodic extraction of aliquots from the reaction mixture. These aliquots were purified via precipitation and filtering and analyzed with GPC which allowed insight into the evolution of molecular weight over time.

Figure 2.10 and Figure 2.11 represents the PS and PAS molecular weight and PDI as a function of reaction time with reaction temperature at 125 ˚C. Here, the molecular weight increased rapidly and then plateaued, while the PDI continued to increase. This experiment provided clear insight into the optimal approach to achieve controlled molecular weight and low PDI. Since reasonable molecular weight and low PDI can be achieved at shorter reaction times, reaction time should be limited. Also, increasing the relative monomer to initiator ratio should also increase the reaction rate and reduce the required reaction time. Furthermore, bulk polymerization should also be used since it increases the monomer concentration and polymerization rate. However, it must be noted

that bulk polymerization prevents periodic sampling of aliquots due to the high viscosity of the bulk polymerization solution.

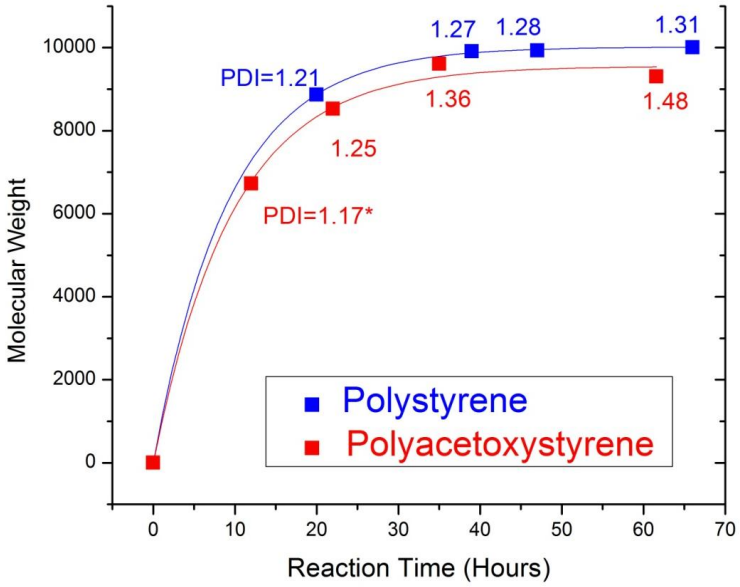

Figure 2.10 Number average molecular weight (g/mol) versus solution polymerization time for styrene (blue) and acetoxystyrene (red) using TEMPO initiator (polymerization temperature was 125 ˚C).

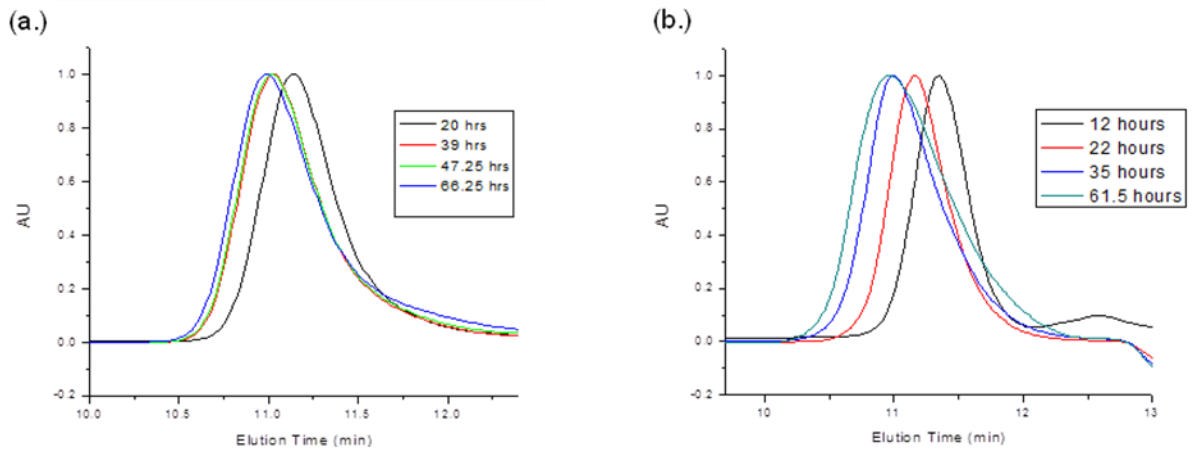

Figure 2.11 GPC traces for the solution polymerization using TEMPO initiator for (a.) styrene and (b.) acetoxystyrene with different reaction times (polymerization temperature was 125 ˚C).

Next, the living nature of poly(styrene) and poly(acetoxystyrene) was investigated by using these materials as macro-initiators to initiate the growth of the second polymer block. Here, the PS-TEMPO readily facilitated the continued growth of styrene polymer with high molecular weight and low PDI (Figure 2.12). However, PS-b-PAS synthesized with the PAS-TEMPO macro-initiator exhibited a higher PDI with a lower molecular weight tail observed on the GPC trace, which suggested premature termination of the growing polymer chains (Figure 2.13). Also, PAS-b-PS synthesized from the PAS-TEMPO macro-initiator exhibited a bimodal molecular weight distribution which suggested a considerable portion of the PAS-TEMPO failed to initiate polymerization (Figure 2.14). These results suggested PAS-TEMPO does not exhibit living polymerization, and other NMP initiators with improved compatibility with acetoxystyrene should be investigated.

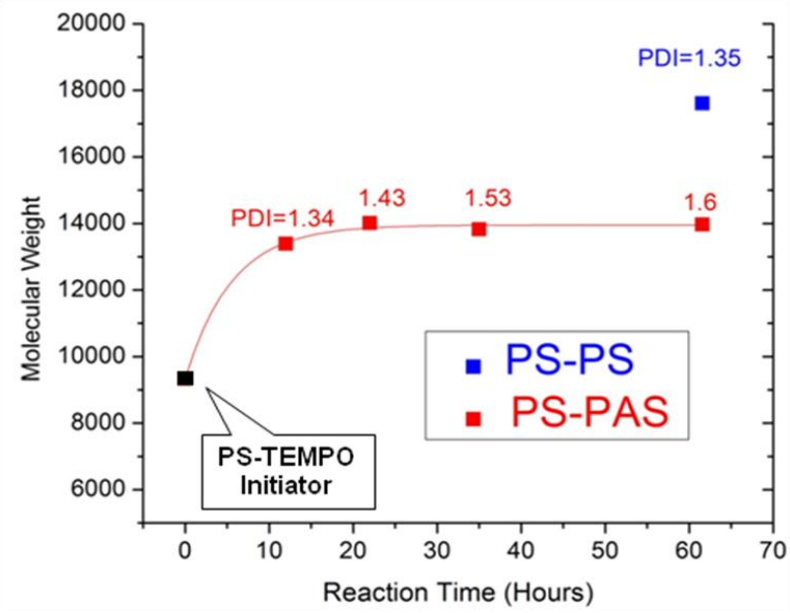

Figure 2.12 Number average molecular weight (g/mol) versus reaction time for solution polymerization of the second block of PS-b-PAS (red) and PS-b-PS (blue) using PS TEMPO macro-initiator (black) at 125 ˚C.

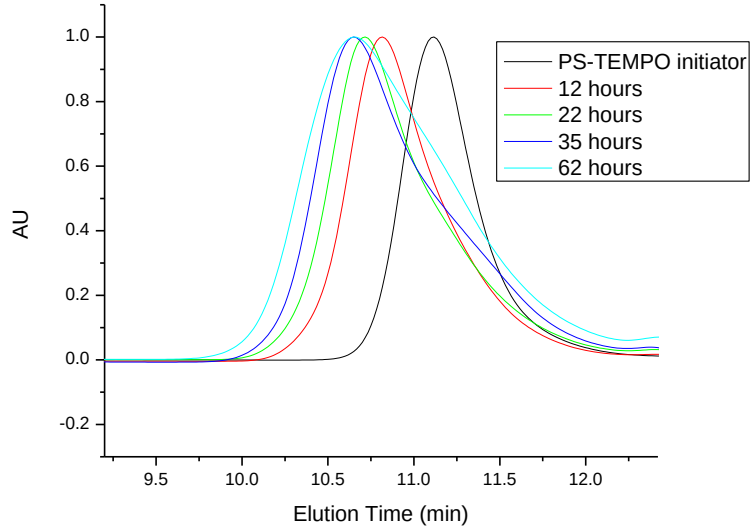

Figure 2.13 GPC traces for the solution polymerization (at 125 ˚C) of PS-b-PAS with different reaction times using PS-TEMPO macro-initiator.

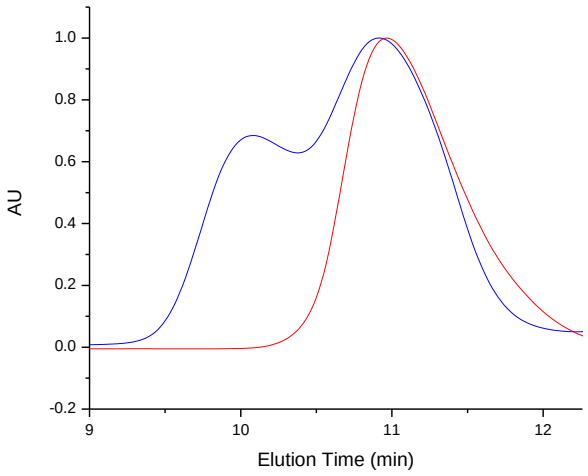

Figure 2.14 GPC traces of the solution polymerization (at 125 ˚C) of PAS-TEMPO macro-initiator (red), and PS-b-PAS(blue) using the PAS-TEMPO macro-initiator. The bimodal distribution of the PS-b-PAS trace suggested non-living polymerization.

2.3.2 Polymerization Using the Universal Nitroxide Initiator

To overcome the deficiencies associated with TEMPO, alternative nitroxide initiator structures were investigated. The most significant breakthrough in the design of improved nitroxides was the use of alicyclic nitroxides in previous studies by the Hawker group. Here, the presence of a hydrogen atom on one of the alpha carbons, which is traditionally associated with unstable nitroxide derivatives, seemed to have some bearing on the success of these materials[20]. In this work, the universal initiator, *N*-*tert*-butyl-*N*-(2-methyl-1-phenylpropyl)-*O*-(1-phenylethyl)hydroxylamine, was used to prepare PS-b-PHOST.

2.3.3 Poly(styrene)-b-Poly(acetoxystyrene) (PS-b-PAS) via the Universal Nitroxide Initiator

In order to synthesize PAS with targeted molecular weights and low PDI, bulk polymerization with high monomer to initiator ratio was used and reaction time was limited. Here, the rapid increase in molecular weight was followed by a plateau, which could be due to the increased viscosity of the reaction mix (Figure 2.15, Figure 2.16, and Table 2.2).

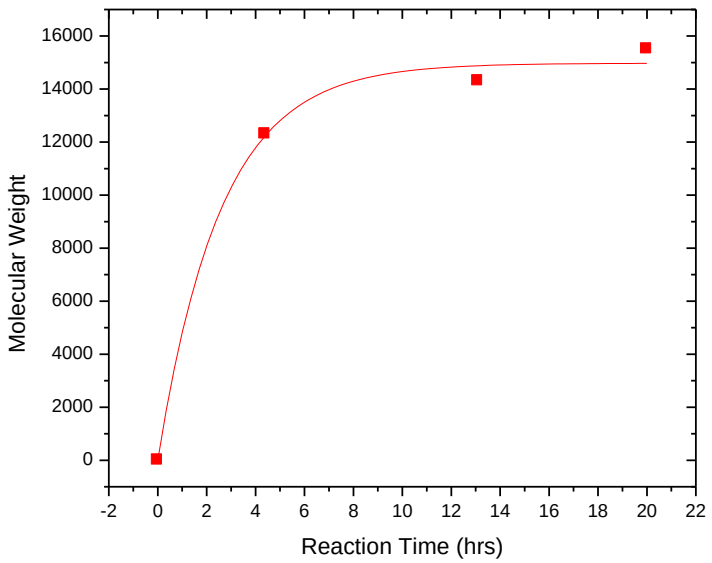

Figure 2.15 Number average molecular weight (g/mol) versus bulk polymerization time for acetoxystyrene (red) using universal nitroxide initiator (polymerization temperature was 125 ˚C).

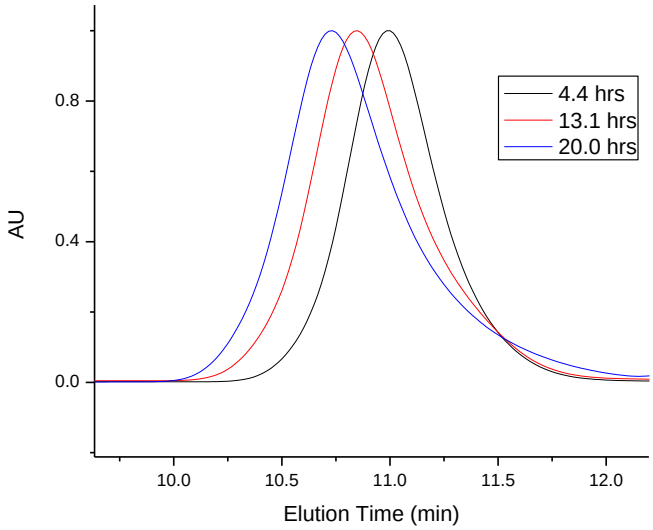

Figure 2.16 GPC traces for the bulk polymerization of acetoxystyrene using universal nitroxide initiator with different reaction times.

Table 2.2 The theoretical molecular weight, molecular weight as measured by GPC, and PDI for given polymerization time of acetoxystyrene using universal nitroxide initiator (polymerization temperature was 125 ˚C).

Monomer	Theoretical M_n (g/mol)	M_n (g/mol)	PDI	Reaction Time (hours)
Acetoxystyrene	32700	12300	1.20	4.4
Acetoxystyrene	32700	14300	1.27	13.1
Acetoxystyrene	32700	15500	1.36	20.0

The PAS macro initiator efficiently initiated growth of the polystyrene block.

The mono-modal molecular weight distribution and low polydispersity were indicative of

controlled living polymerization (Figure 2.17, Figure 2.18, and Table 2.3). The polymerization times for the second block were tailored to allow growth of the PS block with roughly equal volume fraction in relation to the first block.

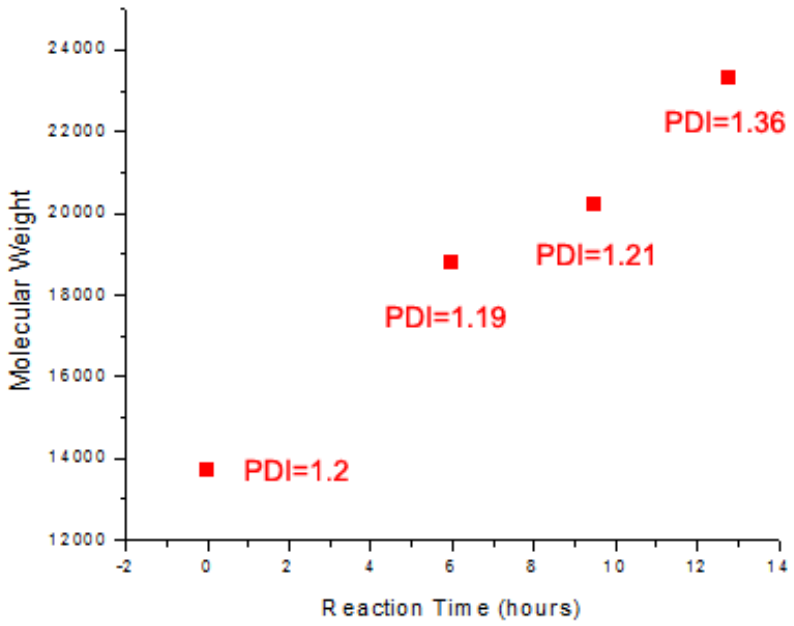

Figure 2.17 Number average molecular weight (g/mol) and PDI versus reaction time for bulk polymerization of the PS block of PAS-b-PS using universal nitroxide initiator with different reaction times (polymerization temperature was 125 ˚C).

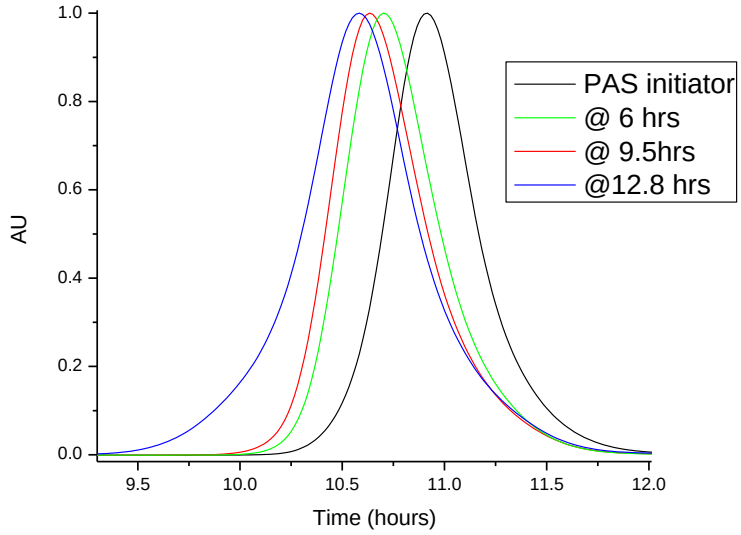

Figure 2.18 GPC traces for the bulk polymerization of PS-b-PAS with different reaction times using PAS macro-initiator (polymerization temperature was 125 ˚C).

Table 2.3 The molecular weight, degree of polymerization, and PDI of PAS-b-PS materials prepared with a series of reaction times for the PS block (polymerization temperature was 125 ˚C).

First Block: PAS		Second Block: PS		PAS-b-PS Block Copolymer	
M_n 1st Block (g/mol)	PDI 1st Block	M_n 2nd Block (g/mol)	Reaction Time For 2nd Block (hours)	M_n (Total) (g/mol)	PDI (total)
13700	1.21	6500	6	20200	1.21
13700	1.21	5100	9.5	18800	1.19
13700	1.21	9600	12.8	23300	1.36

2.3.4 Low Molecular Weight Poly(styrene)-b-Poly(acetoxystyrene) (PS-b-PAS)

Interest in block copolymer patterns with sub 20 nm pitch motivated the synthesis of low molecular weight PS-b-PAS. Synthesis of low molecular weight PAS macro-initiator followed similar conditions for the higher molecular material, except reaction temperature was decreased to 115 ˚C, and reaction time was limited to provide lower molecular weight material. The synthetic results of lower molecular weight PAS are represented in Figure 2.19 Inconsistent results of molecular weight in comparison with previous results in Figure 2.15 were attributed to differences in reaction time, temperature, and volume. Once the low molecular weight PAS was synthesized, this macro-initiator was used to grow the PS chain using similar conditions for the synthesis of the high molecular material, except the reaction time was limited to about 30 to 60 min to provide lower molecular material.

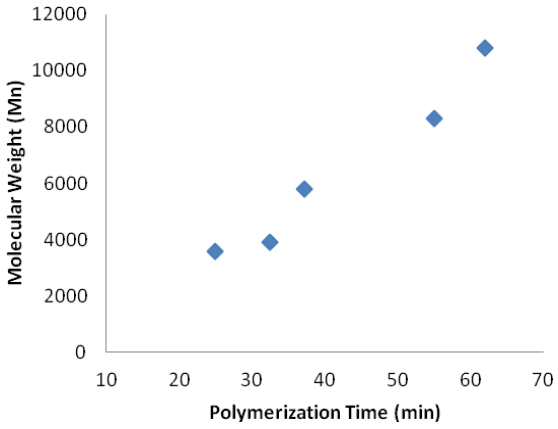

Figure 2.19 Number average molecular weight versus bulk polymerization time for acetoxystyrene using universal nitroxide initiator and short reaction times (polymerization temperature was 115 ˚C).

2.3.5 Deprotection Reaction of Poly(styrene)-b-Poly(acetoxystyrene) (PS-b-PAS)

Following synthesis of PS-b-PAS, the acetoxystyrene was deprotected using hydrazine hydrate. The polymer was characterized by ^{1}H-NMR, and FTIR analysis. Loss of the acetoxy peak at 2.25 ppm indicates complete deprotection of the acetoxy group (Figure 2.20). Loss of the carbonyl peak at 1757 cm^{-1} and appearance of the hydroxyl peak at 3350 cm^{-1} also indicate deprotection (Figure 2.21). See Appendix A for full spectroscopic analysis.

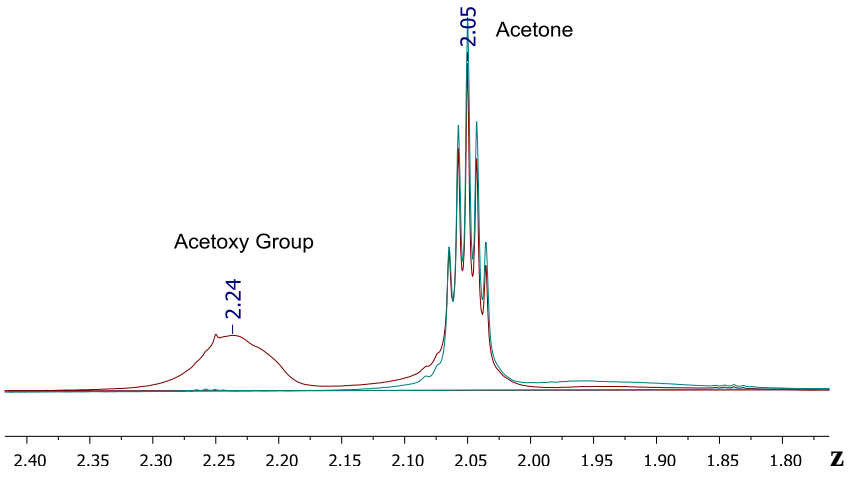

Figure 2.20 ^{1}H-NMR spectra of the deprotection of PS-b-PAS (red) providing PS-b-PHOST (blue).

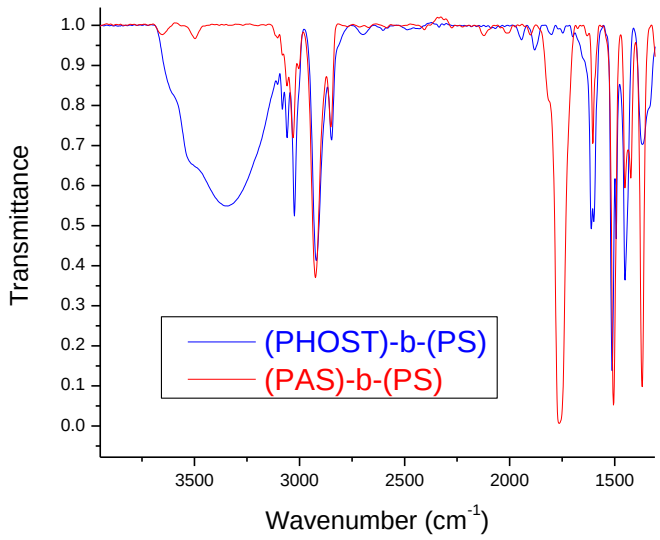

Figure 2.21 FTIR spectra of the deprotection of PS-b-PAS (red) providing PS-b-PHOST (blue).

2.3.6 Summary of the Synthetic Results of Poly(styrene)-b-poly(hydroxystyrene) (PS-b-PHOST)

A summary of PS-b-PHOST materials synthesized and phase separated in this study is represented in Table 2.4. Here, the a range of molecular weights were prepared which correspond to observed pitches ranging from 13-40 nm (See Chapter 3). The low PDI indicated controlled polymerization of these materials. The volume fraction of these materials (estimated from the density and molecular weight of each block) was between 40 and 60 percent PS, and corresponded to lamellar morphology when annealed as a thin film (See Chapter 3 for full discussion).

Table 2.4 Summary of the molecular weight, degree of polymerization, and PDI of PS-b-PHOST materials synthesized and phase separated in this study.

PHOST (M_n) (g/mol)	PS (M_n) (g/mol)	M_n Total (g/mol)	PHOST (N)	PS (N)	N total	PDI total	Estimated Volume fraction of PS
14300	14900	29200	119	143	262	1.39	0.44
10500	7400	17900	88	72	160	1.38	0.54
6840	8528	15368	57	82	139	1.24	0.60
4679	3910	8589	39	38	77	1.23	0.50

2.3.7 Synthesis and Characterization of Poly(styrene)-r-poly(hydroxystyrene)-r-poly(glycidyl methacrylate) (PS-r-PHOST-r-PGMA) Neutral Cross-linked Underlayer

A series of random copolymer materials, poly(styrene)-r-poly(hydroxystyrene)-r-poly(glycidylmethacrylate) or PS-r-PHOST-r-PGMA, were prepared by traditional radical polymerization for use as neutral underlayer substrates (Table 2.5). The relative volume fraction was determined via ^{1}H-NMR analysis. This material utilized glycidyl methacrylate to cross link the material after spin coating to form an insoluble cross-linked mat. GPC analysis confirmed this material was not cross-linked during the deprotection step (Figure 2.22). The relative neutrality of these materials in thin films was determined by contact angle analysis. Here, the contact angle of PS65-r-PHOST21-r-PGMA14 is approximately the average between PHOST and PS suggesting this material is neutral toward the PS-b-PHOST block copolymer (Figure 2.23).

Table 2.5 The molar feed ratio, polymer composition, molecular weight, and PDI of PS-r-PHOST-r-PGMA materials prepared in this investigation.

Molar Feed Ratio			Polymer Composition			% Yield	MW (g/mol) and PDI Before Deprotection
S	AS	GMA	S	AS	GMA		
80	5	15	65	21	14	64	14900 (1.54)
60	20	20	55	29	16	71	8200 (1.6)
52	28	20	51	37	12	79	11700 (1.7)
44	36	20	50	43	07	78	11000 (1.5)

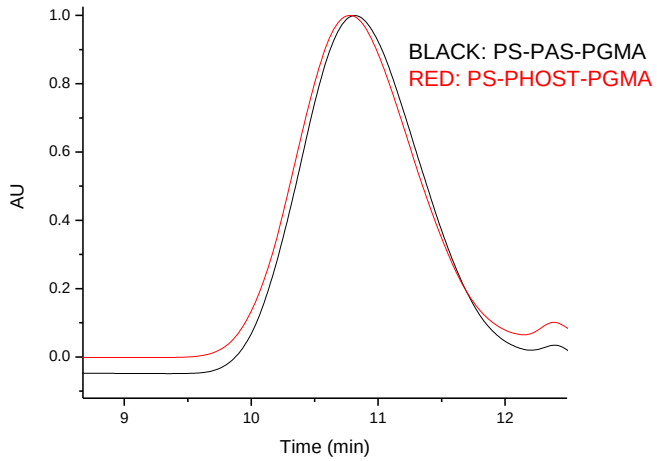

Figure 2.22 GPC analysis of (PS-r-PAS-r-PGMA) (black) and (PS-r-PHOST-r-PGMA) (red) illustrates no significant cross-linking occurred during the deprotection reaction.

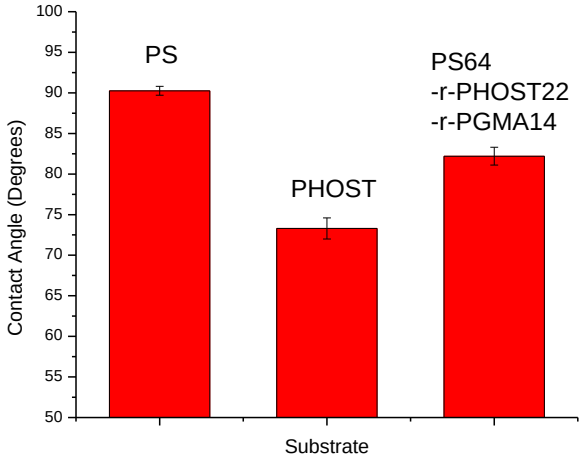

Figure 2.23 Measured contact angle of PS, PHOST, and (PS64-r-PHOST22-r-PGMA14) thin films.

2.4 Conclusions

Targeted polymer molecular weights with low polydispersities are required for directed self assembly patterning since the pitch and morphology of the BCP is dependent on the characteristic length scale (or degree of polymerization) of each block on the polymer chain. In this work, nitroxide mediated polymerization (NMP) techniques were utilized to produce the diblock copolymers. NMP provided good molecular weight control and low PDI without the use of metallic reagents that can contaminate the polymer samples and cause contamination problems in subsequent processing of block copolymers in clean room facilities. Block copolymers synthesized with the universal nitroxide initiator exhibited improved PDI in comparison with block copolymers

synthesized with the traditional TEMPO initiator. Here, PS-b-PHOST polymers were synthesized with a range of molecular weights (M_n=8500-30000 g/mol) with low PDI approaching 1.2. Also, a series of random copolymers were synthesized for use as neutral underlayer substrates for the PS-b-PHOST system.

2.5 References

1. Odian, G., *Principles of Polymerization*. John Wiley and Sons, Inc.: Hoboken, New Jersey, 2004.

2. Matsushita, Y.; Mori, K.; Saguchi, R.; Nakao, Y.; Noda, I.; Nagasawa, M. *Macromolecules* **1990,** 23, (19), 4313-4316.

3. Lynd, N. A.; Meuler, A. J.; Hillmyer, M. A. *Prog Polym Sci* **2008,** 33, (9), 875-893.

4. Matsushita, Y.; Noro, A.; Iinuma, M.; Suzuki, J.; Ohtani, H.; Takano, A. *Macromolecules* **2003,** 36, (21), 8074-8077.

5. Noro, A.; Okuda, M.; Odamaki, F.; Kawaguchi, D.; Torikai, N.; Takano, A.; Matsushita, Y. *Macromolecules* **2006,** 39, (22), 7654-7661.

6. Lynd, N. A.; Hillmyer, M. A. *Macromolecules* **2005,** 38, (21), 8803-8810.

7. Georges, M. K.; Veregin, R. P. N.; Kazmaier, P. M.; Hamer, G. K. *Macromolecules* **1993,** 26, (11), 2987-2988.

8. Stevens, M., *Polymer Chemistry*. Oxford University Press: New York, New York, 1999; p 551.

9. Darling, T. R.; Davis, T. P.; Fryd, M.; Gridnev, A. A.; Haddleton, D. M.; Ittel, S. D.; Matheson, R. R.; Moad, G.; Rizzardo, E. *J Polym Sci Pol Chem* **2000,** 38, (10), 1706-1708.

10. Darling, S. B.; Yufa, N. A.; Cisse, A. L.; Bader, S. D.; Sibener, S. J. *Adv Mater* **2005,** 17, (20), 2446.

11. Greszta, D.; Matyjaszewski, K. *Macromolecules* **1996,** 29, (24), 7661-7670.

12. Matyjaszewski, K.; Xia, J. H. *Chem Rev* **2001,** 101, (9), 2921-2990.

13. Hawker, C. J.; Bosman, A. W.; Harth, E. *Chem Rev* **2001,** 101, (12), 3661-3688.

14. Moad, G.; Rizzardo, E.; Thang, S. H. *Accounts Chem Res* **2008,** 41, (9), 1133-1142.

15. Chiefari, J.; Chong, Y. K.; Ercole, F.; Krstina, J.; Jeffery, J.; Le, T. P. T.; Mayadunne, R. T. A.; Meijs, G. F.; Moad, C. L.; Moad, G.; Rizzardo, E.; Thang, S. H. *Macromolecules* **1998,** 31, (16), 5559-5562.

16. Braunecker, W. A.; Matyjaszewski, K. *Prog Polym Sci* **2007,** 32, (1), 93-146.

17. Patel, K. *Material Matters:* **2010,** 5, (1), 1-32.

18. Barclay, G. G.; Hawker, C. J.; Ito, H.; Orellana, A.; Malenfant, P. R. L.; Sinta, R. F. *Macromolecules* **1998,** 31, (4), 1024-1031.

19. Hawker, C. J.; Barclay, G. G.; Orellana, A.; Dao, J.; Devonport, W. *Macromolecules* **1996,** 29, (16), 5245-5254.

20. Benoit, D.; Chaplinski, V.; Braslau, R.; Hawker, C. J. *J Am Chem Soc* **1999,** 121, (16), 3904-3920.

21. In, I.; La, Y. H.; Park, S. M.; Nealey, P. F.; Gopalan, P. *Langmuir* **2006,** 22, (18), 7855-7860.

22. Edwards, E. W.; Stoykovich, M. P.; Solak, H. H.; Nealey, P. F. *Macromolecules* **2006,** 39, (10), 3598-3607.

23. Han, E.; Stuen, K. O.; La, Y. H.; Nealey, P. F.; Gopalan, P. *Macromolecules* **2008,** 41, (23), 9090-9097.

24. Chen, X. Y.; Jankova, K.; Kops, J.; Batsberg, W. *J Polym Sci Pol Chem* **1999,** 37, (5), 627-633.

CHAPTER 3

PS-b-PHOST AS A HIGH χ BLOCK COPOLYMER FOR HIGH RESOLUTION DIRECTED SELF-ASSEMBLY PATTERNING

Directed self assembly (DSA) of block copolymers (BCP) could enable high resolution secondary patterning via pitch multiplication from lower resolution primary lithographic patterns. For example, DSA could enable dense feature production with pitch less than 15 nm via alignment from primary patterns generated using 193 nm exposure tools. According to theory, microphase separation of block copolymers can only occur when the critical condition that χN>10.5 is met, where χ is the Flory Huggins interaction parameter and N is the total degree of polymerization for the block copolymer. In order to generate patterns with smaller pitch, the degree of polymerization must be decreased thereby lowering the characteristic length scale for the polymer. In order to maintain the χN>10.5 relationship which allows phase separation, the decrease in degree of polymerization must be balanced by an increase in χ. Current materials, such as poly(styrene)-b-poly(methyl methacrylate), PS-b-PMMA, exhibit a relatively low χ value of 0.04, which limits the practical DSA pitch to approximately 20 nm. In this paper, we investigate alternative materials, namely poly(styrene)-b-poly(hydroxystyrene) (PS-b-PHOST), which exhibits high χ via hydrogen bonding interactions, enabling phase separation of dense patterns with improved resolution. Here, PS-b-PHOST was synthesized with targeted molecular weight and low PDI via nitroxide mediated polymerization. Also, the random copolymer poly(styrene)-r-poly(hydroxystyrene)-r-

poly(glycidyl methacrylate), PS-r-PHOST-r-PGMA, was prepared via radical polymerization as a neutral underlayer substrate. High resolution PS-b-PHOST fingerprint lamellar patterns with 13 nm pitch were prepared using ethyl acetate solvent annealing. Graphoepitaxy with SU-8 primary patterns was used to align PS-b-PHOST secondary patterns with 18 nm pitch. This work shows styrene based block copolymer systems with hydrogen bonding functionality, such as PS-b-PHOST, are a promising alternative to PS-b-PMMA for sub 20 nm pitch DSA patterning applications.

3.1 Introduction

Moore's law, the primary driving force of the semiconductor industry, states that the number of transistors on a chip will approximately double every two years. The key enabler of this trend is the printing of features at continuously smaller dimensions. Next generation lithography techniques, including double patterning and EUV, could facilitate the patterning of dense lines space features with pitch of 20 nm and below[1]. However, issues with EUV, including efficiency and cost motivate investigation into alternative techniques[2]. Other various patterning options, such as multiple patterning (e.g. double patterning, triple patterning, etc.), generally add significant complexity and cost to the lithographic process[3]. Alternatively, directed self assembly of block copolymers could allow secondary patterns with pitch below 20 nm via pitch multiplication of low resolution primary patterns[4, 5]. For example, DSA could be used to print 15 nm features using guiding patterns of relaxed pitch fabricated from 193 immersion techniques.

The pitch of such lamellar patterns in the strong segregation regime is proportional to the statistical segment length (a), Flory Huggins interaction parameter (χ), and the degree of polymerization (N) as shown in Equation 1.5[6-8]. Hence, lowering the degree of polymerization of the block copolymer directly facilitates high resolution BCP patterning. However, according to theory, microphase separation of lamellae forming block copolymers can only occur when the critical thermodynamic condition of χN>10.5 is met, where χ is the Flory Huggins interaction parameter and N is the total degree of polymerization for the block copolymer (Equation 2)[9-11]. In order to maintain the χN>10.5 relationship which allows phase separation, the decrease in degree of polymerization must be balanced by an increase in χ.

$$D \sim a\chi^{1/6}N^{2/3} \quad (1)$$

$$\chi N > 10.5 \quad (2)$$

The goal lithographically is to utilize the natural tendency of block copolymers to phase separate, forming aligned self-assembled BCP patterns on lithographically made guiding patterns. This process, which allows pitch reduction of the primary pattern, is commonly referred to as directed self assembly (DSA)[12, 13]. Currently the most widely studied block copolymer (BCP) for DSA is poly(styrene)-block-poly(methylmethacrylate) or PS-b-PMMA. PS-b-PMMA possess an extremely modest χ value of approximately 0.04, which translates into a minimum practical DSA pitch for such materials on the order of 20 nm[14]. If χ could be increased by an order of magnitude,

the attainable pitch would extend beyond 10 nm. Production of diblock copolymers with higher χ values can be achieved by incorporating polymer blocks that have stronger interactions between monomers of the same type and which have interactions that are orthogonal in nature to the types of interaction between monomers of the second block type. One such example is poly(styrene)-b-poly(hydroxystyrene) (PS-b-PHOST) in which the PHOST block exhibits hydrogen bonding interactions in conjunction with the PS block that interacts primarily though quadrupolar interactions (Figure 3.1). The goal in this work has been to explore this high χ polymer PS-b-PHOST and the associated processes required to achieve DSA using this materials in order to achieve higher resolution pitch.

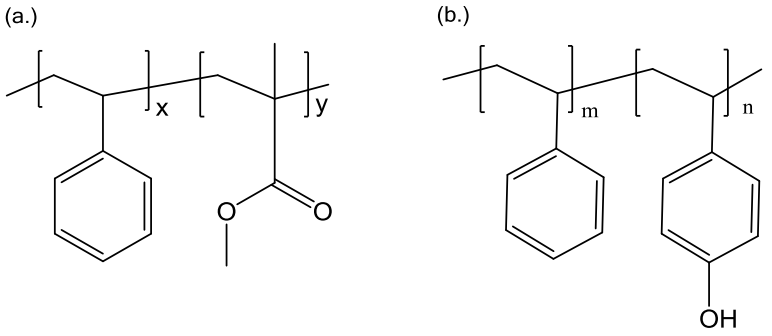

Figure 3.1 (a.) poly(styrene)-b-poly(methylmethacrylate) or PS-b-PMMA; (b.) poly(styrene)-b-poly(hydroxystyrene) or PS-b-PHOST.

The χ interaction parameter of PS-b-PHOST can be predicted from solubility parameters using a method developed by Hildebrand and Scott[15]. This approach uses Equation 3, where V_o is the average monomer volume, R is the gas constant, and T is

temperature in Kelvin. The solubility parameter δ is determined experimentally and is related to the cohesive energy density of the material. Utilizing δ_{PHOST} of 24.6 $MPa^{1/2}$, δ_{PS} of 18.5 $MPa^{1/2}$, and V_o of 99.1 cm^3/mol, this approach provides $\chi_{PS\text{-}PHOST}$ of 1.46 (compared with $\chi_{PS\text{-}PMMA}$ of 0.04) [16, 17]. This approach assumes species interact mainly by dispersion forces, and ignores the highly polar and hydrogen bonding interactions of PHOST, hence these results are only qualitative in value. More importantly, experimental predictions suggest $\chi_{PS\text{-}PHOST}$ is at least an order of magnitude greater than PS-b-PMMA, thus making it attractive for fabricating nano-scale patterns below 10 nm[18].

$$\chi = \frac{V_0}{RT}\left(\delta_{PS} - \delta_{PHOST}\right)^2 \tag{3}$$

Thin film lamellar morphologies produced from block copolymer microphase separation which are oriented perpendicular to a substrate surface are of particular interest to semiconductor device manufacturing. Such morphologies allow formation of dense line-space patterns that can be transferred into the substrate through processes such as plasma etching. The equilibrium morphology of a diblock BCP pattern is primarily governed by the volume fraction of the two blocks, where 50:50 volume fraction of blocks provides lamellar domains[11]. Because the morphology is integrally dependent on volume fraction, polymerization techniques with precise control of molecular weight and low polydispersities (as commonly characterized by the polydispersity index, i.e. PDI) are required. Controlled nitroxide mediated polymerization techniques were utilized to produce the diblock copolymers reported here[19-23]. Such methods were used since they can provide for good molecular weight control and low PDI without the use of metallic

reagents that can contaminate the polymer samples and cause contamination problems in subsequent processing of block copolymers in clean room facilities.

Additionally, the morphology is critically dependent on the chemical potential at the block copolymer/substrate interface. In order to form vertical lamellae, the underlayer must be approximately neutral with respect to its interactions with each block of the BCP. This avoids preferential wetting of either block with the substrate, a situation that results in lamellae oriented parallel to the substrate surface. Polymer mats, which are thin film cross-linked polymer networks, are used in this study to control the interfacial interactions and wetting behavior of the BCP substrate[24]. By adjusting the monomer composition and cross-link density, the chemical composition of the surface can be modified to be neutral with respect to each block of the BCP[25, 26]. In this work, the neutral cross-linked random copolymer substrate poly(styrene)-r-poly(hydroxystyrene)-r-poly(glycidyl methacrylate (PS-r-PHOST-r-PGMA) is utilized as the neutral underlayer for BCP phase separation.

The goal in this work has been to explore the high χ polymer PS-b-PHOST and the associated processes required to achieve DSA of this materials in order to achieve higher resolution pitch. The process of PS-b-PHOST phase separation is summarized in Figure 3.2. Here, the neutral underlayer is first spin coated onto the silicon substrate and cross-linked via UV exposure. The PS-b-PHOST is then spin coated and annealed (either thermally or with solvent annealing) resulting in phase separated features. While thermal annealing is generally utilized due to its simplicity and facile integration with industrial semiconductor processing, PHOST exhibits a high glass transition temperature (180 ˚C) and low decomposition temperature (200 ˚C) limiting the processing window and

efficiency of this approach. Alternatively solvent vapor annealing is utilized to provide chain mobility resulting in phase separated structures with annealing time much less than 10 hours[27-29]. Phase separation of low molecular weight PS-b-PHOST via ethyl acetate solvent annealing provides thin film vertically oriented lamellae with 13 nm pitch, which are among the smallest BCP thin film lamellar patterns to date.

Also, we demonstrate the directed self assembly of lamellar patterns via graphoepitaxy (Figure 3.3). Here, lithographically patterned SU-8 lines on the neutral underlayer provide guiding walls for physical alignment. The BCP is spin coated and solvent annealed on these substrates resulting in directed self assembly of PS-b-PHOST with 18 nm pitch within the trench.

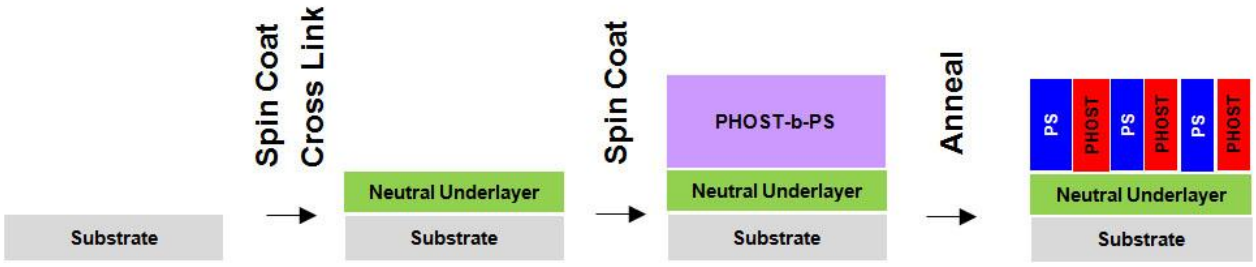

Figure 3.2. Phase separation process flow consisting of spin coating and cross-linking the neutral underlayer PS-r-PHOST-r-PGMA, spin coating of PS-b-PHOST, and solvent annealing to provide lamellar fingerprint patterns.

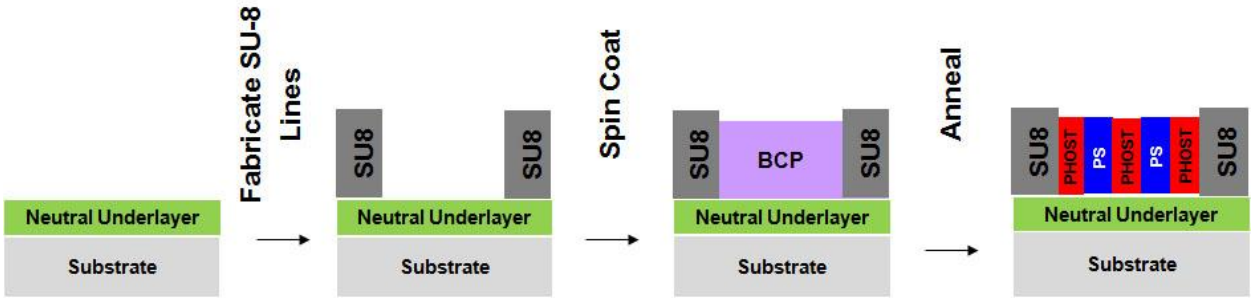

Figure 3.3 Graphoepitaxy process flow consisting of fabrication of SU-8 guiding lines on neutral underlayer PS-r-PHOST-r-PGMA, spin coating of PS-b-PHOST, and solvent annealing to provide aligned lamellar patterns.

3.2 Experimental Section

3.2.1 Materials

All reagents were purchased from Sigma Aldrich or Acros Organics unless otherwise noted. Inhibitor was removed from the monomers with a glass column containing neutral alumina oxide immediately before polymerization. All other reagents were used as received. ^{1}H-NMR spectra were obtained using a Varian Mercury Vx 400 MHz spectrometer. All spectra were referenced to the residual solvent proton signal. Fourier transform infrared (FTIR) spectra from bulk samples (KBr pellet) were obtained using a Bruker Vertex 80v in transmission mode. Gel-permeation chromatography (GPC) analysis was carried out using a Waters 1515 isocratic pump coupled to a Waters 2489 UV detector with THF as the eluant. All GPC measurements were carried out at a flow rate of 0.3 mL/min and 35 ºC, and calibrated using narrow molecular weight polystyrene standards. Film thicknesses were measured using a Woollam M-2000V

ellipsometer over a wavelength range of 350 nm to 1000 nm. Patterned samples were imaged using a Carl Zeiss Ultra60 SEM with 2 keV acceleration voltage.

3.2.2 Poly(styrene)-b-poly(hydroxystyrene) (PS-b-PHOST) Block Copolymer

In this work, nitroxide mediated polymerization was used to prepare PS-b-PHOST with controlled molecular weights and low PDI. See Chapter 2 for full discussion of synthesis and characterization methods.

3.2.3 Neutral Cross-linked Underlayer, (PS79-r-PHOST19-r-PGMEA5)

In this work, the neutral cross linked random copolymer substrate (poly(styrene)-r-poly(hydroxystyrene)-r-poly(glycidyl methacrylate) (PS-r-PHOST-r-PGMA) was synthesized via radical polymerization with the thermal initiator azoisobutyronitrile (AIBN). See Chapter 2 for full discussion of synthesis and characterization methods.

Neutral cross-linked underlayer films were made by spin casting in PGMA with commercial TPS-N1 photoacid generator (5 wt% of polymer) followed by baking at 120 ºC for 2 min to remove the casting solvent, which resulted in 20 nm films as measured by spectroscopic ellipsometry. Films were cross-linked via deep ultraviolet exposure (Oriel Instruments 500W Hg-Xe arc lamp with a 248 nm band-pass filter) followed by post exposure bake at 120 ºC for 120 s and sonication for 10 min in PGMEA to remove uncross-linked polymer (normalized remaining thickness was 0.92).

3.2.4 Poly(styrene)-b-poly(hydroxystyrene) (PS-b-PHOST) Fingerprint Patterns by Solvent Annealing

Solutions of 1-3 wt% PS-b-PHOST in PGMEA were spin cast on neutral underlayers using a poly(tetrafluoroethylene) (PTFE) filter (0.2 μm pore size), and baked at 110 °C for 2 min to remove casting solvent. BCP films were solvent annealed in sealed flasks with 0.4 mL dry ethyl acetate liquid added to each 250 mL flasks. Sealed flasks were purged with nitrogen before and after annealing to remove any excess water. Anneal time was varied according to the polymer molecular weight and film thickness.

3.2.5 Graphoepitaxy with SU-8

Graphoepitaxy of PS-b-PHOST was performed using 100 nm tall SU-8 guiding lines on neutral underlayer substrates. The SU-8 (Microchem) patterns for graphoepitaxy were exposed using a JEOL JBX-9300FS electron-beam lithography system with a 100keV acceleration voltage, 2 nA current, 20 uC/cm^2 exposure dose, and 10 nm single-pixel shot pitch. SU-8 processing included 95º C post apply bake (PAB) for 60 s, 95 ºC post exposure bake (PEB) for 90 s, and soak in SU-8 developer solution and isopropyl alcohol for 60 s and 20 s respectively. Solutions of 1-3 wt% PS-b-PHOST in PGMEA were spin cast on neutral underlayers with patterned SU-8 lines using a poly(tetrafluoroethylene) (PTFE) filter (0.2 μm pore size), and baked at 110 °C for 2 min to remove casting solvent. Samples were solvent annealed in nitrogen purged sealed containers with 0.4 mL dry ethyl acetate added per 250 mL flask. The effect of water on

phase separation and alignment was investigated by adding known amounts of water to the annealing flasks.

3.2.6 Thin Film Characterization

Film thicknesses were measured using a Woollam M-2000V ellipsometer over a wavelength range of 350 nm to 1000 nm. Contact angle goniometry was conducted using a VCA 2500-XE contact angle system with 1 μl drop size. Patterned samples were imaged using a Carl Zeiss Ultra60 SEM with 2 keV acceleration voltage. Dimensions of fingerprint patterns were determined from SEM analysis by averaging from 5 different areas with an inspection length of about 400 nm. Dimensions were verified by 2D fast Fourier transform analysis (Gwyddion 2.26 data visualization and analysis tool). Here, the SEM images were cropped to remove the data label, then 2D FFT filtered to remove long range artifacts due to charging from the SEM exposure. The resulting SEM image was processed by fast Fourier transform (FFT) analysis. The pitch was determined by taking a cut line through the FFT and measuring the distance from the center to the area of high intensity.

3.3 Results and Discussion

3.3.1 Polymerization of Poly(styrene)-b-poly(hydroxystyrene) (PS-b-PHOST)

PS-b-PHOST was prepared by nitroxide mediated polymerization of PS-b-PAS followed by deprotection of the acetoxystyrene. Here, a thermally labile alkoxyamine initiator was used which showed improved control of molecular weight and PDI of styrenic derivatives in comparison with the commonly used TEMPO initiator[19]. Also, acetoxystyrene has a 50% higher propagation rate coefficient than styrene, hence additional nitroxide radical was added to control the rate providing PAS with low PDI[30]. Initial attempts to use the PS macro-initiator to grow the PAS block were unsuccessful. GPC analysis of the material after polymerization of the second block showed a low molecular weight shoulder. The nature of the shoulder, whether unreacted polystyrene or early terminated PS-b-PAS, is unknown. The reverse strategy using poly(acetoxystyrene) to initiate the growth of the polystyrene block proved successful, providing PS-b-PAS with controlled molecular weight and low PDI (See Chapter 2). To prepare materials with targeted molecular weight and low PDI, reaction times were limited and relatively high monomer to initiator ratios were used. This general procedure allowed preparation of a large compositional range of materials (M_n=8500-30000 g/mol, PDI=1.2-1.4) (Table 3.1).

Table 3.1 The molecular weight (g/mol), degree of polymerization, and PDI of PS-b-PHOST materials prepared in this investigation. Also shown is the observed pitch for each associated molecular weight.

PHOST (M_n)	PHOST (N)	PS (M_n)	PS (N)	Mw Total	N total	PDI total	Volume % PS	Morphology	Pitch
14300	119	14900	143	29200	262	1.39	0.44	Lamellae	47
10500	88	7400	72	17900	160	1.38	0.54	Lamellae	32
6840	57	8528	82	15368	139	1.24	0.41	Lamellae	18
4679	39	3910	38	8589	77	1.23	0.50	Lamellae	13

3.3.2 Neutral Underlayer, Poly(styrene)-r-poly(hydroxystyrene)-r-poly(glycidyl methacrylate) (PS-r-PHOST-r-PGMA)

A series of random copolymer materials (PS-r-PHOST-r-PGMA) was prepared by radical polymerization for potential neutral underlayer substrates (See Chapter 2). This material utilized glycidyl methacrylate to cross link the material after spin coating to form an insoluble cross-linked mat. Here, the random copolymer PS65-r-PHOST21-r-PGMA14 was used, with tailored composition to provide a neutral underlayer for the block copolymer. The neutrality of this underlayer was verified by contact angle goniometry. This underlayer provided a contact angle of 82.2±1.1 which is an approximate average of the contact angle for PS (90±0.5) and PHOST(73.0±1.3).

3.3.3 Anneal Processes Associated with Phase Separation

Initial investigation of the phase separation behavior of PS-b-PHOST utilized thermal annealing (Figure 3.4). Samples were annealed for 7 days under N_2 atmosphere at 190 ˚C, a temperature above the glass transition temperature of PHOST (180 ˚C). Higher anneal temperature was not applied to prevent polymer degradation[31]. While this approach provided phase separated PS-b-PHOST lamellar patterns, the long anneal time associated with low annealing temperature motivated the investigation of alternative annealing methods.

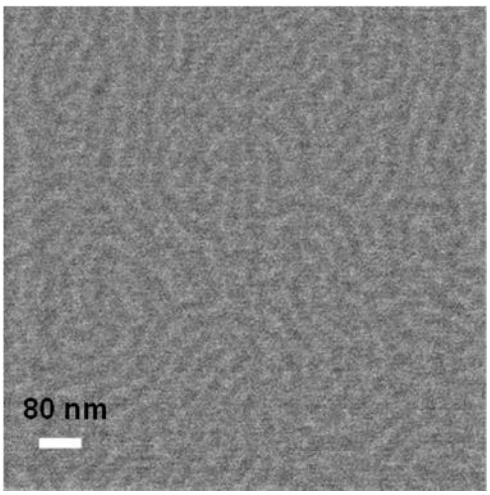

Figure 3.4 SEM analysis of PS-b-PHOST (14900-b-14300 g/mol) films thermally annealed at 190˚C under nitrogen atmosphere for 5 days.

As an alternative to thermal annealing, solvent annealing was used to promote sufficient mobility allowing for phase separation of the BCP. Choice of annealing solvent was critical to avoid cylinder formation via preferential swelling of one of the

blocks, and to avoid dewetting of the BCP films upon annealing[32, 33]. Hence, annealing solvent should exhibit similar compatibility between both polymer blocks. In order to screen potential annealing solvents, relative solubility parameters of the polymer and solvents were calculated and compared. Specifically, Hansen solubility parameters were used which take into account the nonpolar, polar and hydrogen bonding interactions since the free energy of mixing depends by a variety of intermolecular interactions (Equation 4). While these solubility parameters can be estimated from group contribution methods, experimentally determined solubility parameters were used, which should provide more accurate comparisons (Table 3.2) [16, 34]. Table 3.3 represents the calculated Rsolv/PS and Rsolv/PHOST, where the smaller difference in R values ((Rsolv/PS-Rsolv/PHOST)^2) suggests similar compatibility between the solvent and the PS and PHOST block. Using these calculated solubility parameters, ethyl acetate provided the most similar compatibility with each block. Also, as a further test, homopolymer films of PHOST and PS were annealed in ethyl acetate atmosphere which remained homogeneous with no observed dewetting.

$$R^2 = 4(\delta_{d1} - \delta_{d2})^2 + (\delta_{p1} - \delta_{p2})^2 + (\delta_{h1} - \delta_{h2})^2 \quad (4)$$

Table 3.2 Relevant values, including Mw (monomer molecular weight), V (volume), ρ (density), and Hansen solubility parameters (δ), used to calculate polymer solvent compatibility.

	Mw (g/mol)	V (cm^3/mL)	ρ (g/cm^3)	δ_d ($MPa^{1/2}$)	δ_p ($MPa^{1/2}$)	δ_h ($MPa^{1/2}$)
PS	104.15	99.2	1.05	18.4	1.0	3.3
PHOST	120.15	104.5	1.15	17.6	10	13.7

Table 3.3 Calculated R(polymer/solvent) values use to compare the relative solvent compatibility with the solvent and each block of the PS-b-PHOST polymer.

Solvent	Vapor Pressure at ~20 ˚C (Torr)	Rsolv/PS ($MPa^{1/2}$)	Rsolv/PHOST ($MPa^{1/2}$)	[(R(solv/PS)-R(solv/PHOST)]^2 (MPa)
Acetone	184.5	11.7	7.9	14.4
Chloroform	158.4	3.4	10.6	51.8
Acetonitrile	88.8	18.3	12	39.7
Ethyl Acetate	73	7.8	8.8	1
MIBK	16	8.1	11.3	10.2
Cyclohexanone	5	5.7	9.4	13.7

All samples were annealed with 0.4 mL liquid ethyl acetate per 250 f flask. Anneal times were varied according to the BCP molecular weight and film thickness. When excess water was present in the annealing experiment (either from the atmosphere or from the solvent) defects and dewetting were observed in the phase separated sample.

This could be a result of condensation of the water at the end of the annealing experiment when the solvent evaporates, since the BCP film rapidly cools due to endothermic heat of vaporization. In order to avoid these detrimental effects, special care was used to remove water from the chamber throughout the solvent anneal process. This included using extra dry solvent and purging the anneal chamber with dry nitrogen gas both before and after annealing.

To further investigate the effect of water on the phase separated result, controlled amounts of water were added to a series of solvent annealed experiments (0-0.02 g water per 250 mL flask) (Figure 3.5). Note, at saturated conditions 0.4 mL of ethyl acetate holds 0.026 g water and the 250 mL flask holds 0.005 g of water vapor. The amount of water that the film absorbs is negligible in relationship to the amount in the solvent and flask. Here, moderate amounts of water present in the anneal experiment results in higher contrast between the PS and PHOST domains, while the pitch remains relatively the same (Pitch= 47 nm). However, excessive amounts of water caused the fingerprint domains to swell and distort. This suggests that the presence of water in the atmosphere promotes a higher proportion of PHOST at the surface (relative to PS), thereby increasing the SEM contrast in the PHOST domain. This is consistent with previous studies showing water prefers the PHOST material. In fact, PHOST homopolymer films absorb ~10 wt % water under saturated conditions[35].

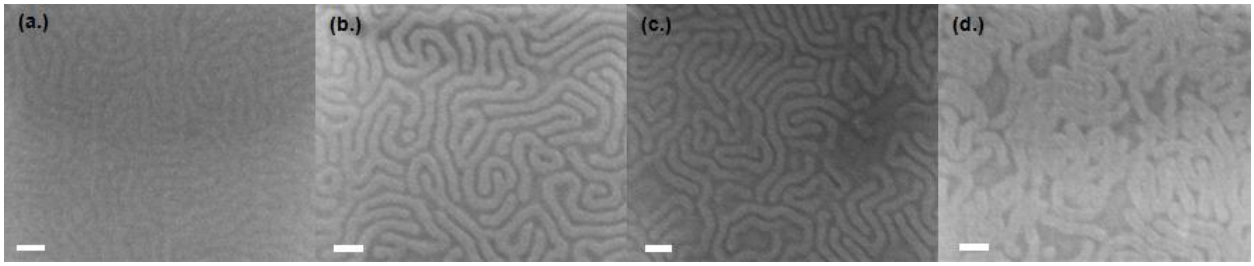

Figure 3.5 SEM analysis of PS-b-PHOST (14900-b-14300 g/mol) films annealed with 0.4 mL dry ethyl acetate in nitrogen purged 250 mL flask with (a.) 0 g water, (b.) 0.05 g water, (c.) 0.1g water (d.) 0.2 g water. Scale bar 100 nm.

In order to test the hypothesis that water in the solvent anneal experiment increases the relative amount of PHOST at the surface of the phase separated thin films, samples annealed with and without water were processed with atomic layer deposition (ALD) (Figure 3.6 and 3.7). See Chapter 4 for full ALD methods and discussion. Here, samples annealed in the presence of water exhibited considerably more TiO_2 coverage in comparison with samples annealed in the absence of water. Since the hydroxyl functionality on the PHOST serves as the reactive site for ALD nucleation and growth, the fact that samples annealed in the presence of water exhibit improved and more continuous titania coverage suggests a higher proportion of PHOST at the surface of these samples.

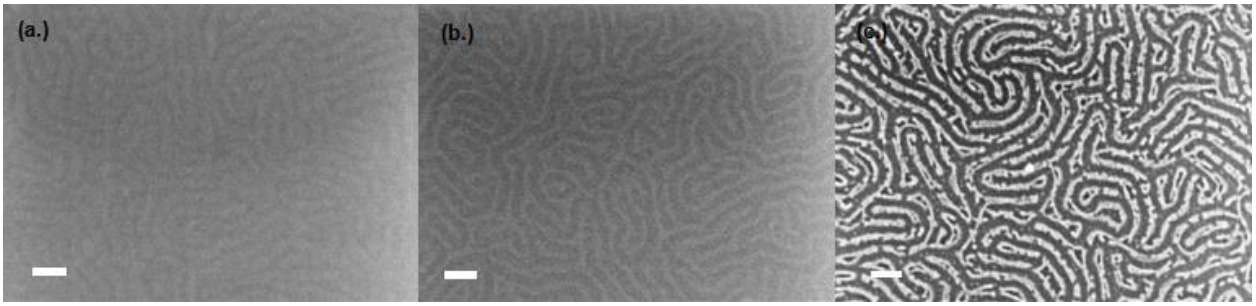

Figure 3.6 SEM imaging of PS-b-PHOST (14900-b-14300 g/mol) finger print patterns with 47 nm pitch, (a) after ethyl acetate anneal in the absence of water , (b) after 200 ALD cycles, (c) and after etching for 15s with of 5 sccm O2, 5 sccm Ar, 100 W, 0.035 mTorr. Scale bar is 100 nm.

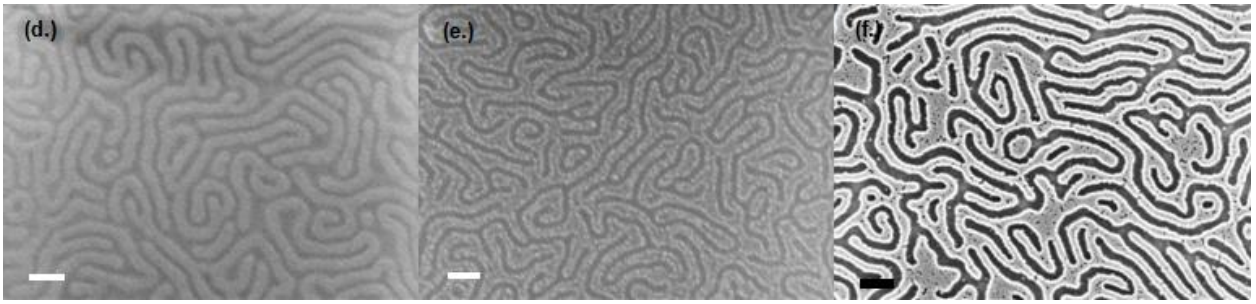

Figure 3.7 SEM imaging of PS-b-PHOST (14900-b-14300 g/mol) finger print patterns with 47 nm pitch, (a) after ethyl acetate anneal with 0.05 g water added to annealing flask, (b) after 200 ALD cycles, (c) and after etching for 15 s with of 5 sccm O2, 5 sccm Ar, 100 W, 0.035 mTorr. Scale bar is 100 nm.

Table 3.1 and Figure 3.8 summarizes the observed pitch and the associated degree of polymerization. Typical scaling (where $D \sim N^{2/3}$) observed in block copolymers in the strong segregation limit was not observed due to solvent swelling during the annealing process. Solvent anneal of PS-b-PHOST (3900-b-4700 g/mol) provided thin film lamellar patterns with 13 nm pitch, which is the among the smallest reported pitch for

thin film lamellar patterns to date. Smaller pitch has been observed for silicon containing materials, yet the morphology for those systems was imbedded cylinders[36]. The fact that lower molecular weight PS-b-PHOST phase separated provides a lower bound on the Flory Huggins interaction parameter for this system. Utilizing the χN=10.5 relationship at the order disorder transition of a symmetrical BCP system, one finds χ>0.14.

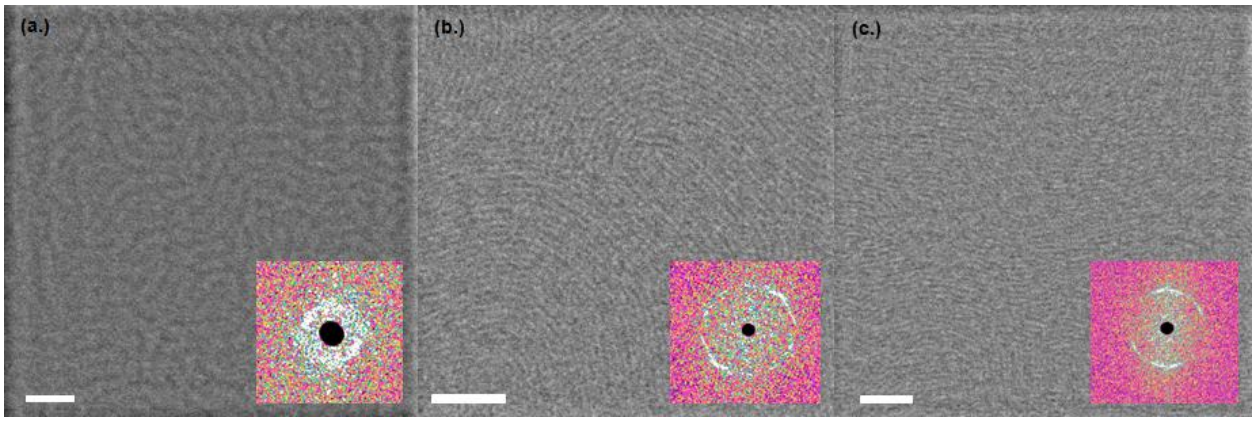

Figure 3.8 SEM images of BCP annealed with 0.4 mL ethyl acetate in 250 mL nitrogen purged flasks: (a.) PS-b-PHOST (7400-b-10500 g/mol), 32 nm pitch; (b.) PS-b-PHOST (8500-b-6900 g/mol), 18 nm pitch; (c.) PS-b-PHOST (3900-b-4700 g/mol), 13 nm pitch.

3.3.4 Directed Self Assembly

Directed self assembly via graphoepitaxy was performed using SU-8 guiding lines on top of the neutral underlayer[37, 38]. Graphoepitaxy was used for alignment in part because the dimensions of the primary lithographic pattern are readily analyzed by SEM. SU-8 is an epoxy based negative tone resist used in industry and is readily patterned with electron beam lithography with high mechanical stability. Also, SU-8 favorably wets

PHOST which should promote alignment of the block copolymer along the length of the trench.

Since water was shown to affect the phase separation of unaligned fingerprint patterns, the effect of water on directed self assembly of aligned patterns was also investigated. PS-b-PHOST (14900-b-14300 g/mol) on SU-8 guiding substrates was solvent annealed with controlled amounts of water (0-0.23 g) added to the solvent anneal experiment (0.4 mL dry ethyl acetate in 250 mL purged flask) (Figure 3.9). Here, the presence of water is necessary for alignment, however, the addition of excess water resulted in swelling and deformation of the material and loss of alignment.

This set of optimized water/solvent anneal conditions was used to phase separate low molecular weight PS-b-PHOST on SU-8 patterned substrates resulting in high resolution aligned BCP patterns. Figure 3.10 summarizes graphoepitaxy results, with aligned PS-b-PHOST patterns with 47 nm, 31 nm, and 18 nm pitch. Also, alignment with graphoepitaxy was observed even when the trench width was incommensurate with the natural pitch of the BCP. Here, the BCP polymer stretched or compressed to match the width of the SU-8 trench. [39].

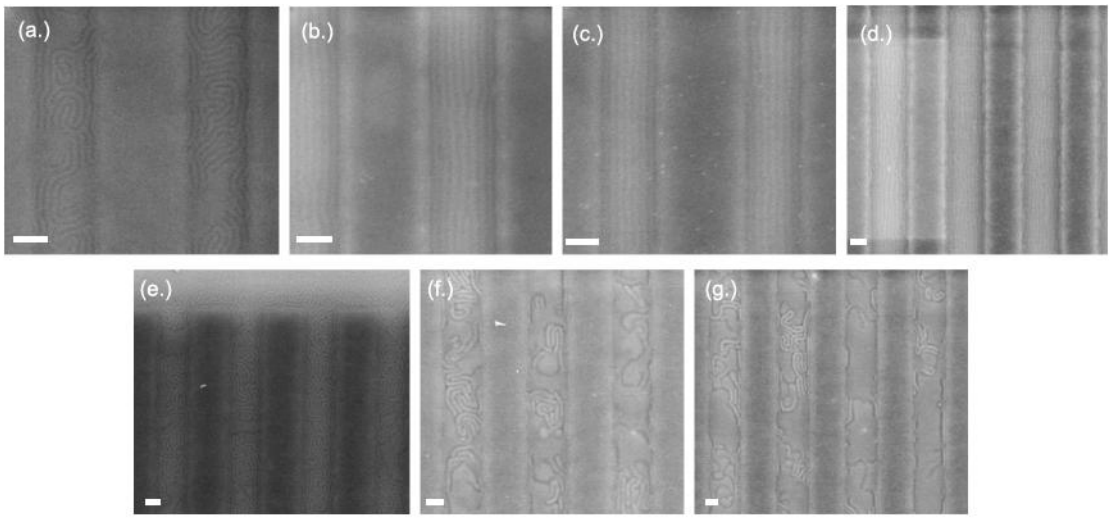

Figure 3.9 SEM images of aligned PS-b-PHOST (14900-b-14300 g/mol) via graphoepitaxy using SU-8 guiding lines and ethyl acetate solvent annealing with added water per 250 mL annealing flask: (a.) 0 g water , (b.) 0.002 g water , (c.) 0.005 g water , (d.) 0.01 g water , (e.) 0.02 g water, (f.) 0.038 g water , (g.) 0.058 g water. Scale bar is 200 nm.

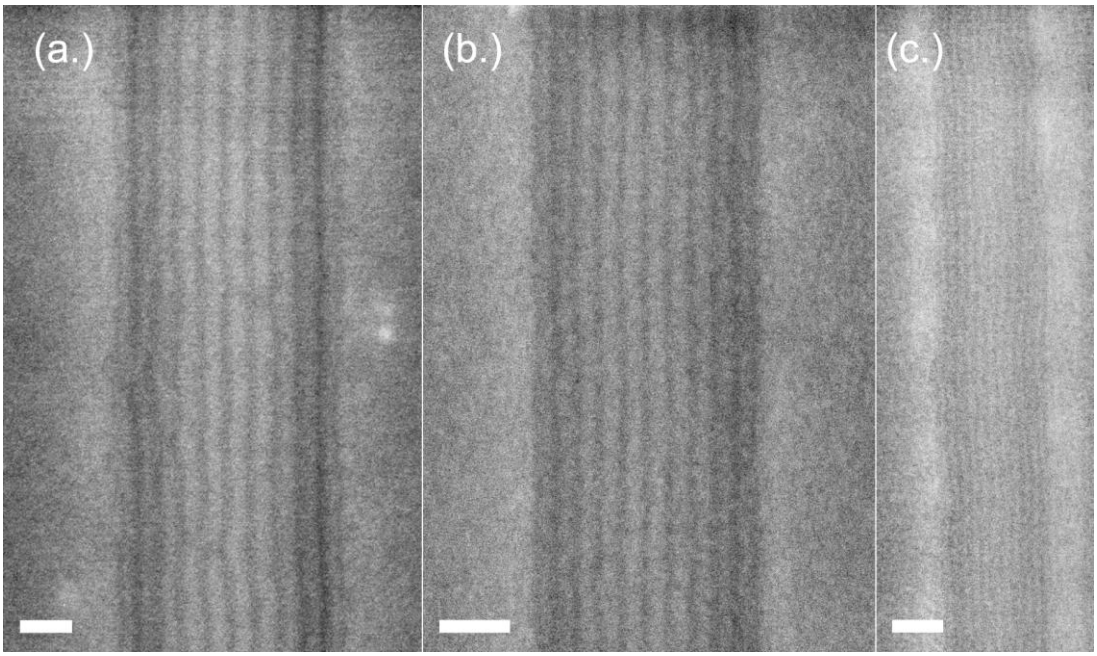

Figure 3.10 SEM images of aligned PS-b-PHOST via graphoepitaxy using SU-8 guiding lines: (a.) PS-b-PHOST (14900-b-14300 g/mol), 47 nm pitch (b.) PS-b-PHOST (7400-b-10500 g/mol), 32 nm pitch; (c.) PS-b-PHOST (8500-b-6900 g/mol), 18 nm pitch. Scale bar is 100 nm.

3.4 Conclusion

In summary, PS-b-PHOST was utilized as a high χ block copolymer for high resolution DSA patterning. PS-b-PHOST was synthesized with controlled molecular weight and low PDI via nitroxide mediated polymerization. Also, PS-r-PHOST-r-PGMA was prepared via radical polymerization as a neutral underlayer substrate. High resolution PS-b-PHOST fingerprint lamellar patterns with 13 nm pitch were prepared using ethyl acetate solvent anneal. Graphoepitaxy with SU-8 primary patterns was used to align PS-b-PHOST secondary patterns with 18 nm pitch. This work indicates styrene based block copolymers with hydrogen bonding functionality, such as PS-b-PHOST, are a promising alternative to PS-b-PMMA for sub 20 nm pitch DSA patterning applications.

While PS-b-PHOST exhibits high χ enabling high resolution DSA patterns, this material exhibits poor etch contrast necessary for pattern transfer into the underlying substrate. This is because PS and PHOST exhibit similar organic composition and similar Ohnishi number[40]. Hence, this material requires some modification to allow selective block removal. Ongoing work in this lab includes utilizing the OH functionality already present on the PHOST domain to selectively grow an etch resistant oxide layer directly on the PHOST domain through a selective atomic layer deposition process. Here, an oxide layer formed on the surface of the PHOST domain is highly etch resistant, while the PS domain is easily removed. An alternative approach includes synthesizing the styrene block with silicon containing functionality such as trimethyl silane[36, 41, 42]. When exposed to oxygen plasma, the silane is converted to an inorganic oxide which is

highly etch resistant. Upon reactive ion etching the silane containing block remains, while the other block is easily removed.

3.5 References

1. Brunner, T. A. *J Vac Sci Technol B* **2003,** 21, (6), 2632-2637.

2. Wagner, C.; Harned, N. *Nat Photonics* **2010,** 4, (1), 24-26.

3. Herr, D. J. C. *J Mater Res* **2011,** 26, (2), 122-139.

4. Kim, H. C.; Hinsberg, W. D. *J Vac Sci Technol A* **2008,** 26, (6), 1369-1382.

5. Stoykovich, M. P.; Nealey, P. F. *Mater Today* **2006,** 9, (9), 20-29.

6. Bates, F. S.; Fredrickson, G. H. *Annu Rev Phys Chem* **1990,** 41, 525-557.

7. Bates, F. S.; Fredrickson, G. H. *Phys Today* **1999,** 52, (2), 32-38.

8. Matsushita, Y.; Mori, K.; Saguchi, R.; Nakao, Y.; Noda, I.; Nagasawa, M. *Macromolecules* **1990,** 23, (19), 4313-4316.

9. Bates, F. S. *Science* **1991,** 251, (4996), 898-905.

10. Leibler, L. *Macromolecules* **1980,** 13, (6), 1602-1617.

11. Khandpur, A. K.; Forster, S.; Bates, F. S.; Hamley, I. W.; Ryan, A. J.; Bras, W.; Almdal, K.; Mortensen, K. *Macromolecules* **1995,** 28, (26), 8796-8806.

12. Bang, J.; Jeong, U.; Ryu, D. Y.; Russell, T. P.; Hawker, C. J. *Adv Mater* **2009,** 21, (47), 4769-4792.

13. Cheng, J. Y.; Rettner, C. T.; Sanders, D. P.; Kim, H. C.; Hinsberg, W. D. *Adv Mater* **2008,** 20, (16), 3155-3158.

14. Russell, T. P.; Hjelm, R. P.; Seeger, P. A. *Macromolecules* **1990,** 23, (3), 890-893.

15. Rubinstein, M., *Polymer Physics*. Oxford University Press: Oxford, New York, 2003.

16. Arichi, S.; Himuro, S. *Polymer* **1989,** 30, (4), 686-692.

17. Mangaraj, D.; Bhatnagar, S. K.; Rath, S. B. *Makromolekul Chem* **1963,** 67, 75-83.

18. Quinn, J. D.; Register, R. A. *Journal of Polymer Science: Part B: Polymer Physics* **2009,** 47, 2106-2113.

19. Benoit, D.; Chaplinski, V.; Braslau, R.; Hawker, C. J. *J Am Chem Soc* **1999,** 121, (16), 3904-3920.

20. Chen, X. Y.; Jankova, K.; Kops, J.; Batsberg, W. *J Polym Sci Pol Chem* **1999,** 37, (5), 627-633.

21. Hawker, C. J.; Bosman, A. W.; Harth, E. *Chem Rev* **2001,** 101, (12), 3661-3688.

22. Patel, K. *Material Matters:* **2010,** 5, (1), 1-32.

23. Barclay, G. G.; Hawker, C. J.; Ito, H.; Orellana, A.; Malenfant, P. R. L.; Sinta, R. F. *Macromolecules* **1998,** 31, (4), 1024-1031.

24. Han, E.; Stuen, K. O.; La, Y. H.; Nealey, P. F.; Gopalan, P. *Macromolecules* **2008,** 41, (23), 9090-9097.

25. In, I.; La, Y. H.; Park, S. M.; Nealey, P. F.; Gopalan, P. *Langmuir* **2006,** 22, (18), 7855-7860.

26. Ham, S.; Shin, C.; Kim, E.; Ryu, D. Y.; Jeong, U.; Russell, T. P.; Hawker, C. J. *Macromolecules* **2008,** 41, (17), 6431-6437.

27. Zhao, J. C.; Jiang, S. C.; Ji, X. L.; An, L. J.; Jiang, B. Z. *Polymer* **2005,** 46, (17), 6513-6521.

28. Cavicchi, K. A.; Berthiaume, K. J.; Russell, T. P. *Polymer* **2005,** 46, (25), 11635-11639.

29. Peng, J.; Kim, D. H.; Knoll, W.; Xuan, Y.; Li, B. Y.; Han, Y. C. *J Chem Phys* **2006,** 125, (6).

30. Li, N.; Cho, A. S.; Broadbelt, L. J.; Hutchinson, R. A. *Macromol Chem Physic* **2006,** 207, (16), 1429-1438.

31. Rahman, S. S. A.; Kawaguchi, D.; Matsushita, Y. *Macromolecules* **2011,** 44, (8), 2799-2807.

32. Bosworth, J. K.; Paik, M. Y.; Ruiz, R.; Schwartz, E. L.; Huang, J. Q.; Ko, A. W.; Smilgies, D. M.; Black, C. T.; Ober, C. K. *ACS Nano* **2008,** 2, (7), 1396-1402.

33. Paik, M. Y.; Bosworth, J. K.; Smilges, D. M.; Schwartz, E. L.; Andre, X.; Ober, C. K. *Macromolecules* **2010,** 43, (9), 4253-4260.

34. Brandrup, J.; Immerguy, E.; Grulke, A., *Polymer Handbook*. Fourth ed.; John Wiley and Sons: New York, 1999.

35. Berger, C. M.; Henderson, C. L. *Polymer* **2003,** 44, (7), 2101-2108.

36. Cushen, J. D.; Otsuka, I.; Bates, C. M.; Halila, S.; Fort, S.; Rochas, C.; Easley, J. A.; Rausch, E. L.; Thio, A.; Borsali, R.; Willson, C. G.; Ellison, C. J. *ACS Nano* **2012,** 6, (4), 3424-3433.

37. Park, S. M.; Stoykovich, M. P.; Ruiz, R.; Zhang, Y.; Black, C. T.; Nealey, P. E. *Adv Mater* **2007,** 19, (4), 607.

38. Bilenberg, B.; Jacobsen, S.; Schmidt, M. S.; Skjolding, L. H. D.; Shi, P.; Boggild, P.; Tegenfeldt, J. O.; Kristensen, A. *Microelectron Eng* **2006,** 83, (4-9), 1609-1612.

39. Cheng, J. Y.; Mayes, A. M.; Ross, C. A. *Nat Mater* **2004,** 3, (11), 823-828.

40. Suzuki, M.; Saigo, K.; Gokan, H.; Ohnishi, Y. *J Electrochem Soc* **1983,** 130, (9), 1962-1964.

41. Cushen, J. D.; Bates, C. M.; Rausch, E. L.; Dean, L. M.; Zhou, S. X.; Willson, C. G.; Ellison, C. J. *Macromolecules* **2012,** 45, (21), 8722-8728.

42. Watanabe, F.; Ohnishi, Y. *J Vac Sci Technol B* **1986,** 4, (1), 422-425.

CHAPTER 4

NANOSCALE PATTERN FORMATION VIA AREA SELECTIVE ATOMIC LAYER DEPOSITION AND ETCH ON MICRO-PHASE SEPARATED BLOCK COPOLYMER THIN FILMS

A general new process for forming nano-scale relief patterns by area selective atomic layer deposition (ALD) on micro-phase separated block copolymer thin films is described. Such relief patterns can be turned into high aspect ratio relief patterns by subsequent selective etching of the block copolymer thin film, using the ALD grown surface features as an etch hard mask. The key requirement is that the block copolymer used in the process selectively nucleates growth of the ALD derived inorganic material on only one of the two microphase separated domains formed by the block copolymer. This process was demonstrated using micro-phase separated thin films of poly(hydroxystyrene)-b-poly(styrene) (PS-b-PHOST) to selectively nucleate ALD growth of titania (TiO_2) onto the exposed surface regions of the reactive PHOST domains. Subsequent oxygen plasma etching of the partially titania covered micro-phase separated PS-b-PHOST thin film allows for production of high aspect ratio nanostructures in the shape and size of the original block copolymer thin film surface pattern. This method allows formation of nanometer scale patterns using block copolymers that are not amenable to direct selective etching of one block, and thus

expands the useful range of copolymers for directed self-assembly (DSA) based patterning techniques.

4.1 Introduction

Fabrication of nano-scale structures on surfaces is an enabling technology for a variety of established fields such as semiconductor manufacturing and for an array of emerging fields such as bit patterned media. Conventionally, the most common methods for fabrication of nano-scale structures on surfaces have been based on various forms of lithography, including both electron beam and optical lithography, in which radiation exposure of a photoresist film is used to form an initial relief pattern that is transferred into other materials via etching or deposition processes through the photoresist pattern[1]. While electron beam lithography can form patterns at feature sizes down to single nanometer length scales, such direct-write e-beam tools and processes are too slow to be useful in high volume applications such as fabrication of consumer semiconductor devices[2, 3]. Instead, optical lithography has dominated commercial microfabrication for the last five decades and is still the critical technology for production of the high volumes of patterned nano-scale features that underlie modern semiconductor devices. Unfortunately, the evolution of optical lithography using refractive lens-based exposure tools in conjunction with single layer photoresist technology has recently reached its practical resolution limits at feature sizes of approximately 40 nm and pattern feature pitches of approximately 80 nm using exposure tools operating at 193 nm[4, 5]. In order to enable high-volume production of patterned surfaces with feature sizes and pitches

significantly below these limits, alternative methods beyond conventional optical lithography are required. While there is significant industrial interest in lower wavelength exposure lithographic technologies, e.g. extreme-ultraviolet lithography (EUVL) operating with ~13nm radiation, no other commercially useful lithographic exposure technology for creating large area patterns beyond the current 193 nm optical lithography has been successfully commercialized[6]. Likewise, efforts are underway to develop multi-beam electron and ion beam based exposure systems, but thus far none of these technologies € near commercial readiness for high volume manufacturing. There is a critical need for development of methods that can extend currently available optical lithography to large areas of patterns at sub-40 nm feature sizes.

In looking for alternative methods for producing nano-scale patterned or structured materials, block copolymers have attracted significant attention. The interest in block copolymers for making nanostructured materials arises from their propensity to micro-phase separate and to form domains that are commensurate in size with the size of individual polymer blocks[7]. A block copolymer in simplest terms is a polymer consisting of two or more homopolymer chains linked end to end via a covalent bond[8]. In such block copolymers, the thermodynamic immiscibility of the different homopolymer blocks drives phase separation, but bulk macro-phase separation is prevented due to the covalent bonds linking the individual copolymer blocks. Thus, when block copolymers are annealed at temperatures above their effective glass transition temperature, either by heating or by introduction of solvent, they tend to micro-phase separate to form domains of essentially pure homopolymer whose size is proportional to the number of monomers in the block. Such domain sizes are typically on the order of a few nanometers to ~ 100

nm based on the block molecular weights that are achievable using current block copolymer synthesis methods. Micro-phase separated block copolymers can adopt a variety of morphologies, including lamellar and cylindrical forms, which depend primarily on the relative volume fractions of the polymer blocks[9]. More recently, the possible utility of self-assembly and, more significantly, *directed* self-assembly (DSA) of nanometer scale features in thin block copolymer films has attracted considerable attention as one method for breaking through current optical lithography resolution limits to produce large areas of nanometer scale features in a fast and cost-effective manner[10, 11].

While disordered nanometer scale patterns over large areas, which could have applications as optical coatings and in other fields, can be achieved by casting and phase separation of block copolymers on unpatterned surfaces, recent research efforts have focused more heavily on production of nanometer scale patterns with both long range order and spatial registration using directed self-assembly methods[12-14]. In block copolymer DSA, some version of a traditional lithographic process, such as optical lithography, is first used to form chemical or topographical patterns at comparatively large length scales on a surface. These large scale patterns then induce long range order and pattern registration in the features formed from annealing block copolymer thin films on top of these guiding structures. In such DSA lithography processes, control over the feature shapes and sizes formed is not limited by the size scales and shapes achievable by the lithographic method used to produce the guiding patterns. Instead, feature sizes and shapes are controlled by factors that can be manipulated or "programmed" into the block copolymer during its creation. The choice of the two monomers from which the polymer is made (i.e. which controls the thermodynamic driving force for phase separation which

is often characterized using the Flory-Huggins χ parameter) and the degree of polymerization of each block (i.e. which control the volume fractions (*f*) of each monomer/block type and the total degree of polymerization (*N*)) pre-determine the size and type of features that will be made by the polymer[15-21]. Thus, the feature sizes possible in the DSA process are not determined by the lithographic method used to create the guiding patterns, allowing for creation of pattern sizes below the resolution capability of a given lithographic technology. Instead, it is only a requirement that the lithographic patterning technology can successfully create patterns at an appropriate multiple of the copolymer micro-phase separated domain pitch such that appropriate morphology and long range order can be directed by the lithographically derived guiding layer. These types of pitch and feature size reduction strategies are often referred to as "pitch sub-division" methods. One potential application of block copolymer DSA is in high volume patterning for nanoelectronic devices[22-24]. In such cases, the micro-phase separated block copolymer thin film pattern is transformed into a physical relief pattern that can serve as a lithographic template, e.g. as a resist mask for plasma etching, so that the pattern can be transferred into a layer of material used to build the device.

One common requirement for use of block copolymer patterns to form nano-scale structures in other materials for many applications, such as in DSA lithography for nanoelectronic device fabrication, is that methods exist for selective removal of one of the blocks from the block copolymer thin film to form a relief pattern. Currently, due largely to compatibility with current semiconductor industry processes, selective polymer block removal is most commonly performed through reactive ion etching of the ordered block copolymer thin film. This requires block copolymers which naturally have

differential etch rates of their homopolymer blocks in a particular plasma etch chemistry (e.g. oxygen reactive ion etching)[10, 25-27]. For example, the most commonly used block copolymer thus far for DSA patterning studies has been poly(styrene)-b-poly(methylmethacrylate) (PS-b-PMMA), due in part to the fact that PS exhibits significantly higher etch resistance as compared with PMMA in oxygen based plasma, thus allowing for formation of PS relief patterns from PS-b-PMMA thin films[28, 29]. Unfortunately, PS-b-PMMA possesses a relatively modest χ value of ~0.04, which limits the minimum practical feature size achievable using that particular polymer to approximately 20 nm[16]. In order to achieve smaller pattern sizes and pitches, new block copolymers with larger χ values must be integrated into DSA processes. However, the requirement that one polymer block possesses a significantly faster plasma etch rate than the other polymer block greatly restricts the choice of copolymer blocks and thus places an inherent limit on the feature sizes achievable. It can also be difficult to obtain very large etch rate ratios in organic polymers, thus limiting the aspect ratios of patterns that can be formed using such DSA processes in organic block copolymers. Therefore, the goal of the work reported here was to develop a DSA process for nano-scale pattern formation that can utilize a wider variety of block copolymers by employing block copolymers with poor direct plasma etch contrast but which can be converted via chemical transformation to produce significantly higher etch contrast between the polymer blocks.

In large part this goal was motivated by our initial work on developing high χ block copolymers for block copolymer DSA lithography[30, 31]. In the search for block copolymer designs that could produce high χ values, it was observed that polymers

containing hydrogen bonding motifs in one polymer block coupled with other blocks that possess orthogonal modes of interaction could produce very large χ-values Our early work focused on developing structure-property relations for a series of block copolymers with one block containing hydrogen-bonding moieties coupled to a poly(styrene) block whose main interaction is quadrupolar in nature. Since some of the polymers that were predicted to have large χ values were not expected to exhibit an inherently large etch contrast between the two blocks based on etch rate predictions such as their Ohnishi parameter[32], creation of alternative methods that could be used to achieve DSA and selective block removal in such polymers with poor inherent plasma etch contrast were explored. One such example of a block copolymer with a predicted poor plasma etch contrast between its blocks but a large predicted χ value was poly(styrene)-b-poly(hydroxystyrene) (PS-b-PHOST). Its χ value, based on several different experimental results including domain size scaling with molecular weight, was estimated to be at least an order of magnitude greater than PS-b-PMMA, thus making it attractive for fabricating small nano-scale patterns below 10 nm[33]. Unfortunately, since both the PS and PHOST blocks possess styrene backbones differing only by the presence of a single oxygen atom in the PHOST monomer, their plasma etch rates under a variety of plasma etch conditions were found to be nearly identical.

Considering the similarity of the functionality of the PS-b-PHOST polymer to modern photoresist polymer compositions and the common need in both traditional photoresist processing and DSA lithographic processing to form relief patterns, it is appropriate to examine the extant photoresist literature for methods to enable relief pattern formation. In particular, it is instructive to revisit the extensive work that was

performed on silylation methods for thin-film and top-surface imaging[34-37]. In such studies, photoresist thin films patterned using conventional lithographic exposure techniques were selectively infiltrated with silicon-containing agents to provide a means for selective plasma etch removal and "development" of relief patterns. Initially, differences in the rate of diffusion of the silylation compounds into either the exposed or unexposed regions of the resist film, e.g. as can be generated based on photochemically induced cross-linking reactions, were used to allow for selective silylation. Later, schemes based more on chemically selective reaction of the silylation reagents with portions of the resist film were investigated as a means to improve the silylation contrast over that achieved via the simple diffusion-biased schemes. For example, photodeprotection of protected poly(hydroxystyrene) polymers such as APEX-E allowed for area selective production of phenol groups in the photoresist film that could react with silylating agents such as hexamethyldisilazane (HMDS). Similar treatments of micro-phase separated PS-b-PHOST block copolymer films with reactively selective silylating agents such as HMDS were attempted as a means to provide an etch contrast between the PS and PHOST films. Results similar to those observed in the original photoresist silylation efforts were achieved, with the advantage that the phenol content and contrast in the block copolymer films was even higher than that achieved by optical lithographic patterning of protected chemically amplified resists. Plasma etch resistance of the silylated PHOST regions was greatly improved and selective plasma etch removal of the PS domains was possible. However, a significant drawback to methods such as silylation which rely on incorporation of additional atoms selectively into one block of the copolymer film is the propensity for such methods to cause swelling and volume changes

in the patterns due to the addition of mass to the films. In general, this was observed to cause image distortion and pattern dimensional changes that were difficult to control.

In designing alternative methods for selective block removal of block copolymers, it was hypothesized that the thin film patterns formed by such block copolymers which contain different functional groups spatially segregated in a relatively pure manner across their surface could also be a perfect substrate on which to perform spatially selective surface reactions to alter the block copolymer film properties after micro-phase separation. In order to prevent potential pattern distortion such as that observed in the silylation attempts, a methodology that led only to reactions on the surface of the phase separated block copolymer film was desired, with the goal being creation of a thin robust etch mask on the block copolymer pattern surface that could allow for further pattern transfer through the entire thickness of the block copolymer film. Previous work by Sinha and coworkers on area-selective atomic layer deposition techniques (ASALDT) using thin polymer relief patterns has shown that polymer such as PS are excellent inert barriers for ALD growth on inorganic surfaces[38-41]. It was hypothesized that, in a complementary fashion to the inert properties of materials such as PS, polymers and polymer surfaces containing reactive functional groups such as alcohols (–OH) and carboxylic acids (–COOH) could serve as surfaces on which to nucleate and grow metal or metal oxide films via ALD. Using the short ALD precursor exposure times available in modern ALD tools serves to limit precursor diffusion into the polymer films, thus preventing bulk incorporation of reactive precursors into the block copolymer film. Likewise, the comparatively long purge cycle times used in ALD to remove unreacted metal precursor or oxidant compounds helps to ensure complete removal of any

precursors adsorbed onto or absorbed into the polymer film from the last ALD precursor exposure cycle. ALD also has the advantage that it is possible to grow dense dielectric and metal films on surfaces at relatively modest temperatures and with exquisite control of film thickness, both characteristics that are important for possible use with polymer film patterns made via DSA[42]. Thus, it was anticipated that the reactive block surface presented by a phase separated block copolymer film could be used to selectively grow metal oxide features directly on only one block phase of a copolymer thin film.

Related work in other laboratories has demonstrated the use of ALD-like processes to perform so-called "sequential infiltration synthesis" (SIS) in micro-phase separated block copolymers[43, 44]. In such sequential infiltration synthesis, the basic concept has been to exploit differences in the solubility and diffusion rates of ALD precursors in the different polymer block domains of phase separated block copolymers to selectively nucleate and grow dielectric materials within the block copolymer. For example, Al_2O_3 and H_2O precursors have been selectively infiltrated into the PMMA domain of a phase separated PS-b-PMMA block copolymer film to produce hybrid organic-inorganic ordered nanostructures. As observed in our work in selective silylation of block copolymer film patterns, the reactants in such SIS schemes can swell and distort the material, resulting in different feature sizes and morphologies as compared to the original block copolymer template pattern. Also, the standard angstrom scale layer by layer growth control characteristic of ALD has not been demonstrated in the case of SIS. Furthermore this method exhibited poor selectivity as demonstrated by the fact that after several ALD cycles, significant oxide growth was observed in both the PS and PMMA domains of the block copolymer. Since DSA lithographic processes demand precise

pattern dimensional control, the work presented here has focused on achieving high contrast selective growth between block copolymer domains and on achieving traditional layer-by-layer linear growth rate control.

In this paper, such a highly selective ALD deposition of metal oxide and selective etch contrast enhancement is demonstrated for PS-b-PHOST. First, the plasma etch characteristics of PS and PHOST homopolymer films and homopolymer films treated with ALD deposited oxides are characterized using thin film growth and etch studies. Selective growth of oxide patterns on micro-phase separated PS-b-PHOST thin films is then demonstrated. Finally, use of such oxide surface patterns on a micro-phase separated PS-b-PHOST film to allow for selective block removal of one polymer phase (i.e. PS in this case) through plasma etching is demonstrated to yield large area, high resolution nano-scale patterns. Thus, a method for producing nano-scale relief patterns in high-χ block copolymers that inherently exhibit no simple method for liquid or plasma removal of one of its blocks is described and validated in this work.

4.2 Experiment, Results, and Discussion

4.2.1 Atomic Layer Deposition on Poly(styrene) (PS) and Poly(hydroxystyrene) (PHOST) Homopolymer Films

A Cambridge NanoTech Plasma ALD system was used throughout this study. The ALD reactor was kept at 170 ˚C and ~1 Torr pressure. The ALD cycle consisted of a 0.06 s H_2O pulse and 40 s purge (70 sccm N_2), followed by 0.06 s pulse of

tetrakis(dimethylamido titanium(IV)) (TDMAT), and a 40 s purge (70 sccm N_2). Titanium precursors with organic ligands were used for area selective ALD because they exhibit relatively lower reactivity with materials such as PS and slower diffusion rates into the polymer films due to their larger size as compared to smaller and more reactive precursors such as $TiCl_4$[39]. Changes in film thickness were monitored using spectroscopic ellipsometry (Woollam M-2000V) over a series of ALD cycles on PS, PHOST, and SiO_2 substrates (Figure 4.1). Linear growth was observed on SiO_2 and PHOST films (0.42 Å/cycle and 0.37 Å/cycle, respectively). This growth rate was similar to previous ALD reports using TDMAT[45]. Also, TiO_2 film growth on PS substrates was not observed after 80 cycles demonstrating the selective nature of this technique.

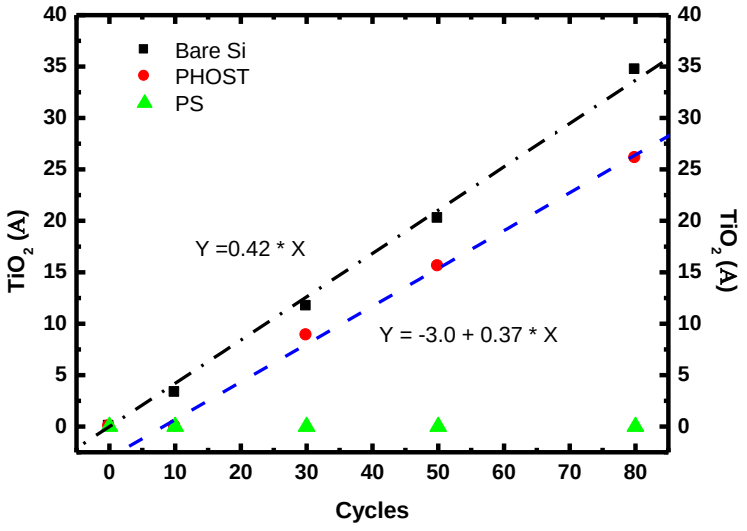

Figure 4.1 Growth rate of TiO_2 layer as a function of ALD deposition cycles on homopolymer films of PS and PHOST, as measured by spectroscopic ellipsometry. ALD growth occurred at 170 ^{o}C, with Ti-TDMAT and water precursors.

To further verify the selective growth of TiO_2 on the PHOST surface, X-ray photoelectron spectroscopy (thermo K-Alpha XPS) was performed, with the source of an Al Kα micro-focused monochromator at the pressure of 10^{-9} mbar. A value of 285 eV for the C_{1s} binding energy was used to correct the XPS data for charging effects under irradiation. Figure 4.2 represents the XPS spectra of the Si substrate, PHOST film, and PS film exposed for 0 and 80 ALD cycles. Titanium content on these surfaces was analyzed using the Ti 2p3 peak at 458.8 eV which is characteristic of titanium in TiO_2. The signal representing Ti 2p was clearly observed for both the Si substrate and PHOST films exposed to the ALD process, indicating TiO_2 growth on these substrates. In contrast, TiO_2 was not detected on PS film surfaces exposed at 80 cycles. These results further indicate that TiO_2 selectively grew on PHOST substrates, yet ALD did not occur on the PS substrate. Also, no nitrogen signal was observed on the TiO_2 films indicating the Ti-N bonds were fully broken (at least to the detection limit of the XPS) and converted to Ti-O bonds during the growth process.

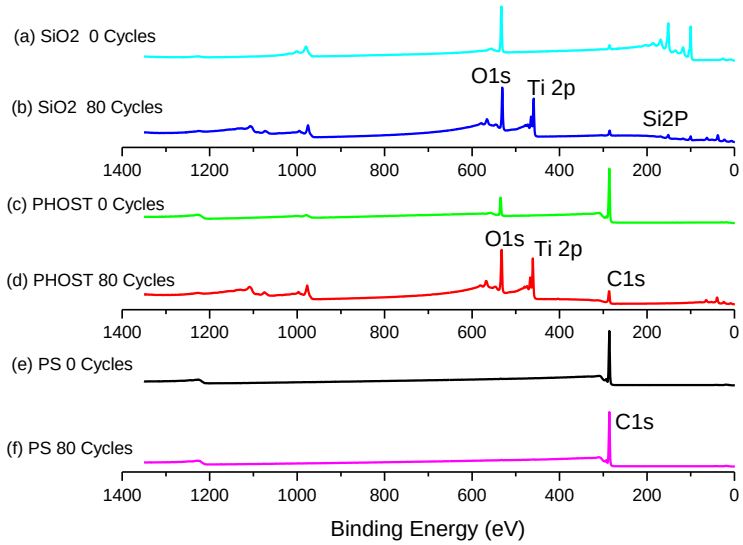

Figure 4.2 XPS spectra of bare Si exposed for (a) 0 cycles and (b) 80 cycles. XPS spectra of PHOST exposed for (c) 0 cycles and (d) 80 cycles. XPS spectra of PS exposed for (e) 0 cycles and (f) 80 cycles. The signal at 458.8 eV, representing the Ti 2p3 peak, demonstrated selective growth on Si and PHOST substrates, but no growth on PS substrates.

4.2.2 Etch Analysis of Poly(styrene) (PS) and Poly(hydroxystyrene) (PHOST) Homopolymer Films Exposed to the Atomic Layer Deposition Process

Since selective growth of TiO_2 on PHOST was demonstrated, studies were performed to verify the ability of the TiO_2 mask to allow for selective etching of the polymers. Following the growth of thin titanium dioxide films on polymer substrates, the bulk films were reactive-ion etched (RIE) using 5 sccm O_2 and 5 sccm argon at 100 W power and 35 mTorr pressure (Oxford Endpoint RIE Plasmalab 80Plus). Such an oxygen-based plasma allows selective removal of the organic material while minimally damaging the titania patterns, with argon ion bombardment assisting in improving the

anisotropy of the etch to minimize under-cutting of the oxide pattern. In Figure 4.3, PS films (both with and without ALD exposure) exhibit an etch rate of ~1.3 nm/sec under the particular plasma conditions used here. In comparison, the PHOST films without exposure to ALD deposition of oxide exhibit an etch rate of ~1.6 nm/s. Although the PHOST films do etch slightly faster, by a factor of ~1.2, than the PS films as one might expect from incorporation of oxygen into the PHOST polymer and structure-etch correlations such as the Ohnishi parameter, this level of etch contrast is insufficient to produce any significant relief patterns using PS-b-PHOST block copolymer thin films directly. The etch rate for the PHOST film decreases as the number of ALD cycles increases, and reaches approximately zero after approximately 50 ALD cycles. This suggests that a sufficiently continuous TiO_2 film is formed on the PHOST substrate after approximately 50 cycles, corresponding to approximately 2 nm TiO_2 film thickness, which prevented plasma etching into the underlying PHOST polymer.

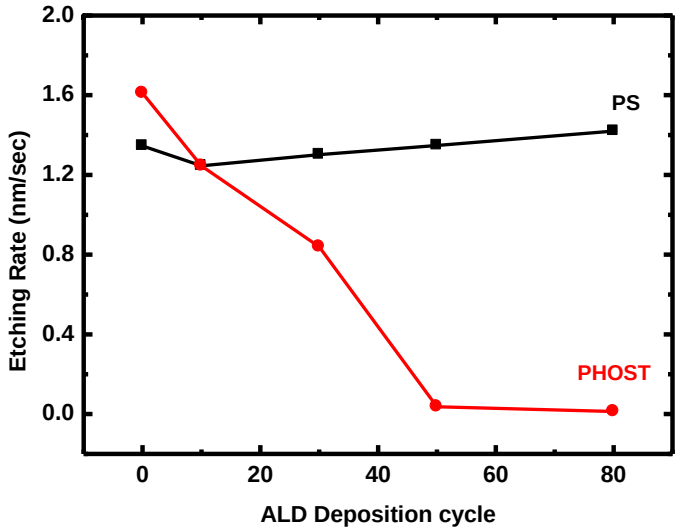

Figure 4.3 Average etch rate of homopolymer films as a function of ALD deposition cycles, as measured by spectroscopic ellipsometry. Etch conditions included 5 sccm O_2 and 5 sccm Ar, 100 W, and 0.035 Torr.

4.2.3 Area Selective Atomic Layer Deposition (ALD) and Etch of Poly(styrene)-b-poly(hydroxystyrene) (PS-b-PHOST) Phase Separated Thin Film Vertical Lamellar Patterns

Once the process requirements for selective ALD and etch were established on bulk films, demonstration of the ability to produce high aspect ratio nano-scale relief patterns using a combined ALD and etch process with micro-phase separated block copolymer thin films was accomplished. Figure 4.4 illustrates the processes involved in producing the desired nano-scale relief features: BCP self-assembly, selective ALD of the etch barrier, and selective plasma etch removal of one polymer block. Here, a cross-linkable random copolymer, poly(styrene-r-hydroxystyrene-r-glycidyl methacrylate),

consisting of 65 mole fraction styrene, 21 mole percent hydroxystyrene, and 14 mole percent glycidyl methacrylate, was utilized as a chemically neutral underlayer to avoid preferential wetting of either the PS or PHOST domain in the BCP material, and to promote vertical lamellae formation (see Supporting Information for details). The molar composition of PS and PHOST in this random copolymer was tailored to provide the neutral interface for both PS and PHOST domains of the BCP. This material also utilized glycidyl methacrylate to crosslink the material (via photoacid generator doping, UV exposure, and bake of spin coated films) to form an insoluble cross-linked mat with 20 nm film thickness.

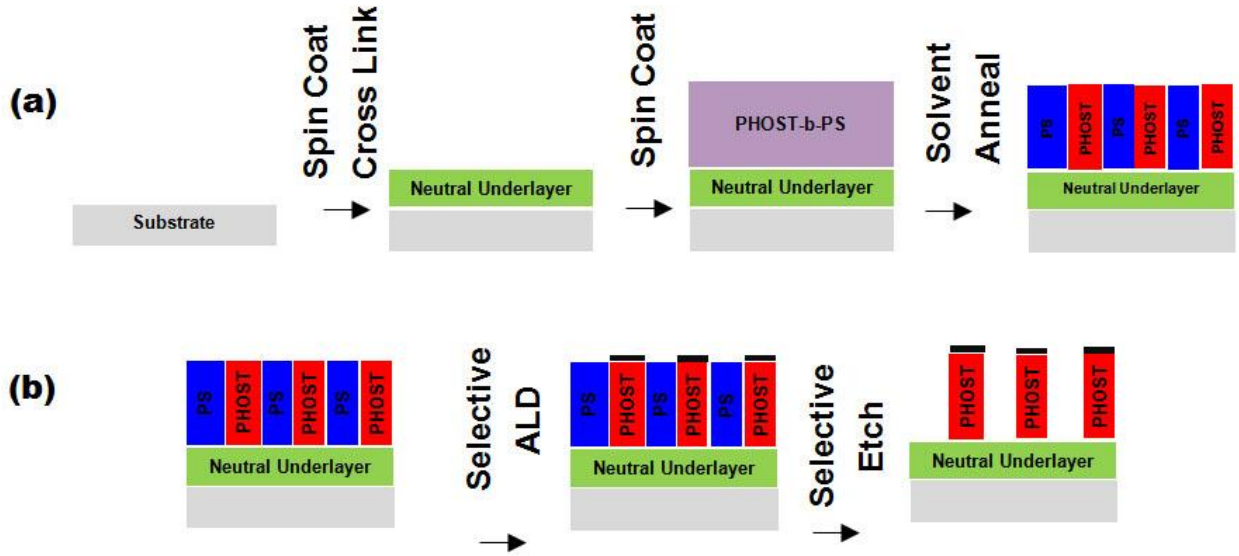

Figure 4.4. Selective block removal process flow: (a.) spin coating and cross-linking the neutral underlayer PS-r-PHOST-r-PGMA, spin coating of PS-b-PHOST, and solvent annealing to provide vertical lamellar fingerprint patterns; (b.) selective ALD and etch resulting in the relief pattern of the original block copolymer pattern.

PS-b-PHOST (14900-b-14300 g/mol) was prepared via nitroxide mediated polymerization with 0.44 volume fraction PS which consistently results in a vertical lamellar morphology after solvent anneal processing on a neutral underlayer (under conditions where the film thickness creates a frustrated condition for lamellae formation parallel to the substrate surface). Here, these block copolymer samples were spin coated from a 1.25 wt% propylene glycol monomethyl ether acetate (PGMEA) solution onto the neutral underlayer substrate to provide a BCP film thickness of 22 nm (with post apply bake at 120 ˚C for 2 min). Solvent annealing for at least 8 hours provided excellent, uniform fingerprint patterns consisting of lamellae oriented normal to the substrate surface. Analysis of 2-D Fast Fourier Transforms (FFT) of SEM images of these fingerprint patterns showed that the pattern was 47.2±2.8 nm.

These phase separated PS-b-PHOST block copolymer patterns were exposed to ALD using the titania deposition conditions described earlier. 200 ALD cycles were utilized in the patterning experiments to ensure successful formation of a dense etch mask on the PHOST domains of the copolymer film. These TiO_2 functionalized PS-b-PHOST patterns were etched by RIE for approximately 23 seconds to completely remove the PS domain leaving the desired nanometer scale relief pattern.

Top down SEM imaging was used to analyze the fingerprint patterns and confirmed the selectivity of the ALD growth and RIE etch processes (Carl Zeiss Ultra60 SEM, with 2-5 keV acceleration voltage) (Figure 4.5). The ALD grown TiO_2 pattern on the PS-b-PHOST film surface closely resembles that of the original block copolymer fingerprint pattern while no nucleation or growth of TiO_2 was observed within the PS

domain. The oxide layer grown with 200 ALD cycles was sufficient to provide high etch resistance and to maintain pattern fidelity when exposed to reactive ion etching. In fact, the pitch of the fingerprint pattern remained the same throughout the processing steps confirming that the TiO_2 features preserved the original pattern of the PHOST-b-PS fingerprint template (47.2±4.8 nm after anneal, 47.4±3.2 nm after ALD, and 47.7±4.0 nm after etch). The PHOST domain width was also preserved throughout the processing steps (27.4±2.8 nm after anneal, 28.1±4.1 nm after ALD, and 26.9±3.0 nm after etch). This indicates that under the conditions reported here, the TiO_2 layer did not appear to significantly widen the effective PHOST domain width due to isotropic oxide growth at the domain edges. Figure 4.6 shows the conformal oxide coating is uniform and homogeneous without breaks or defects across large areas of the substrate.

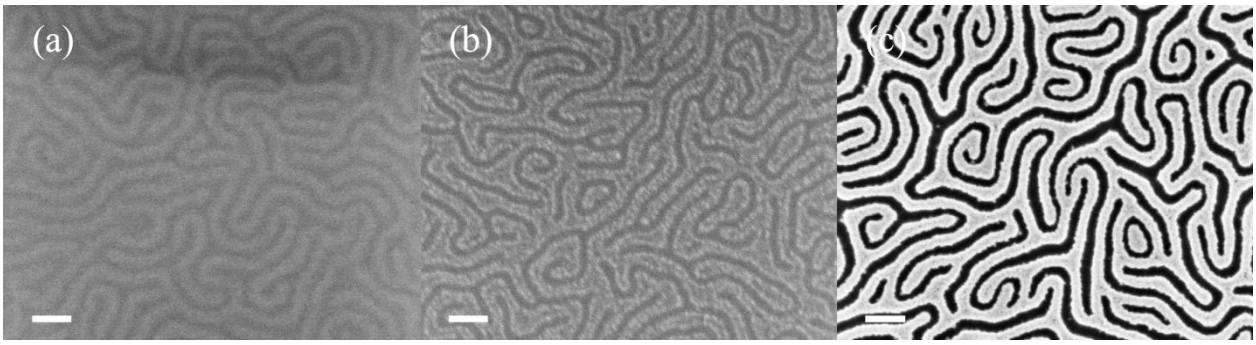

Figure 4.5 SEM imaging of block copolymer fingerprint patterns with 47 nm pitch, (a) after anneal, (b) after ALD, (c) and after etching. The 23 s etching step consisted of 5 sccm O2, 5 sccm Ar, 100 W, 35 mTorr. Scale bar is 100 nm.

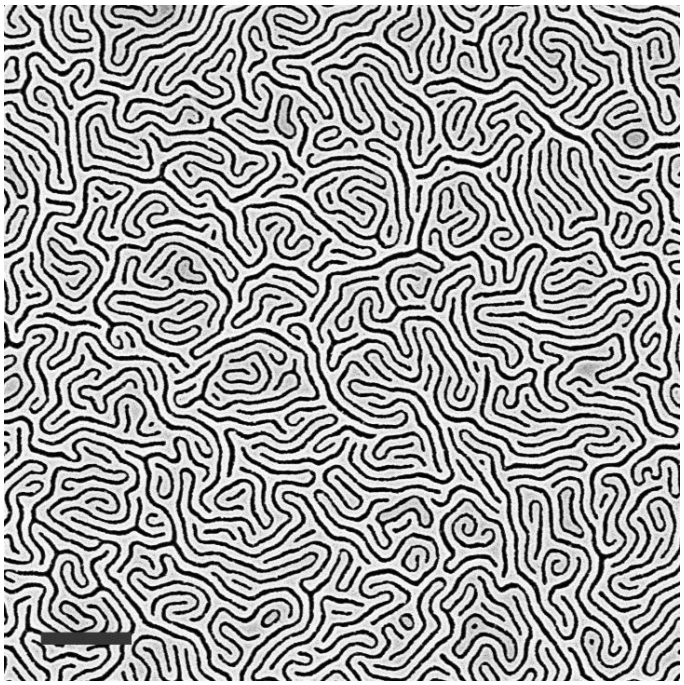

Figure 4.6 SEM imaging of PHOST-b-PS finger print patterns (47 nm pitch) after 200 ALD cycles and 23 s reactive ion etching. Scale bar is 400 nm.

Cross sectional SEM imaging of the patterns after ALD and block removal via plasma etch is shown in Figure 4.7. Again, no evidence of nucleation or growth of oxide in the PS domain regions of the PS-b-PHOST films was observed as signified by the lack of any significant etch residue artifacts in the trench features formed. Also, minimal undercutting of the oxide patterns during the etching step was observed and the features produced appeared to have relatively vertical sidewalls. Since no significant optimization of the etch process was performed, it is expected that better etch profiles and etch contrast could be achieved with further process optimization.

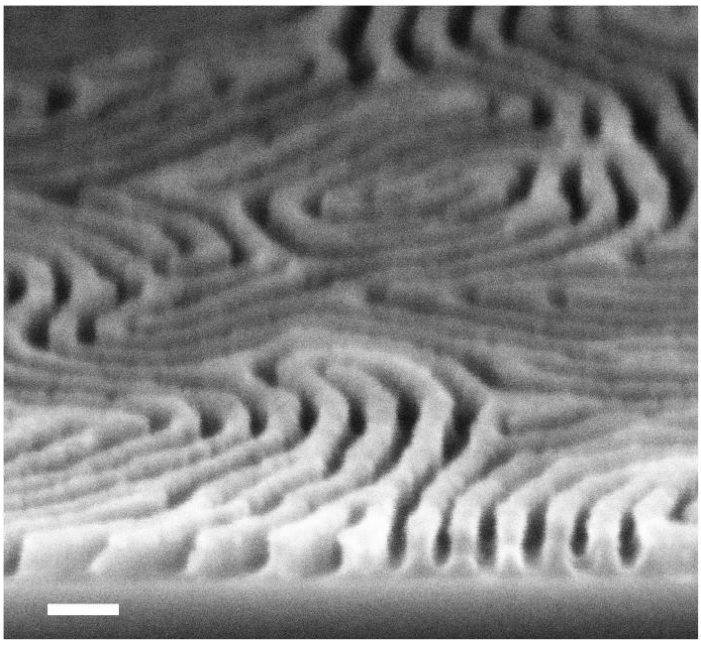

Figure 4.7. 45^{o} cross sectional imaging of block copolymer finger print patterns (47 nm pitch) after anneal, ALD, and etching steps. 200 ALD deposition cycles resulted in 7.5 nm TiO_2 (as measured on homopolymer PHOST films used as control). The 23 nm etch step consisted of 5 sccm O2, 5 sccm Ar, 100 W, 0.035 mTorr. Scale bar is 60 nm.

4.3 Conclusion

In conclusion, we have demonstrated a highly selective ALD and plasma etch process that allows for selective block removal from micro-phase separated block copolymer patterns to form nano-scale relief patterns. The key to such a process was the use of block copolymers that contain a reactive polymer block which can selectively nucleate ALD growth. The highlights of this process are as follows: Oxide growth occurred on top of the polymer avoiding infiltration, deformation, and swelling of the underlying pattern, thereby preserving the underlying template pattern. Oxide growth occurred layer-by-layer in a linear fashion indicative of atomic layer deposition providing a continuous film on the PHOST domain, free of breaks or defects. Also, ALD growth

was highly selective utilizing the hydroxy functionality present only in the PHOST domain, providing a high fidelity mapping of the oxide onto the patterned PHOST domain. Upon etching, the PS domain was removed while the oxide coated PHOST remained leaving a high fidelity etch relief image of the original block copolymer pattern. This general methodology could be applied to a much wider range of oxide precursor chemistries and block copolymer substrates resulting in a broad range of nano-scale thin film patterns. Further study is needed to determine the practical resolution limits of such a process. Ongoing work includes optimization of ALD and etch conditions, allowing selective block removal of lower molecular weight block copolymer patterns with smaller pitch.

4.4 References

1. Thompson, L. F.; Willson, C. G.; Bowden, M. J., *Introduction to microlithography*. 2nd ed.; American Chemical Society: Washington, DC, 1994; p xiv, p. 527.

2. May, G. S.; Sze, S. M., *Fundamentals of semiconductor fabrication*. Wiley international ed.; Wiley: New York, 2004; p xiii, p. 305.

3. Ito, T.; Okazaki, S. *Nature* **2000,** 406, (6799), 1027-1031.

4. Brunner, T. A. *J Vac Sci Technol B* **2003,** 21, (6), 2632-2637.

5. Rothschild, M. *MRS Bulletin* **2005,** 30, 942-946.

6. Wagner, C.; Harned, N. *Nat Photonics* **2010,** 4, (1), 24-26.

7. Kim, H. C.; Hinsberg, W. D. *J Vac Sci Technol A* **2008,** 26, (6), 1369-1382.

8. Odian, G., *Principles of Polymerization*. John Wiley and Sons, Inc.: Hoboken, New Jersey, 2004.

9. Kim, H. C.; Park, S. M.; Hinsberg, W. D. *Chem Rev* **2010,** 110, (1), 146-177.

10. Jung, Y. S.; Ross, C. A. *Nano Lett* **2007,** 7, (7), 2046-2050.

11. Bang, J.; Jeong, U.; Ryu, D. Y.; Russell, T. P.; Hawker, C. J. *Adv Mater* **2009,** 21, (47), 4769-4792.

12. Cheng, J. Y.; Rettner, C. T.; Sanders, D. P.; Kim, H. C.; Hinsberg, W. D. *Adv Mater* **2008,** 20, (16), 3155-3158.

13. Cheng, J. Y.; Mayes, A. M.; Ross, C. A. *Nat Mater* **2004,** 3, (11), 823-828.

14. Chai, J.; Buriak, J. M. *ACS Nano* **2008,** 2, (3), 489-501.

15. Matsushita, Y.; Mori, K.; Saguchi, R.; Nakao, Y.; Noda, I.; Nagasawa, M. *Macromolecules* **1990,** 23, (19), 4313-4316.

16. Russell, T. P.; Hjelm, R. P.; Seeger, P. A. *Macromolecules* **1990,** 23, (3), 890-893.

17. Rahman, S. S. A.; Kawaguchi, D.; Matsushita, Y. *Macromolecules* **2011,** 44, (8), 2799-2807.

18. Bates, F. S. *Science* **1991,** 251, (4996), 898-905.

19. Leibler, L. *Macromolecules* **1980,** 13, (6), 1602-1617.

20. Khandpur, A. K.; Forster, S.; Bates, F. S.; Hamley, I. W.; Ryan, A. J.; Bras, W.; Almdal, K.; Mortensen, K. *Macromolecules* **1995,** 28, (26), 8796-8806.

21. Bates, F. S.; Fredrickson, G. H. *Phys Today* **1999,** 52, (2), 32-38.

22. Herr, D. J. C. *J Mater Res* **2011,** 26, (2), 122-139.

23. Stoykovich, M. P.; Nealey, P. F. *Mater Today* **2006,** 9, (9), 20-29.

24. Ruiz, R.; Kang, H. M.; Detcheverry, F. A.; Dobisz, E.; Kercher, D. S.; Albrecht, T. R.; de Pablo, J. J.; Nealey, P. F. *Science* **2008,** 321, (5891), 936-939.

25. Cushen, J. D.; Otsuka, I.; Bates, C. M.; Halila, S.; Fort, S.; Rochas, C.; Easley, J. A.; Rausch, E. L.; Thio, A.; Borsali, R.; Willson, C. G.; Ellison, C. J. *ACS Nano* **2012,** 6, (4), 3424-3433.

26. Hirai, T.; Leolukman, M.; Liu, C. C.; Han, E.; Kim, Y. J.; Ishida, Y.; Hayakawa, T.; Kakimoto, M.; Nealey, P. F.; Gopalan, P. *Adv Mater* **2009,** 21, (43), 4334.

27. Chuang, V. P.; Ross, C. A.; Gwyther, J.; Manners, I. *Adv Mater* **2009,** 21, (37), 3789-3793.

28. Liu, C. C.; Nealey, P. F.; Ting, Y. H.; Wendt, A. E. *J Vac Sci Technol B* **2007,** 25, (6), 1963-1968.

29. Ting, Y. H.; Park, S. M.; Liu, C. C.; Liu, X. S.; Himpsel, F. J.; Nealey, P. F.; Wendt, A. E. *J Vac Sci Technol B* **2008,** 26, (5), 1684-1689.

30. Cheng, J.; Lawson, R.; Yeh, W.; Jarnagin, N.; Peters, A.; Tolbert, L.; Henderson, C. L. *Proceedings of SPIE* **2012,** 8323, 83232R.

31. Jarnagin, N.; Cheng, J.; Peters, A.; Yeh, W.; Lawson, R.; Tolbert, L.; Henderson, C. L. *Proceedings of SPIE* **2012,** 8323, 832310.

32. Gokan, H.; Esho, S.; Ohnishi, Y. *J Electrochem Soc* **1983,** 130, (1), 143-146.

33. Quinn, J. D.; Register, R. A. *Journal of Polymer Science: Part B: Polymer Physics* **2009,** 47, 2106-2113.

34. Roland, B. *Microelectron Eng* **1991,** 13, (1-4), 11-18.

35. Macdonald, S. A.; Schlosser, H.; Ito, H.; Clecak, N. J.; Willson, C. G. *Chem Mater* **1991,** 3, (3), 435-442.

36. Somervell, M. H.; Fryer, D. S.; Osborn, B.; Patterson, K.; Byers, J.; Willson, C. G. *J Vac Sci Technol B* **2000,** 18, (5), 2551-2559.

37. Pierrat, C.; Tedesco, S.; Vinet, F.; Lerme, M.; Dalzotto, B. *J Vac Sci Technol B* **1989,** 7, (6), 1782-1786.

38. Sinha, A.; Hess, D. W.; Henderson, C. L. *Electrochem Solid St* **2006,** 9, (11), G330-G333.

39. Sinha, A.; Hess, D. W.; Henderson, C. L. *J Electrochem Soc* **2006,** 153, (5), G465-G469.

40. Sinha, A.; Hess, D. W.; Henderson, C. L. *J Vac Sci Technol B* **2006,** 24, (6), 2523-2532.

41. Sinha, A.; Hess, D. W.; Henderson, C. L. *J Vac Sci Technol B* **2007,** 25, (5), 1721-1728.

42. George, S. M. *Chem Rev* **2010,** 110, (1), 111-131.

43. Peng, Q.; Tseng, Y. C.; Darling, S. B.; Elam, J. W. *ACS Nano* **2011,** 5, (6), 4600-4606.

44. Peng, Q.; Tseng, Y. C.; Darling, S. B.; Elam, J. W. *Adv Mater* **2010,** 22, (45), 5129.

45. Xie, Q.; Jiang, Y. L.; Detavernier, C.; Deduytsche, D.; Van Meirhaeghe, R. L.; Ru, G. P.; Li, B. Z.; Qu, X. P. *J Appl Phys* **2007,** 102, (8).

CHAPTER 5

HIGH χ SILICON CONTAINING BLOCK COPOLYMER: SYNTHESIS, PHASE SEPARATION, AND SELECTIVE BLOCK REMOVAL

A PTMSS-b-PHOST material was investigated as a high χ block copolymer with high oxygen plasma etch contrast between the domains. PTMSS-b-PHOST with symmetric volume fraction between the blocks was synthesized with controlled molecular weight (M_n=17300-26800 g/mol) and low PDI (~1.2) using nitroxide mediated polymerization techniques. Processing conditions were explored and optimized to facilitate phase separation of vertical lamellar patterns (pitch 32-40 nm). A random copolymer, poly(trimethylsilylstyrene)-r-poly(hydroxystyrene)-r-poly(glycidyl methacrylate) (i.e. PTMSS-r-PHOST-r-PGMA), was synthesized which exhibited a relatively neutral contact angle for PTMSS-b-PHOST and facilitated vertical lamellae formation. Phase separation was attempted with both thermal and solvent annealing, with ethyl acetate solvent annealing providing vertical lamellar patterns. PTMSS and PHOST homopolymer films exhibited high etch contrast when exposed to oxygen plasma etching. The film thickness loss of PTMSS homopolymer films rapidly plateaued at 10 nm after about 20 s etch time, while the PHOST exhibited a linear etch rate (~1.9 nm/s). PTMSS-b-PHOST phase separated patterns were exposed to oxygen plasma allowing selective block removal of the PHOST domain as indicated by SEM cross section analysis.

5.1 Introduction

Block copolymer (BCP) thin film patterns have shown excellent promise as templates for semiconductor device manufacturing, since they have the potential to produce patterns with dimensions at relevant nanometer length scales[1, 2]. The most widely used block copolymer in current studies is poly(styrene)-b-poly(methylmethacrylate) (i.e. PS-b-PMMA); however, it lacks the thermodynamic driving force necessary for phase separation at 20 nm pitch length scales and below[3]. According to theory, phase separation of lamellar morphologies in diblock copolymers only occurs when χN>10.5, where χ is the Flory Huggins interaction parameter, and N is the total degree of polymerization for the diblock copolymer[4, 5]. Since block copolymer domain sizes scale as $\sim N^{2/3}$ in the strong segregation limit, to achieve small feature sizes requires the use of shorter block chain lengths[6-8]. In order to satisfy the requirement that χN>10.5 at the same time means that polymers with higher χ values must be used to achieve the smallest possible DSA feature sizes and pitches.

Production of diblock copolymers with higher χ values can be achieved by incorporating polymer blocks that have stronger interactions between monomers of the same type and which have interactions that are orthogonal in nature to the types of interactions between monomers of the second block type. One such example is poly(styrene)-b-poly(hydroxystyrene), PS-b-PHOST, which exhibits extensive hydrogen bonding networks in the PHOST block in conjunction with the PS polymer block that interacts primarily through quadrupolar interactions (Figure 5.1) [9]. In fact, recent studies show phase separation of thin film PS-b-PHOST provides sub 15 nm pitch lamellar morphology (Chapter 3).

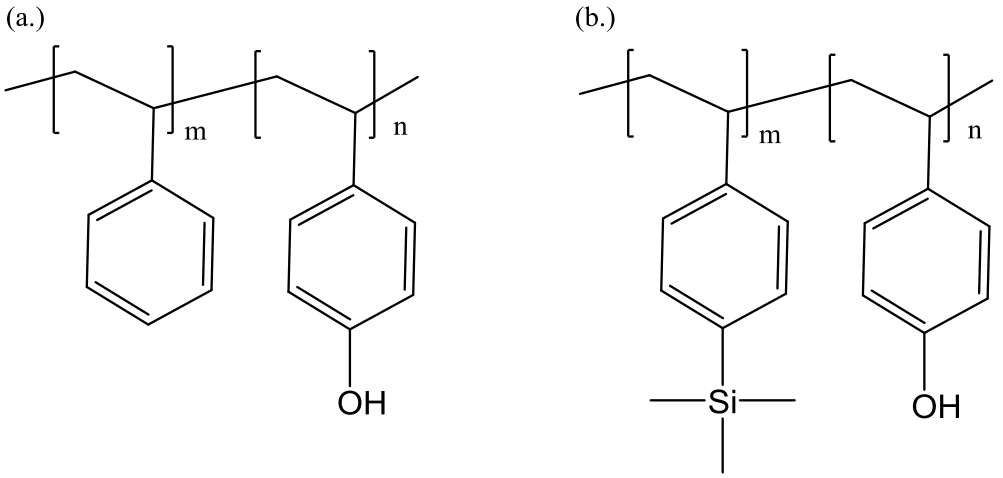

Figure 5.1 (a.) poly(styrene)-b-poly(hydroxystyrene) or PS-b-PHOST, (b.) poly(trimethylsilylstyrene)-b-poly(hydroxystyrene) or PTMSS-b-PHOST.

A key application of self assembled block copolymer films is high volume patterning of nanoelectronic devices[1, 10, 11]. Here, the block copolymer pattern serves as a lithographic template which can be transferred into the underlying silicon substrate[12]. Pattern transfer is performed through processes such as reactive ion etching, in which one of the blocks is selectively etched away, leaving the other block to serve as an etch resistant mask for pattern transfer to the underlying substrate. While PS-b-PHOST may exhibit the appropriate thermodynamic properties for high resolution block copolymer patterning, this material exhibits no etch contrast given PS and PHOST exhibit similar organic composition and similar Ohnishi number[13].

In order for PS-b-PHOST to exhibit selective block removal, some modification of the phase separated pattern is necessary. One approach is to use area selective atomic layer deposition to grow an oxide layer directly on the phase separated pattern. This approach utilizes the OH functionality on the PHOST to selective grow the etch barrier

on the PHOST domain. After ALD growth, the etch contrast between the PS and oxide is relatively high, and the PS domain is easily removed upon oxygen plasma etching. While this method has been used to effectively provide selective block removal of PS-b-PHOST patterns, the ALD process adds additional complexity and processing steps to the fabrication process (Chapter 4).

An alternative approach is to utilize a styrene derivative with a chemical functionality which exhibits high etch resistance in comparison with the PHOST block[14]. This approach avoids the additional processing steps associated with ALD, since the polymer itself exhibits high etch contrast. Here, polystyrene with trimethylsilyl functionality is used, which is readily converted to silicon oxide upon oxygen plasma etch, where SiO_2 exhibits high etch resistance and high thermal and mechanical stability in comparison with PHOST (Figure 5.1)[15, 16].

Silicon containing styrene derivatives are readily polymerized via nitroxide mediated polymerization with controlled molecular weights and low PDI, making these materials attractive candidates for formation of block copolymer patterns with targeted dimensions[17]. In fact, poly(pentamethyldisilylstyrene)-b-poly(acetoxystyrene) (PPMDSS-b-PAS) has been synthesized with NMP with demonstrated phase separation in thin films. However, this material exhibits lower χ in comparison to block copolymers with hydrogen bonding functionality in one of the blocks. If the acetoxy functionality was deprotected resulting in hydroxystyrene, the χ value would be dramatically increased allowing smaller pitch and sharper interface.

Recently, poly(trimethysilylstyrene)-b-polysaccharide (PTMSS-b-XGO) was prepared. Here, the TMS group provides high etch resistance, and the OH group on the

polysaccharide increases the incompatibility (χ) between the blocks (Figure 5.2)[18]. Here, PTMSS-b-XGO was synthesized with asymmetric volume fraction resulting in vertical cylinder morphology. While vertical cylinder forming morphology may be appropriate for bit patterned media applications, vertical lamellar morphology is more appropriate for the elaborate geometries associated with logic applications. Hence, silicon containing high χ block copolymers with symmetric volume fractions that enable lamellae formation should be investigated. Also, the PTMSS-b-XGO material was prepared via controlled anionic polymerization of PTMSS followed by coupling to an oligosaccharide group with defined molecular weight via click chemistry to provide the resulting block copolymer. PTMSS-b-PHOST is a promising alternative because it also contains silicon and hydrogen bonding functionality, yet both blocks are readily synthesized with controlled radical techniques with no coupling step required. Also, PHOST is a well studied material commonly found in semiconductor manufacturing. These issues motivate the investigation of PTMSS-b-PHOST lamellae forming block copolymers.

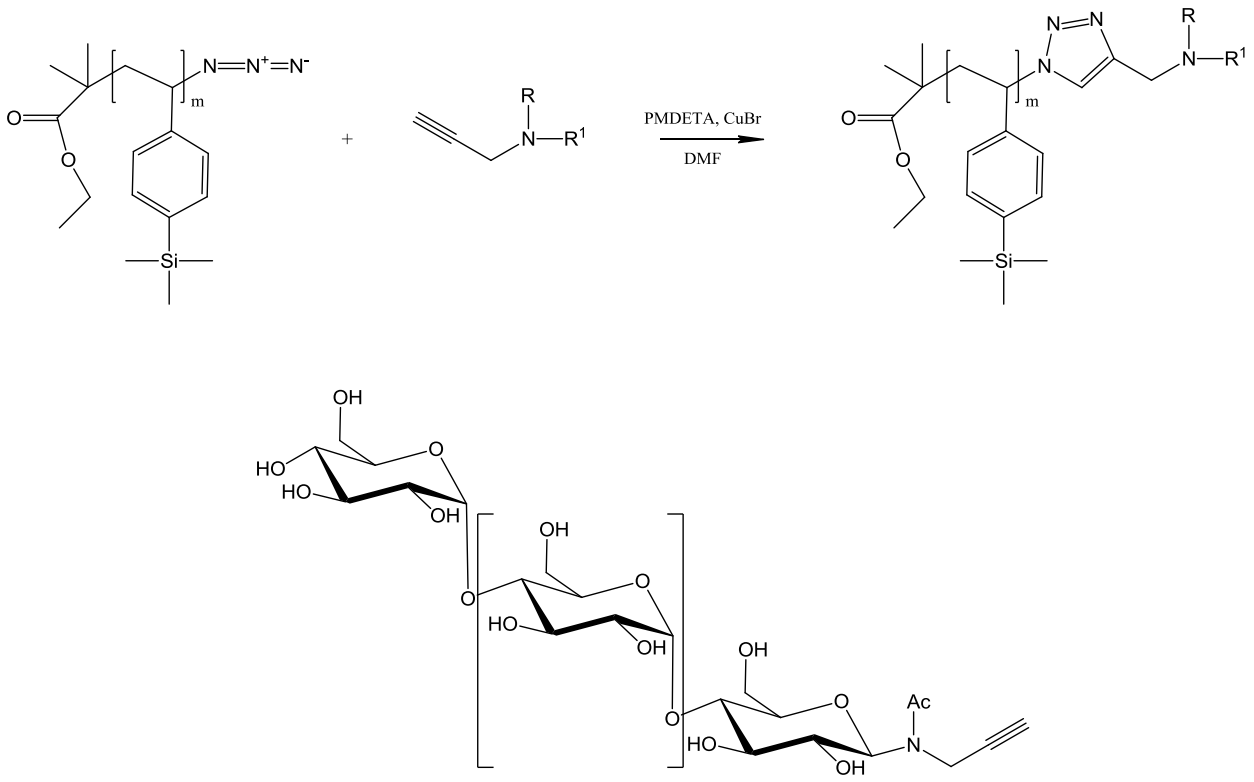

Figure 5.2. Azide-alkyne cycloaddition of the oligosaccharide/silicon containing block copolymer where R presents an oligosaccharide and R^1 represents acetate.

The goal of this work was to explore the high χ block copolymer PTMSS-b-PHOST and the associated processes required to achieve phase separation and selective block removal of vertical lamellar patterns. Here, nitroxide mediated polymerization was used to prepare PTMSS-b-PHOST with roughly 50/50 volume fraction allowing formation of lamellar structures. Figure 5.3 represents the PTMSS-b-PHOST processing scheme consisting of phase separation and selective block removal of the PHOST domain resulting in the high fidelity etch relief image of the fingerprint pattern. Here, the neutral underlayer is first spin coated onto the silicon substrate and cross linked via UV

exposure. The PTMSS-b-PHOST is then spin coated and solvent annealed with ethyl acetate resulting in phase separated vertical lamellar features. These patterns are exposed to oxygen plasma etch processing resulting in selective removal of the PHOST domain.

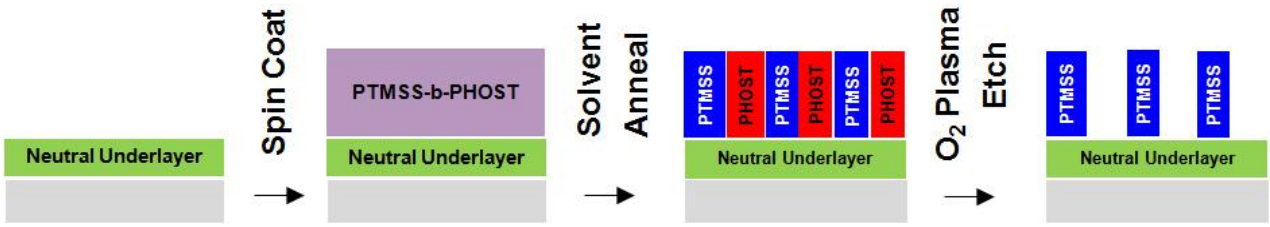

Figure 5.3 Process flow consisting of spin coating PTMSS-b-PHOST on cross-linked neutral underlayer, phase separation via solvent anneal, and selective removal of the PHOST block via oxygen plasma etch.

5.2 Experimental Section

5.2.1 Materials and Methods

All reagents were purchased from Sigma Aldrich or Acros Organics unless otherwise noted. Inhibitor was removed from the monomers immediately before polymerization with a glass column containing neutral alumina oxide. All other reagents were used as received. ^{1}H-NMR spectra were obtained using a Varian Mercury Vx 400 MHz spectrometer. All spectra were referenced to the residual solvent proton signal. Fourier transform infrared (FTIR) spectra from bulk samples (KBR pellet) were obtained using a Bruker Vertex 80v in transmission mode. Gel-permeation chromatography

(GPC) analysis was carried out using a Waters 1515 isocratic pump coupled to a Waters 2489 UV detector with THF as the eluant. All GPC measurements were carried out at a flow rate of 0.3 mL/min and 35 ˚C, and calibrated using narrow molecular weight polystyrene standards. Film thicknesses were measured using a Woollam M-2000V ellipsometer over a wavelength range of 350 nm to 1000 nm. Patterned samples were imaged using a Carl Zeiss Ultra60 SEM with 2-5 keV acceleration voltage.

5.2.2 Synthesis of Trimethylsilystyrene Monomer

About 3 mg iodine and 2.6 g (1.2 molar equiv) of freshly drilled magnesium turnings were added to a 250 mL round bottom flask with stir bar and condenser[19, 20]. The apparatus was flame dried while stirring the magnesium and a purple vapor arose from the iodine. After the apparatus was cooled, about 20 mL of THF was added to the magnesium and vigorously stirred to form a mixture. A solution of 11 mL chlorostyrene (1 molar equiv) and 11 mL THF was slowly added drop wise. Once the reaction began (observed via mild boiling of the reaction mix) the temperature was slowly raised to 55 ˚C. Additional dry THF (10 mL) was added as needed to limit the viscosity and temperature of the reaction.

After two hours when the majority of the magnesium had reacted, the solution was cooled to room temperature and an additional 40 mL of THF was added, next 11.2 mL neat chloro-trimethylsilane (1 equivalent) was slowly added dropwise. The solution was stirred overnight and quenched with excess brine. The product was extracted three times with diethyl ether, and the solvent was removed in vacuo to provide a clear yellow

liquid. The crude product was distilled under reduced pressure at 55 ˚C providing a clear colorless liquid (10.3 g, 78 % yield) (Figure 5.4).

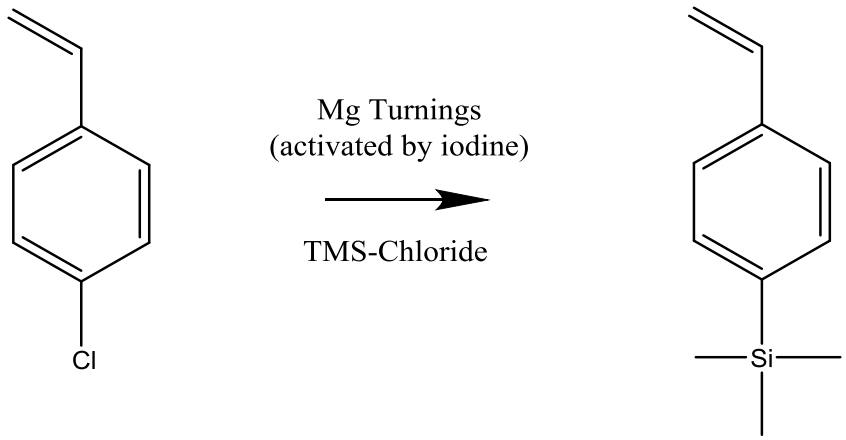

Figure 5.4 Synthesis of TMS-styrene via Grignard reaction of chlorostryrene with TMS-chloride.

5.2.3 Synthesis of Pentamethyldisilylstyrene Monomer

A Grignard reagent was prepared in a similar way to that of the TMS-Styrene using freshly drilled magnesium turnings (0.84 g, 1.2 molar equiv), and chlorostyrene (4.0 g, 1 molar equiv)[17]. Pentamethylchlorosilane (4.8 g, 1 molar equiv) was added to the Grignard solution with additional THF and the solution was stirred overnight, and quenched with excess brine. The product was extracted three times with diethyl ether, and the solvent was removed in vacuo to provided a clear yellow liquid. The crude product was distilled under reduced pressure at 45 ˚C providing a colorless clear liquid (4.5 g, 65 % yield) (Figure 5.5).

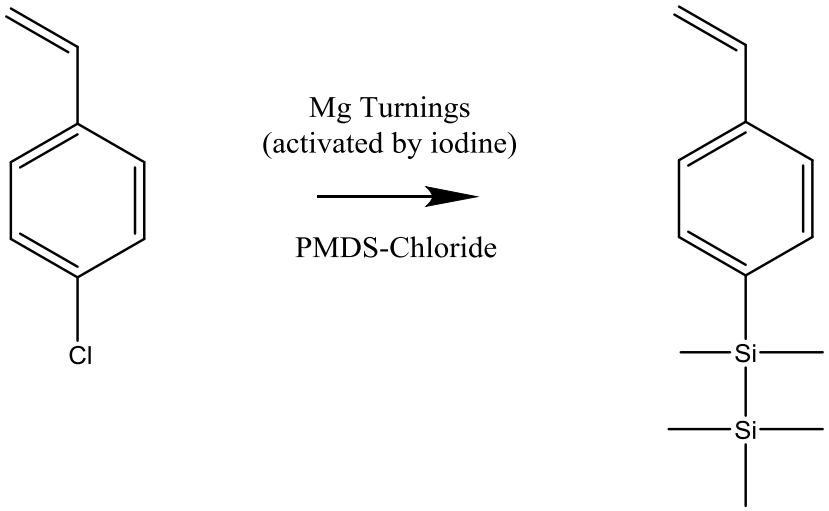

Figure 5.5 Synthesis of PMDS-styrene via Grignard reaction of chlorostryrene with PMDS-chloride.

5.2.4 Synthesis of Poly(trimethylsilylstyrene) (PTMSS) Homopolymer

A mixture of trimethylsilylstyrene (1.25 g, 7.09 mmol, 100 equiv), and universal NMP initiator (23 mg, 0.071 mmol, 1 equivalent), was added to a glass ampoule equipped with a magnetic stir bar. The reaction mixture was degassed through three freeze pump thaw cycles and sealed under vacuum. The mixture was warmed to room temperature, stirred for 10 min, and immersed in a pre-heated oil bath at 130 ˚C. After 14 hours, the reaction was quenched by quick immersion in liquid nitrogen. The viscous reaction mixture was dissolved in THF, precipitated in methanol at 0 ˚C, filtered, and dried under vacuum to yield a white powder. (0.93 g, 75% yield) M_n=17000 g/mol, PDI 1.40 (Figure 5.6).

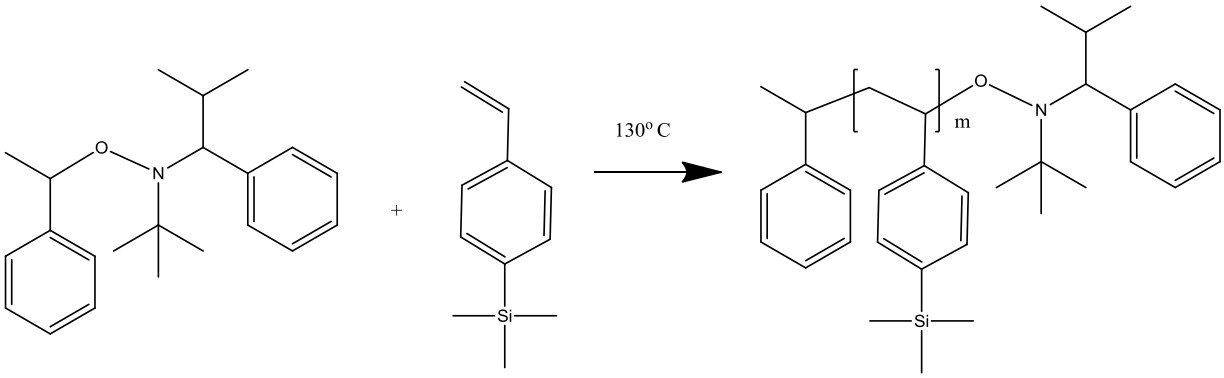

Figure 5.6 Nitroxide mediated polymerization of poly(trimethylstyrene).

5.2.5 Synthesis of Poly(pentamethyldisilystyrene) (PPMDSS) Homopolymer

The homopolymer poly(pentamethyldisilylstyrene) was prepared in a similar way to poly(trimethylsilylstyrene), using pentamethyldisilylstyrene (0.75 g, 3.20 mmol, 100 equiv) and universal NMP initiator (23 mg, 0.071 mmol, 1 equivalent) (Figure 5.7). The reaction mixture was degassed through three freeze pump thaw cycles and sealed under vacuum. The mixture warmed to room temperature, stirred for 10 min, and immersed in a pre-heated oil bath at 130 ˚C. After about 14 hours, the reaction was quenched by quick immersion in liquid nitrogen. The viscous reaction mixture was dissolved in THF, precipitated in methanol at 0 ˚C, filtered, and dried under vacuum to yield a white powder. (0.37 g, 55% yield) M_n=16300 g/mol, PDI 1.37.

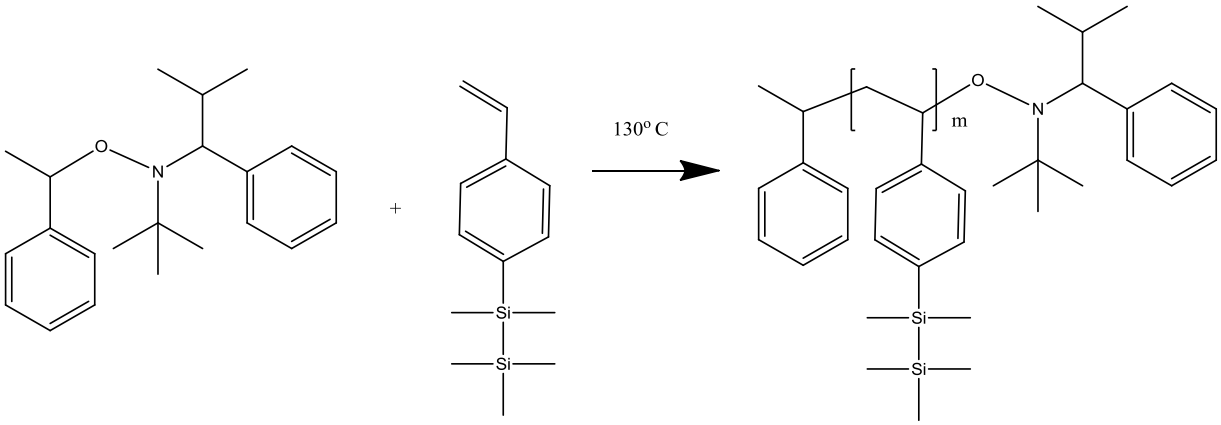

Figure 5.7 Nitroxide mediated polymerization of PPMDSS.

5.2.6 Synthesis of Poly(acetoxystyrene) (PAS) Macro-initiator

A mixture of acetoxystyrene (5.750 g, 37.6 mmol, 200 equiv), universal NMP initiator (60 mg, 0.19 mmol, 1 equivalent), and (2,2,5-trimethyl-4-phenyl-3-azahexane-3-nitroxide) (2 mg, 0.009 mmol, 0.05 equiv) was added to a glass ampoule equipped with a magnetic stir bar. The reaction mixture was degassed through three freeze pump thaw cycles and sealed under vacuum. The mixture was warmed to room temperature, stirred for 10 min, and immersed in a pre-heated oil bath at 125 ºC. After 4 hours, the reaction was quenched by quick immersion in liquid nitrogen. The viscous reaction mixture was dissolved in THF, precipitated with methanol at 0 ˚C, filtered, and dried under vacuum to yield a white powder. (1.48 g, 24% yield) M_n=10100 g/mol, PDI 1.26 (Figure 5.8).

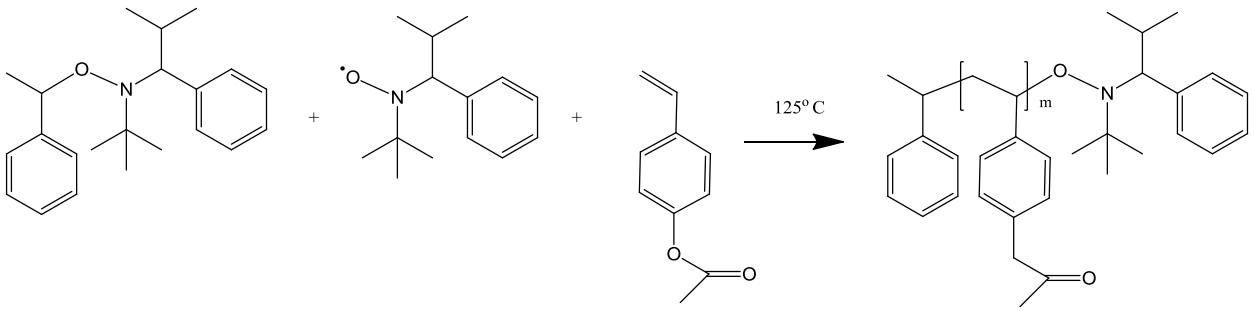

Figure 5.8 Nitroxide mediated polymerization of PAS macro-initiator.

5.2.7 Synthesis of Poly(trimethylsilylstyrene)-block-poly(hydroxystyrene) (PTMSS-b-PHOST) Block Copolymer

A mixture of trimethylsilylstyrene (3.5 g, 19.8 mmol, 400 equiv), and PAS macro-initiator with M_n=10100 g/mol (0.50 g, 0.05 mmol, 1 equivalent) was added to a glass ampoule equipped with a magnetic stir bar (Figure 5.9). Dry DMF (1.4 g) was added to dilute the reactants to about 35 weight percent of the reaction solution. The reaction mixture was degassed through three freeze pump thaw cycles and sealed under vacuum. The mixture was warmed to room temperature, stirred for 10 min, and immersed in a pre-heated oil bath at about 127.5 ˚C. After 1 hour and 40 min, the reaction was quenched by quick immersion in liquid nitrogen. The viscous reaction mixture was dissolved in dichloromethane, precipitated in methanol at 0 ˚C, filtered, and dried under vacuum to yield a white powder (0.48 g , 12% yield). PTMSS-b-PAS (9900-b-10100 g/mol), M_n=20000 g/mol, PDI=1.23.

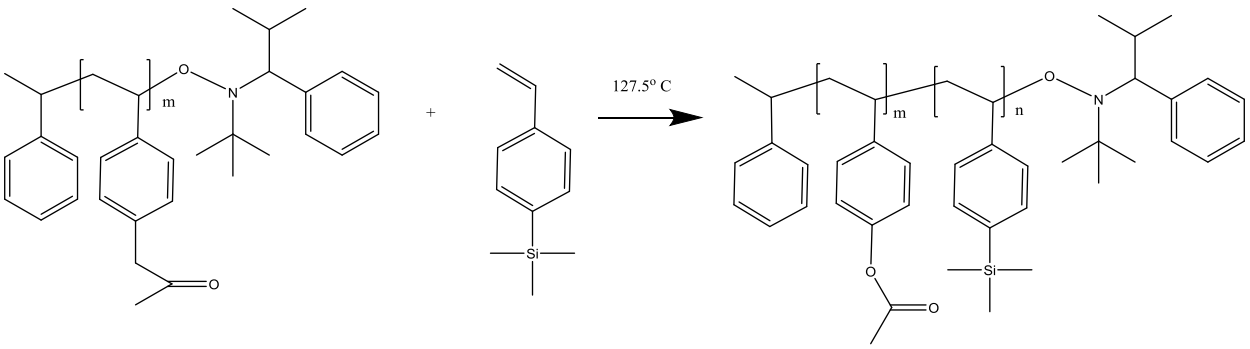

Figure 5.9 Nitroxide mediated polymerization of PAS-b-PTMSS using PAS macro-initiator.

Removal of the acetyl protecting group from the PAS block was accomplished via hydrazinolysis, (hydrazine hydrate in ca. 2:1 ratio by weight of the PAS block) (Figure 5.10) . PTMSS-b-PAS (9900-b-10100 g/mol) (0.21 g) was added to dioxane (1.3 mL) containing hydrazine hydrate (0.16 g) and stirred for 6 hours under nitrogen. The resulting mixture was added to a large excess of 5% aqueous hydrochloric acid and stirred for several hours. The block copolymer product was washed with excess deionized water and isolated by centrifugation, followed by drying under vacuum at room temperature overnight, providing PTMSS-b-PHOST(9900-b-7100 g/mol) with M_n of 17000 g/mol assuming full deprotection. The polymer was characterized by ^{1}H-NMR, and FT-IR analysis.

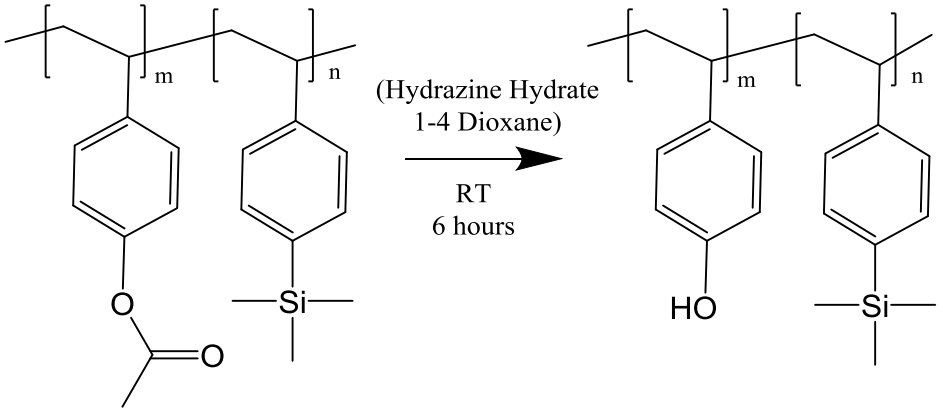

Figure 5.10 Deprotection of acetoxystyrene using hydrazinolysis.

5.2.8 Synthesis of Poly(trimethylsilylstyrene)-r-poly(hydroxystyrene)-r-poly(glycidyl methacrylate) (PTMSS-r-PHOST-r-PGMA) Cross-linked Neutral Underlayer

A mixture of trimethylsilyl styrene (0.28 g, 1.59 mmol, 25 equiv), 4-acetoxystyrene (0.62 g, 3.8 mmol, 60 equiv), glycidyl methacrylate (0.14 g, 0.95 mmol, 15 equiv), and azobisisobutyronitrile (0.02 g, 0.127 mmol, 2 equiv) was added to a glass ampoule with 1 mL DMF and equipped with a magnetic stir bar (Figure 5.11). The reaction mixture was degassed through three freeze pump thaw cycles and sealed under vacuum. The mixture was warmed to room temperature, stirred for 10 min, and immersed in a pre-heated oil bath at 65 ºC. After 18 hours, the reaction was quenched by quick immersion in liquid nitrogen. The viscous reaction mixture was dissolved in THF, precipitated with methanol at 0 ºC, filtered, and dried under vacuum to yield a white powder (0.4 g, 40% yield). M_n=32000 g/mol, PDI=1.4. The molar composition was determined by ^{1}H-NMR analysis to be (PTMSS25-r-PAS72-r-PGMA3). Finally, the

acetoxystyrene was deprotected via hydrazinolysis. *NMR data used in calculating molar composition: ^{1}H-NMR (300MHz, Acetone-d, ppm), δ 0.35-(-0.21) (trimethylsilyl region), 4.10-3.02 (COO-CH$_2$ on glycidyl functional group)2.47-2.10 (acetoxy group).*

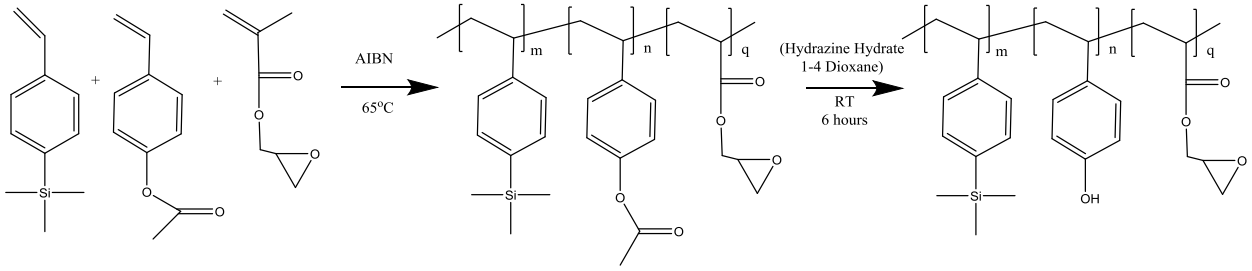

Figure 5.11 Synthesis of PTMSS-r-PAS-r-PGMA using traditional radical polymerization with AIBN initiator followed by deprotection of acetoxystyrene using hydrazinolysis to yield PTMSS-r-PHOST-r-PGMA.

Neutral cross-linked underlayer films were made by spin casting in PGMEA with TPS-N1 photoacid generator (PAG), 5 wt% of polymer, followed by baking at 90º C for 2 min to remove the casting solvent, which resulted in 20 nm films as measured by ellipsometry. Films were cross linked via deep ultraviolet exposure (Oriel Instruments 500W Hg-Xe arc lamp with a 248 nm band-pass filter) followed by post exposure bake at 120 ºC for 120 s and sonication for 10 min in PGMEA to remove uncross-linked polymer (normalized remaining thickness was about 0.9).

5.2.9 Preparation of Poly(trimethylsilylstyrene)-block-poly(hydroxystyrene) (PTMSS-b-PHOST) Fingerprint Patterns by Solvent Annealing

Solutions of 1-3 wt% PTMSS-b-PHOST in PGMEA were spin cast on neutral underlayers using a poly(tetrafluoroethylene) (PTFE) filter (0.2 μm pore size), baked at 120 °C for 2 min to remove casting solvent . BCP films were solvent annealed in sealed flasks with 0.4 mL dry ethyl acetate liquid added to each 250 mL flasks. Sealed flasks were purged with nitrogen before and after annealing to remove excess water. Anneal time was varied according to the polymer molecular weight and film thickness.

5.2.10 Reactive Ion Etching and Thin Film Characterization of Homopolymer and Block Copolymer Thin Films

The polymer films were reactive ion etched (RIE) using 5 sccm O_2, 5 sccm argon, 100 W, and 0.035 Torr (Oxford Endpoint RIE Plasmalab 80Plus). The O_2 allows selective removal of the organic material, while argon bombardment assists in improving the anisotropy of the etch to minimize under cutting of the oxide pattern. Film thicknesses were measured using a Woollam M-2000V ellipsometer over a wavelength range of 350 nm to 1000 nm. Contact angle goniometry was conducted using a VCA 2500-XE contact angle system with 1 μL drop size. Patterned samples were imaged using a Carl Zeiss Ultra60 SEM with 1-5 keV acceleration voltage. Dimensions of fingerprint patterns were determined from SEM analysis by averaging from five different areas with an inspection length of about 400 nm. Dimensions were also verified by 2D fast Fourier transform analysis (Gwyddion 2.26 data visualization and analysis tool). The SEM images were cropped to remove the data label, then 2D FFT filtered to remove long

range artifacts due to charging from the SEM exposure. The resulting SEM image was FFT processed. The pitch was determined by taking a cut line through the FFT and measuring the distance from the center to the area of high intensity.

5.3 Results

5.3.1 Synthesis of Poly(trimethylsilylstyrene)-block-poly(hydroxystyrene) (PTMSS-b-PHOST) Block Copolymer via Nitroxide Mediated Polymerization

PTMSS-b-PHOST was prepared by nitroxide mediated polymerization of PTMSS-b-PAS followed by deprotection of the acetoxystyrene. Here, a thermally labile alkoxyamine initiator was used which showed improved control of molecular weight and PDI of styrene derivatives in comparison with the commonly used TEMPO initiator. Initial attempts to use the PTMSS macro-initiator to grow the PAS block were unsuccessful. GPC analysis of the material after polymerization of the second block showed a low molecular weight shoulder. Nature of the shoulder, whether unreacted poly(trimethylstyrene) or early terminated PTMSS-b-PAS, is unknown. The reverse strategy using poly(acetoxystyrene) to initiate the growth of the polystyrene block proved successful, providing PTMSS-b-PAS with controlled molecular weight and low PDI. The polymer was characterized by NMR, and FT-IR analysis (Appendix B). Loss of the acetoxy peak at 2.25 ppm indicates complete deprotection of the acetoxy group. Loss of the carbonyl peak at 1757 cm^{-1} and appearance of the hydroxyl peak at 3350 cm^{-1} also indicate deprotection. To prepare materials with targeted molecular weight and low

PDI, reaction times were limited and relatively high monomer to initiator ratios were used. This general procedure allowed preparation of PTMSS-b-PHOST with a range of molecular weights (M_n=17300-26800 g/mol), and low PDI (~1.2) (Table 5.1).

Table 5.1 The number average molecular weight, degree of polymerization, and PDI of PTMSS-b-PHOST materials prepared in this investigation. Also shown is the observed pitch and morphology for each associated molecular weight.

Number Average Molecular Weight				Degree of Polymerization			Volume Fraction			
PHOST (g/mol)	PTMSS (g/mol)	Total (g/mol)	PDI	PHOST	PTMSS	N total	PHOST	PTMSS	Morphology	Pitch (nm)
7400	19000	26800	1.22	62	110	172	0.27	0.73	Cylinders	37(±2.3)
7400	9900	17300	1.23	62	56	118	0.42	0.58	Lamellae	32(±1.5)
10300	11000	21300	1.22	86	62	148	0.48	0.52	Lamellae	40(±2.8)

5.3.2 Poly(trimethylsilylstyrene)-r-poly(hydroxystyrene)-r-poly(glycidylmethacrylate) (PTMSS-r-PHOST-r-PGMA) Cross-linked Neutral Underlayer

When a BCP is confined to a thin film, the morphology is critically dependent on the surface energies at the block copolymer/substrate interface. In order to form vertical lamellae, the underlayer must be approximately neutral with respect to its interactions with each block of the BCP. This avoids preferential wetting of either block with the substrate, a situation that results in lamellae oriented parallel to the substrate surface. Polymer mats, which are thin film cross-linked polymer networks, are commonly used as one method to control the interfacial interactions and wetting behavior of the BCP substrate[21]. By adjusting the monomer composition and crosslink density, the chemical composition of the surface can be modified to be neutral with respect to each block of the BCP[22, 23].

In this work, A series of random copolymers were prepared as potential neutral underlayer substrates for PTMSS-b-PHOST. These poly(trimethylsilylstyrene)-r-poly(hydroxystyrene)-r-poly(glycidyl methacrylate) (PTMSS-r-PHOST-r-PGMA) materials were prepared by solution polymerization utilizing azoisobutyronitrile (AIBN) as the radical initiator (Table 5.2). This material utilized glycidyl methacrylate to cross link the material after spin coating to form an insoluble cross-linked mat. The relative neutrality of these materials in thin films was determined by contact angle analysis. Here, the observed contact angle of PTMSS42-r-PHOST56-r-PGMA12 was 90.4˚, which

was approximately the average of the measured contact angle of PHOST (106˚) and PS (73˚) suggesting this material is neutral toward the PTMSS-b-PHOST block copolymer (Figure 5.12). It should be noted that PS brush substrates also exhibited a contact angle of about 90˚, hence this substrate was also used as a neutral underlayer for PTMSS-b-PHOST patterning.

Table 5.2 The molar feed ratio, polymer composition, molecular weight, yield, PDI, and contact angle of PTMSS-r-PHOST-r-PGMA materials prepared in this investigation.

Mole Feed Ratio			Polymer Composition			% Yield	Contact Angle (˚) after deprotection
TMSS	PAS	GMA	TMSS	PAS	GMA		
82.5	2.5	15	82	13	1	33	105 (±0.6)
76.5	8.5	15	76	21	3	68	100 (±2.0)
70	15	15	74	25	1	69	101 (±0.7)
55	30	15	58	40	2	52	96.6 (±0.9)
40	45	15	42	56	2	40	90.4 (±1.2)
25	60	15	25	72	3	38	77.6 (±2.0)

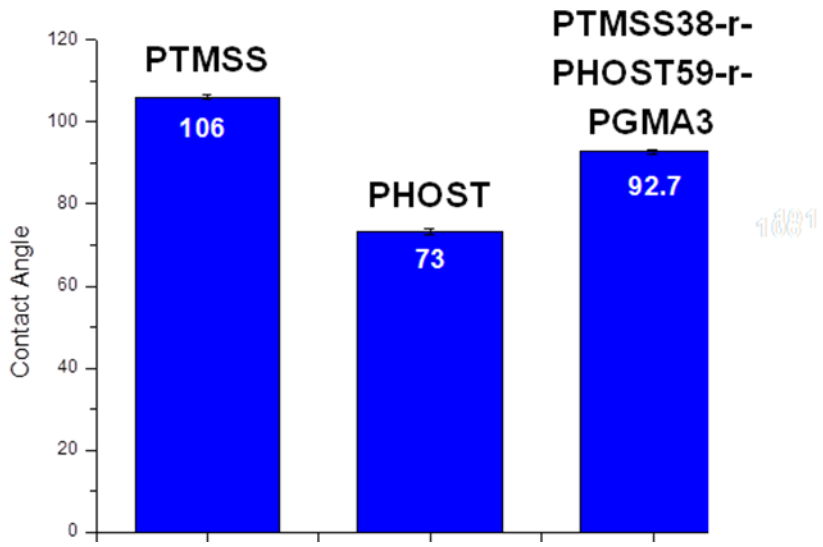

Figure 5.12 Measured contact angle (degrees) of PS, PHOST, and (PTMSS38-r-PHOST59-r-PGMA3) thin films.

5.3.3 Anneal Processes Associated with Phase Separation

Initial investigation of the phase separation behavior of PTMSS-b-PHOST utilized thermal annealing. Samples were annealed for 5 days under N_2 atmosphere at 190 ˚C, a temperature above the glass transition temperature of PTMSS (102 ˚C) and PHOST (180 ˚C). Higher anneal temperatures were not utilized to prevent samples from degrading (See Appendix B for thermogravimetric analysis of PTMSS-b-PHOST). SEM analysis of the thermally annealed PTMSS-b-PHOST(10300-b-11000) block copolymer showed an absence of well formed fingerprint lamellar features (Figure 5.13). This could be due to the favorable interaction of PTMSS (which has relatively low surface energy)

with air resulting in horizontal lamellae or a PTMSS skin on the surface of the thin film[24]. This result motivated the use of solvent annealing for the remainder of this investigation.

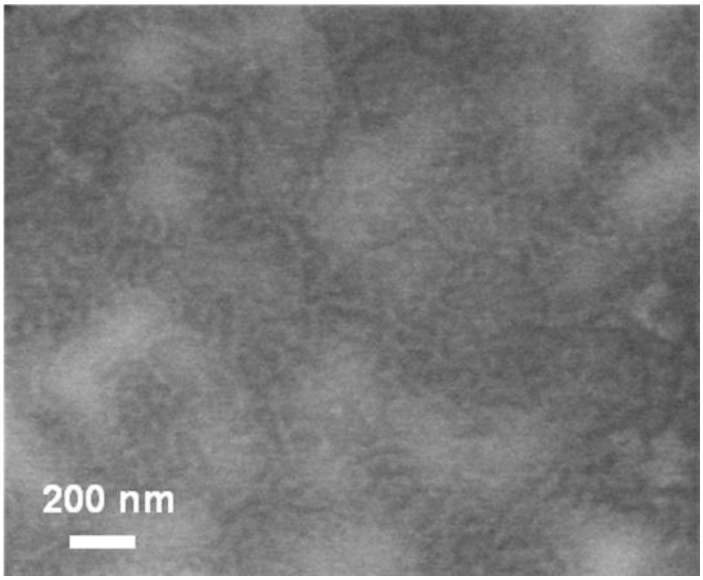

Figure 5.13 Top down SEM analysis of PTMSS10.3k-b-PHOST11k thermally annealed at 190 ˚C for 5 days.

Choice of annealing solvent is critical to avoid cylinder formation via preferential swelling of one of the blocks, and to avoid dewetting of the BCP films upon annealing[25]. Hence, annealing solvent should exhibit similar compatibility between both polymer blocks. Polymer/solvent compatibility was estimated by comparing the relative Hansen solubility parameters (which include dispersion, polar, and hydrogen bonding interactions) of the solvent and each block of the polymer (Equation 5.1)[26]. The solubility parameters of the solvents and PHOST (δ_d=23.6 MPa$^{1/2}$, δ_p=6.6 MPa$^{1/2}$, δ_h=16.1 MPa$^{1/2}$) were experimentally determined, while the solubility parameters of

PTMSS were determined via group contribution methods (δ_d=30.6 $MPa^{1/2}$, δ_p=1.2 $MPa^{1/2}$, δ_h=0 $MPa^{1/2}$)[27]. Table 5.3 represents the calculated Rsolv/PS and Rsolv/PHOST, where the smaller difference in R values ((Rsolv/PS-Rsolv/PHOST)^2) suggests similar compatibility between the solvent and each block of PTMSS-b-PHOST. Based on these calculated solubility parameters, ethyl acetate should provide the most similar compatibility with each block. Also, as a further test, homopolymer films of PHOST and PTMSS where annealed in ethyl acetate atmosphere which remained homogeneous with no observed dewetting. Hence, ethyl acetate was used as the primary annealing solvent for this study.

$$R^2 = 4(\delta_{d1} - \delta_{d2})^2 + (\delta_{p1} - \delta_{p2})^2 + (\delta_{h1} - \delta_{h2})^2 \qquad (5.1)$$

Table 5.3 R(polymer/solvent) represents the compatibility between the polymer and the solvent. [R(PTMSS/solv)-R (PHOST/solv)]^2 represents the relative difference in compatibility with the solvent and each block of the BCP.

	R (PTMSS/solv) ($MPa^{1/2}$)	R (PHOST/solv) ($MPa^{1/2}$)	[R(PTMSS/solv)-R(PHOST/solv)]^2 (MPa)
Acetone	12	8	17.0
Chlorobenzene	8	13	24.7
Chloroform	8	11	7.4
Cyclohexanone	9	9	0.1
Dichloromethane	10	9	2.3
Ethyl acetate	9	9	0.0
MiBK	7	11	20.0
1-Octanol	13	7	31.1
THF	10	7	6.6

5.3.4 Phase Separation of Poly(trimethylsilylstyrene)-block-poly(hydroxystyrene) (PTMSS-b-PHOST) Fingerprint Patterns

Phase separation of PTMSS-b-PHOST followed the same methodology as the phase separation which provided uniform lamellar fingerprint patterns for PS-b-PHOST materials. Here, a non-selective solvent, ethyl acetate, was chosen by Hansen solubility parameters estimates. Dry ethyl acetate and nitrogen purging of annealing flask was utilized to avoid dewetting and condensation of water. A relatively neutral underlayer was used (as indicated by contact angle analysis) to promote vertical lamellae formation.

Also, PTMSS-b-PS films were spin coated at a range of thicknesses and annealed for about 10 hours with 0.4 mL dry liquid ethyl acetate per 250 mL flask. The phase separated results of PTMSS-b-PHOST are summarized in Figures 5.14-5.16. As expected, samples with highly asymmetric volume fractions (0.27 volume fraction of PHOST) exhibited cylinder morphology, while samples with nearly symmetrical volume fraction (between 0.4 and 0.6 volume fraction for the PHOST block) exhibited lamellar fingerprint morphology. Two different substrates, PS brush and PTMSS38-r-PHOST59-r-PGMA3, exhibited a neutral contact angle with respect to PTMSS-b-PHOST and enabled vertical lamellar morphology.

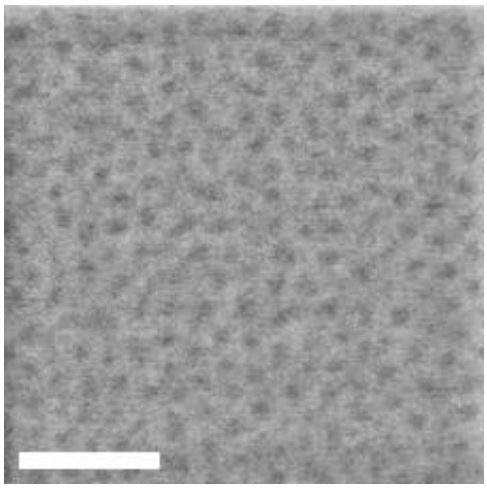

Figure 5.14 SEM analysis of solvent annealed PTMSS-b-PHOST (19300-b-7400) (30 nm thick film) (pitch=37.3 nm ±2.3) on PTMSS42-b-PHOST56-r-PGMA2 underlayer. Scale bar is 100 nm.

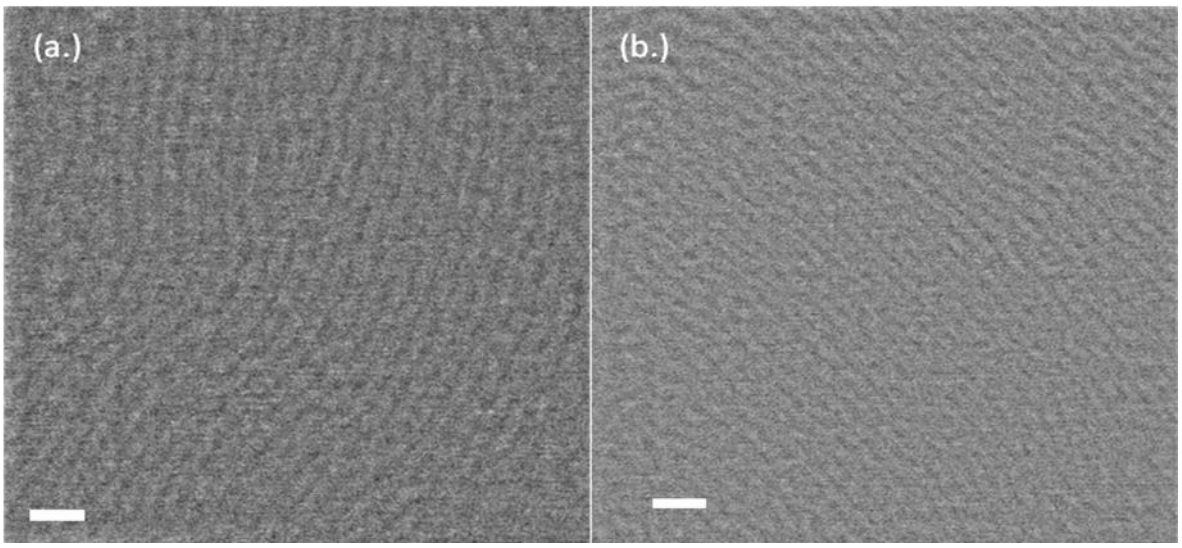

Figure 5.15 SEM analysis of solvent annealed PTMSS-b-PHOST (9900-b-7400) (30 nm thick film) (pitch=32.2 nm ±1.5): (a.) on PS Brush underlayer, (b.) on (PTMSS42-b-PHOST56-r-PGMA2) underlayer. Scale bar is 100 nm.

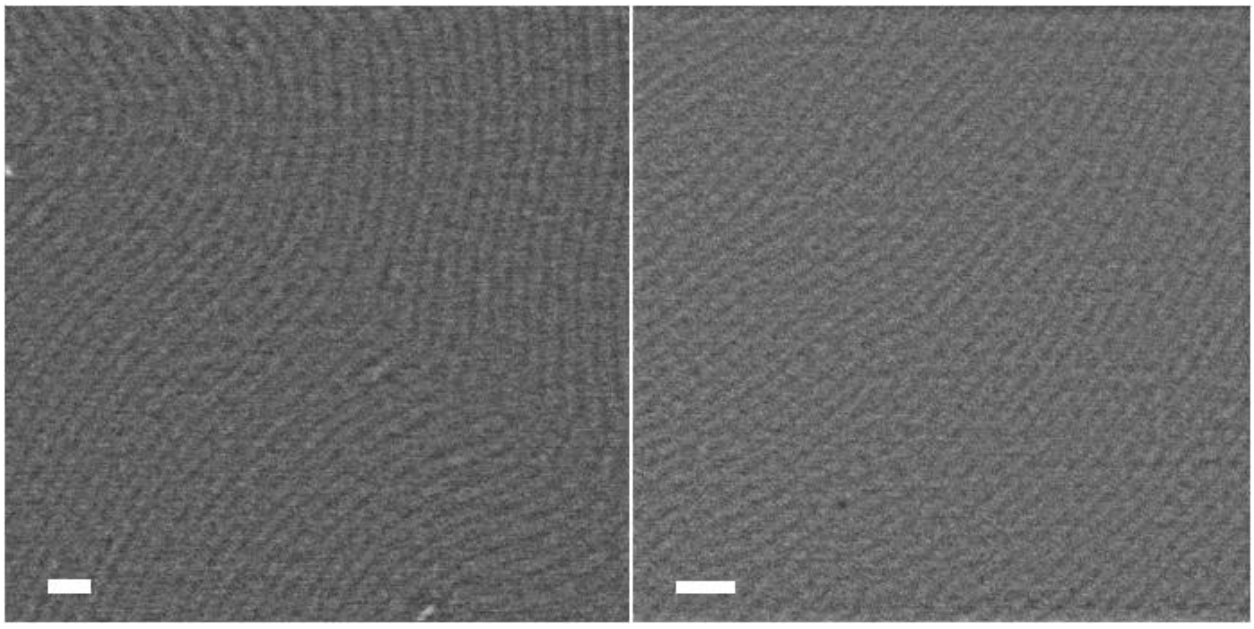

Figure 5.16 SEM analysis of solvent annealed PTMSS-b-PHOST (10300-b-11000) (42 nm thick film) (pitch=41.0 nm ±2.8): (a.) on PS Brush underlayer, (b.) on (PTMSS42-b-PHOST56-r-PGMA2) underlayer. Scale bar is 100 nm.

5.3.5 Etch Studies of Homopolymer Thin Films and Block Copolymer Thin Film Vertical Lamellar Patterns

The etch rate of PTMSS, PPMDSS, and PHOST was investigated by exposing the homopolymer films to oxygen plasma etch, and evaluating the change in thickness via spectroscopic ellipsometry. The PHOST homopolymer films exhibited a linear etch rate of 1.9 nm/s, while the thickness loss of silicon containing homopolymer films plateaued after 20 s (Figure 5.17). It should be noted that the silicon containing homopolymer materials lost about 10 nm of film thickness regardless of the initial film thickness. Both PTMSS and PPMDSS both exhibited similar etch resistance, hence this study simply focused on PTMSS for the remainder of this investigation. Further detailed etch investigation is required to determine the real effect of silicon content on oxygen plasma etch resistance for silicon containing block copolymers After demonstrating high etch contrast between PHOST and the silicon containing homopolymers, this etch process was used to selectively remove the PHOST block in solvent annealed PTMSS-b-PHOST fingerprint patterns. Here, these patterns were exposed to reactive ion etching for 40 s (5 sccm O_2, 5 sccm Ar, 100W, and 0.035 Torr). Cross sectional SEM analysis clearly showed selective block removal of the PHOST and conversion of the PTMSS block into SiO_2 functionality which exhibited high etch resistance (Figure 5.18).

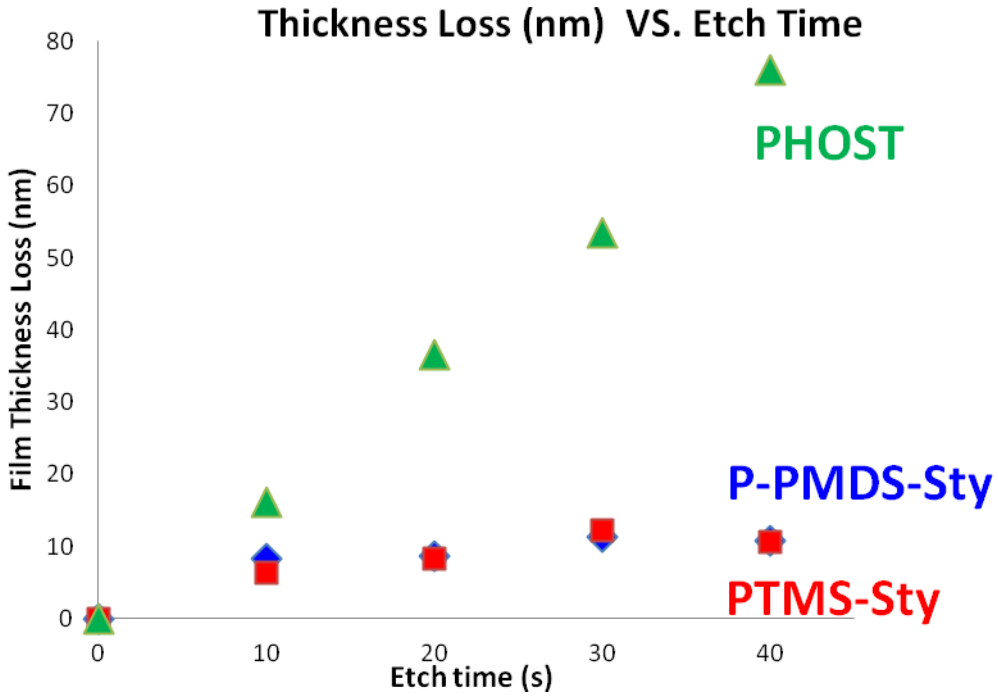

Figure 5.17 Homopolymer film thickness loss as a function of etch time for PHOST (green), PPMDSS (blue), and PTMSS (red). Etch conditions include 5 sccm O_2, 5 sccm Ar, 100 W, 0.035 Torr.

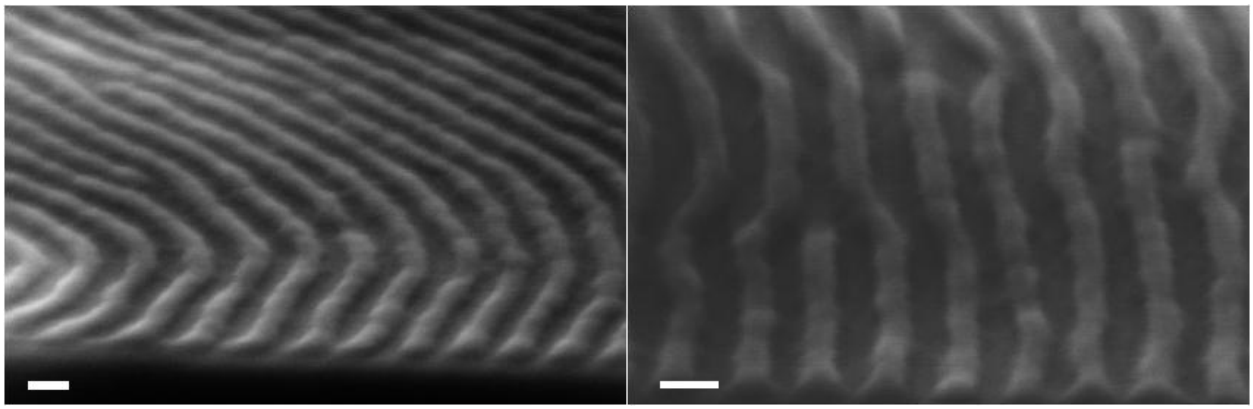

Figure 5.18 Cross sectional SEM analysis of PTMSS-b-PHOST (11000-b-10300) fingerprint patterns (32 nm film thickness) exposed to reactive ion etching. Etch conditions include 5 sccm O_2, 5 sccm Ar, 100 W, 0.035 Torr, and 40 s etch time. Scale bar is 30 nm.

5.4 Conclusions

PTMSS-b-PHOST material was investigated as a high χ block copolymer with large oxygen plasma etch contrast between the domains. PTMSS-b-PHOST with symmetric volume fraction between the blocks was synthesized with controlled molecular weight (17300-26800) and low PDI (~1.2) using nitroxide mediated polymerization techniques. Processing conditions were explored and optimized to facilitate phase separation of vertical lamellar patterns. Here, a random copolymer PTMSS-r-PHOST-r-PGMA was synthesized which exhibited a relatively neutral contact angle for PTMSS-b-PHOST and facilitated vertical lamellae formation. Phase separation was attempted with both thermal and solvent annealing, with solvent annealing (with ethyl acetate) providing vertical lamellar patterns.

PTMSS and PHOST homopolymer films exhibited high etch contrast when exposed to oxygen plasma etching. The film thickness loss of PTMSS homopolymer films rapidly plateaued as a function of etch time (with about 10 nm total film thickness loss), indicating conversion of the TMS group to etch resistant silicon dioxide functionality. PTMSS-b-PHOST phase separated patterns were exposed to oxygen plasma allowing selective block removal of the PHOST domain as indicated by SEM cross section analysis.

5.5 References

1. Herr, D. J. C. *J Mater Res* **2011,** 26, (2), 122-139.

2. Kim, H. C.; Hinsberg, W. D. *J Vac Sci Technol A* **2008,** 26, (6), 1369-1382.

3. Russell, T. P.; Hjelm, R. P.; Seeger, P. A. *Macromolecules* **1990,** 23, (3), 890-893.

4. Leibler, L. *Macromolecules* **1980,** 13, (6), 1602-1617.

5. Bates, F. S. *Science* **1991,** 251, (4996), 898-905.

6. Bates, F. S.; Fredrickson, G. H. *Annu Rev Phys Chem* **1990,** 41, 525-557.

7. Bates, F. S.; Fredrickson, G. H. *Phys Today* **1999,** 52, (2), 32-38.

8. Matsushita, Y.; Mori, K.; Saguchi, R.; Nakao, Y.; Noda, I.; Nagasawa, M. *Macromolecules* **1990,** 23, (19), 4313-4316.

9. Cheng, J.; Lawson, R.; Yeh, W.; Jarnagin, N.; Peters, A.; Tolbert, L.; Henderson, C. L. *Proceedings of SPIE* **2012,** 8323, 83232R.

10. Ruiz, R.; Kang, H. M.; Detcheverry, F. A.; Dobisz, E.; Kercher, D. S.; Albrecht, T. R.; de Pablo, J. J.; Nealey, P. F. *Science* **2008,** 321, (5891), 936-939.

11. Stoykovich, M. P.; Nealey, P. F. *Mater Today* **2006,** 9, (9), 20-29.

12. Ting, Y. H.; Park, S. M.; Liu, C. C.; Liu, X. S.; Himpsel, F. J.; Nealey, P. F.; Wendt, A. E. *J Vac Sci Technol B* **2008,** 26, (5), 1684-1689.

13. Gokan, H.; Esho, S.; Ohnishi, Y. *J Electrochem Soc* **1983,** 130, (1), 143-146.

14. Cushen, J. D.; Bates, C. M.; Rausch, E. L.; Dean, L. M.; Zhou, S. X.; Willson, C. G.; Ellison, C. J. *Macromolecules* **2012,** 45, (21), 8722-8728.

15. Watanabe, F.; Ohnishi, Y. *J Vac Sci Technol B* **1986,** 4, (1), 422-425.

16. Hartney, M. A.; Chiang, J. N.; Hess, D. W.; Soane, D. S. *Appl Phys Lett* **1989,** 54, (16), 1510-1512.

17. Fukukawa, K.; Zhu, L.; Gopalan, P.; Ueda, M.; Yang, S. *Macromolecules* **2005,** 38, (2), 263-270.

18. Cushen, J. D.; Otsuka, I.; Bates, C. M.; Halila, S.; Fort, S.; Rochas, C.; Easley, J. A.; Rausch, E. L.; Thio, A.; Borsali, R.; Willson, C. G.; Ellison, C. J. *ACS Nano* **2012,** 6, (4), 3424-3433.

19. Eckert, T. S. *J Chem Educ* **1987,** 64, (2), 179-179.

20. Schneider, M.; Mulhaupt, R. *Polym Bull* **1994,** 32, (5-6), 545-550.

21. Han, E.; Stuen, K. O.; La, Y. H.; Nealey, P. F.; Gopalan, P. *Macromolecules* **2008,** 41, (23), 9090-9097.

22. In, I.; La, Y. H.; Park, S. M.; Nealey, P. F.; Gopalan, P. *Langmuir* **2006,** 22, (18), 7855-7860.

23. Ham, S.; Shin, C.; Kim, E.; Ryu, D. Y.; Jeong, U.; Russell, T. P.; Hawker, C. J. *Macromolecules* **2008,** 41, (17), 6431-6437.

24. Bates, C. M.; Seshimo, T.; Maher, M. J.; Durand, W. J.; Cushen, J. D.; Dean, L. M.; Blachut, G.; Ellison, C. J.; Willson, C. G. *Science* **2012,** 338, (6108), 775-779.

25. Bosworth, J. K.; Paik, M. Y.; Ruiz, R.; Schwartz, E. L.; Huang, J. Q.; Ko, A. W.; Smilgies, D. M.; Black, C. T.; Ober, C. K. *ACS Nano* **2008,** 2, (7), 1396-1402.

26. Brandrup, J.; Immerguy, E.; Grulke, A., *Polymer Handbook*. Fourth ed.; John Wiley and Sons: New York, 1999.

27. Arichi, S.; Himuro, S. *Polymer* **1989,** 30, (4), 686-692.

CHAPTER 6

SUMMARY AND RECOMMENDATIONS FOR FUTURE WORK

6.1 Summary

Projection optical lithography has enabled tremendous advancements in the semiconductor industry via high throughput and economical mass production of integrated semiconductor devices. However, there is no proven solution using traditional optical techniques to keep pace with increasing resolution demands beyond 20 nm pitch. Block copolymer (BCP) thin film patterns, generated using directed self-assembly (DSA) of diblock copolymers, have shown excellent promise as templates for semiconductor device manufacturing since they have the potential to produce feature pitches and sizes well below 20 nm and 10 nm, respectively, using current 193 nm optical lithography. However, the most widely used block copolymer currently for DSA studies, poly(styrene)-b-poly(methylmethacrylate) (i.e. PS-b-PMMA), lacks the thermodynamic driving force necessary for phase separation at these smallest lengths scales.

Directed self assembly of block copolymers could enable the extension of Moore's law via the formation of patterns at 20 nm pitch length scales and below, yet this technology must address three key challenges. First, current materials do not provide sufficient thermodynamic driving force to achieve useful nanometer dimensions. Second, traditional polymerization techniques do not provide the precise control of molecular weight and low PDI required for DSA applications. Finally, these block copolymer materials must exhibit selective block removal via processes such as reactive ion etching

allowing the transfer of the block copolymer pattern into the underlying substrate. **The goal of this work was to investigate a styrene based block copolymer system, namely PS-b-PHOST, that addresses these challenges.**

Chapter 1 discussed the χ parameter, which describes the enthalpic interactions which drive phase separation, and the necessary conditions to increase χ leading to sub 20 nm pitch BCP patterns. Production of diblock copolymers with higher χ values can be achieved by incorporating polymer blocks that have stronger interactions between monomers of the same type and which have interactions that are orthogonal in nature to the types of interaction between monomers of the second block type. One such example is the use of a polymer block that exhibits hydrogen bonding interactions in conjunction with a polymer block that interacts primarily though quadrupolar interactions. Here, we investigated poly(styrene)-b-poly(hydroxystyrene) (i.e. PS-b-PHOST) which exhibits such a design to achieve a high χ value.

Chapter 2 discussed the necessity of controlled polymerization techniques which provided block copolymers with targeted molecular weights and low PDI. Targeted polymer molecular weights and low polydispersities were required for directed self assembly patterning since the pitch and morphology of the BCP is dependent on the characteristic length scale (or degree of polymerization) of each block on the polymer chain. In this work, nitroxide mediated polymerization (NMP) techniques were utilized to produce the diblock copolymers reported here. NMP provided good molecular weight control and low PDI without the use of metallic reagents that can contaminate the polymer samples and cause contamination problems in subsequent processing of block copolymers in clean room facilities. Block copolymers synthesized with the universal

nitroxide initiator exhibited improved PDI in comparison with block copolymers synthesized with the traditional TEMPO initiator. Here, PS-b-PHOST polymers were synthesized with a range of molecular weights (M_n=8500-30000 g/mol and PDI=1.2) with symmetric volume fraction between the blocks which enabled lamellar morphology. Also, a series of random copolymers (PS-b-PHOST-b-PGMA) were synthesized as potential neutral underlayer substrates for the PS-b-PHOST system.

Chapter 3 described the phase separation and directed self assembly of PS-b-PHOST materials with roughly 50:50 volume fraction in the PS and PHOST blocks . Here, the phase separation of low molecular weight PS-b-PHOST on neutral underlayer substrates via solvent annealing provided thin film vertical lamellae with 13 nm pitch (Figure 6.1). These results illustrated the improved resolution of PS-b-PHOST compared with the current industry standard which is PS-b-PMMA (with 20 nm pitch). Also, the directed self assembly of lamellar patterns via graphoepitaxy was demonstrated. Here, lithographically patterned SU-8 lines on the neutral underlayer provided guiding walls for physical alignment. The BCP was spin coated and solvent annealed on these substrates resulting in directed self assembly of PS-b-PHOST with 18 nm pitch within the trench.

	PS-b-PMMA	PS-b-PHOST
χ	0.04	>0.14
Minimum Demonstrated Pitch (nm)	20	14
Thermal Anneal Time	5 min	5 days
Relative Etch Contrast between the blocks	>2:1	~1.2:1

Figure 6.1 Comparison of PS-b-PMMA and PS-b-PHOST concerning parameters relevant to the DSA self assembly process.

Chapter 4 discussed selective block removal, a key requirement for semiconductor device manufacturing. Here, one of the blocks is selectively removed with processes such as reactive ion etching, leaving the other block to serve as an etch resistant mask for pattern transfer to the underlying substrate. While PS-b-PHOST exhibits favorable thermodynamic properties providing phase separation of patterns with sub 20 nm pitch, this material exhibited no inherent etch contrast. Hence, this material required some modification to allow selective block removal. Here, an area selective atomic layer deposition (ASALD) and etch technique was investigated which provided selective block removal of (PHOST-b-PS) block copolymer patterns which initially exhibited no inherent etch contrast. Layer by layer titanium oxide (TiO_2) growth (0.4 Å/cycle) occurred in the PHOST domain during exposure to ALD precursors (tetrakis(dimethylamido titanium(IV)) and water) while no oxide growth occurred in the PS domain. Scanning electron microscopy (SEM) showed that upon subsequent oxygen plasma etching, the PS domain is removed leaving a high fidelity etch relief pattern of the original block copolymer template.

Chapter 5 presented an alternative to PS-b-PHOST, namely PTMSS-b-PHOST, which inherently exhibited high etch contrast, without the need for additional ALD processing steps. In this study, nitroxide mediated polymerization was used to prepare PTMSS homopolymer materials, and PTMSS-b-PHOST block copolymer materials (M_n=17300-26800 g/mol, and PDI of 1.2) with roughly 50/50 volume fraction allowing formation of lamellar structures (pitch=32-40 nm). Solvent annealing conditions were explored and optimized (including underlayer composition and solvent choice). Etch resistance of homopolymer films composed of TMS styrene and other relevant materials

were explored. The film thickness loss of PTMSS homopolymer films rapidly plateaued as a function of etch time (with about 10 nm film thickness loss), indicating conversion of the TMS group to etch resistant silicon dioxide functionality. PTMSS-b-PHOST phase separated patterns were also exposed to oxygen plasma allowing selective block removal of the PS domain as indicated by SEM cross section analysis.

6.2 Recommendations for Future Work

6.2.1 Evaluation of the Flory Huggins Interaction Parameter (χ) and Polymer/Solvent Compatibility via Investigation of Homopolymer Thin Film Swelling

The Flory Huggins interaction parameter (χ) is a key thermodynamic value that limits the patterning capabilities of the BCP material. Specifically, pitch and interfacial width both depend on this value [1, 2]. While phase separation of PS-b-PHOST thin film lamellae patterns with 13 nm pitch provided a lower bound on χ at 0.14, a precise evaluation of this parameter is required. Typically, χ is determined from the measurement of a scattering profile (neutron or x-ray) for a disordered system at several temperatures[3-5]. A best fit is applied to the profile data to extract a χ value. However, if the χ of PS-b-PHOST is ~1 (as estimated from solubility parameter comparisons), the disordered PS-b-PHOST material required for this technique would have a degree of polymerization of approximately 10. The generalized polymer theory used to evaluate χ from the scattering profile would not apply to this oligomeric material, hence an

alternative method to evaluate χ is required[1]. One possible alternative method is the evaluation of χ through selective solvent uptake studies, in which thin homopolymer films are swollen in controlled atmosphere with various common solvents[6]. From comparison of the degree of swelling of the homopolymers, the polymer/polymer Flory Huggins interaction parameter for PS-b-PHOST is determined. Here, swelling of thin films is readily measured via spectroscopic ellipsometry or mass uptake analysis via a quartz crystal microbalance (QCM)[7].

The BCP phase separated morphology is primarily dependent on the relative volume fraction between the PS and PHOST domain. To avoid excessive swelling of the BCP domains and distortion of the phase separated morphology, the solvent anneal step requires non-preferential solvent uptake between the two domains[8]. Hansen solubility parameter calculations suggest ethyl acetate (the primary solvent used in this study) exhibits similar compatibility with both the PS and the PHOST domain, Also, top down SEM analysis of phase separated PS-b-PHOST with approximately symmetrical volume fraction suggests the formation of lamellar structures which is indicative of limited selective solvent uptake. However, solvent uptake studies in PS and PHOST films (discussed above) would quantitatively describe the solvent compatibility with PS and PHOST.

6.2.2 Investigation of the Resolution Limit of the Area Selective Atomic Layer Deposition and Etch Process

An area selective atomic layer deposition (ASALD) and etch process was demonstrated which provided top surface oxide functionalization and selective block removal of PTMSS-b-PHOST fingerprint patterns with ~40 nm pitch resolution. Anisotropic growth at the domain interface edge could become significant at smaller pitch, hence the resolution limits of this process should be investigated. This investigation would include optimization of the ALD and etch process with high resolution PS-b-PHOST patterns, followed by SEM and AFM analysis of the resulting etch relief image.

6.2.3 Poly(trimethylsilylstyrene)-b-poly(hydroxystyrene) (PTMSS-b-PHOST) Investigation: Evaluation of χ and Resolution Limit of Fingerprint Lamellar Morphology

In this work, PTMSS-b-PHOST synthesis (via nitroxide mediated polymerization), phase separation of vertical lamellar fingerprint patterns, and selective block removal resulting in a high fidelity etch relief image were demonstrated. Future investigation of the Flory Huggins interaction parameter (χ) of PTMSS-b-PHOST is required, since the combination of hydrogen bonding OH functionality in PHOST, and nonpolar interactions of the silane in PTMSS should result in large interaction parameter for this material. In fact, the interaction parameter of PTMSS-b-PLA is 0.41 compared with the interaction parameter of PS-b-PLA of 0.15[5, 9].

While evaluation of the interaction parameter of PTMSS-b-PHOST should elucidate the patterning capabilities of this material, the practical resolution limits of

PTMSS-b-PHOST phase separation should be investigated. This investigation should follow the approach used to provide 13 nm pitch fingerprint patterns with PS-b-PHOST materials. Here, low molecular weight PTMSS-b-PHOST should be synthesized with symmetrical volume fraction between the blocks, followed by solvent annealing which should result in high resolution fingerprint patterns with similar pitch as the low molecular weight PS-b-PHOST system.

6.3 References

1. Leibler, L. *Macromolecules* **1980,** 13, (6), 1602-1617.

2. Bates, F. S. *Science* **1991,** 251, (4996), 898-905.

3. Russell, T. P.; Hjelm, R. P.; Seeger, P. A. *Macromolecules* **1990,** 23, (3), 890-893.

4. Zhao, Y.; Sivaniah, E.; Hashimoto, T. *Macromolecules* **2008,** 41, (24), 9948-9951.

5. Cushen, J. D.; Bates, C. M.; Rausch, E. L.; Dean, L. M.; Zhou, S. X.; Willson, C. G.; Ellison, C. J. *Macromolecules* **2012,** 45, (21), 8722-8728.

6. Elbs, H.; Krausch, G. *Polymer* **2004,** 45, (23), 7935-7942.

7. Berger, C. M.; Henderson, C. L. *Polymer* **2003,** 44, (7), 2101-2108.

8. Bosworth, J. K.; Black, C. T.; Obert, C. K. *ACS Nano* **2009,** 3, (7), 1761-1766.

9. Zalusky, A. S.; Olayo-Valles, R.; Wolf, J. H.; Hillmyer, M. A. *J Am Chem Soc* **2002,** 124, (43), 12761-12773.

APPENDIX A

CHARACTERIZATION OF MATERIALS ASSOCIATED WITH POLY(STYRENE)-b-POLY(HYDROXYSTYRENE)

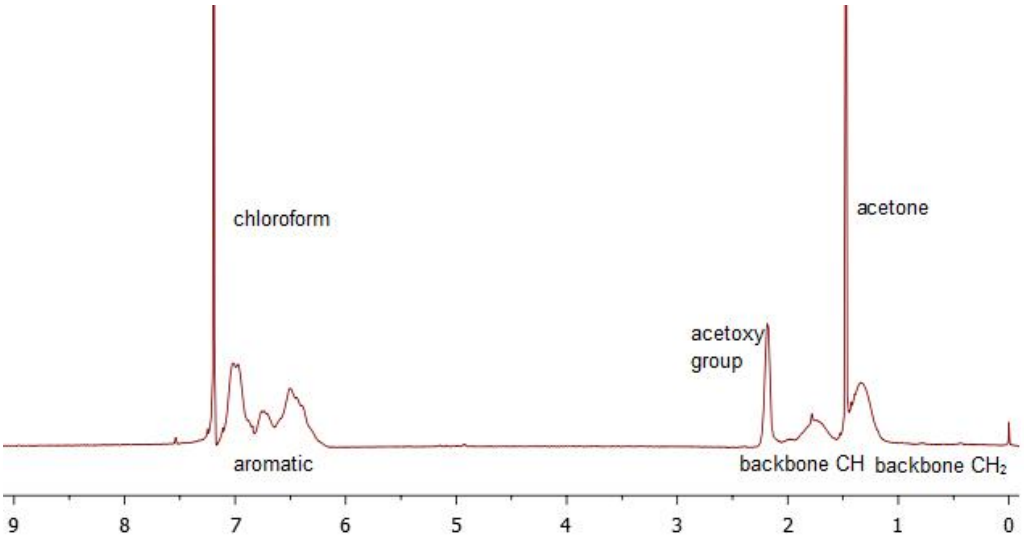

Figure A.1 [1]H-NMR spectrum of PS-b-PAS in Chloroform-D.

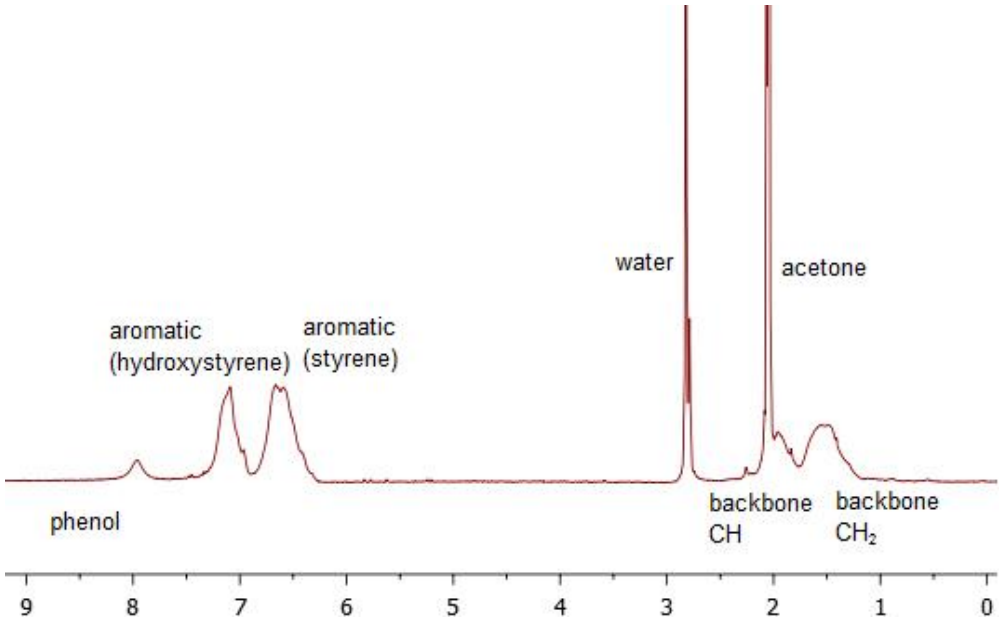

Figure A.2 [1]H-NMR spectrum of PS-b-PHOST in Acetone-d.

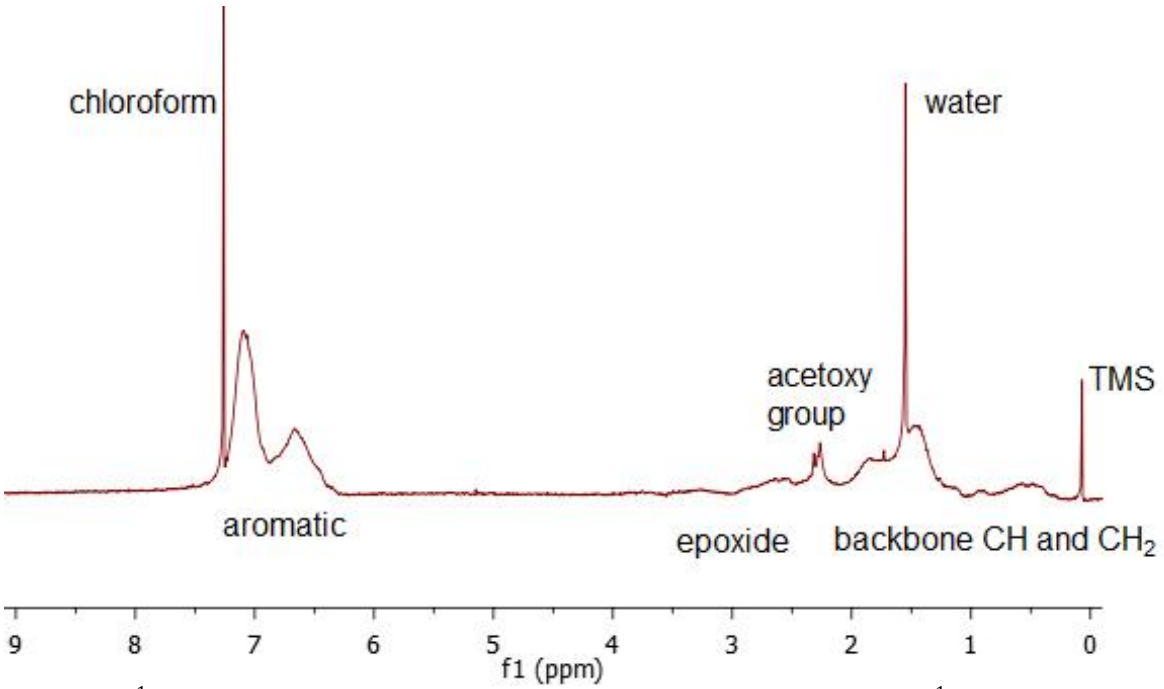

Figure A.3 [1]H-NMR spectrum of PS-r-PAS-r-PGMA in Chloroform-D. *[1]H-NMR data used in calculating molar composition: 1H NMR (300MHz, Acetone-d, ppm) δ 7.25-6.16 (aromatic region), 4.10-3.02 (COO-CH_2 on glycidyl functional group), 2.47-2.10 (acetoxy group).*

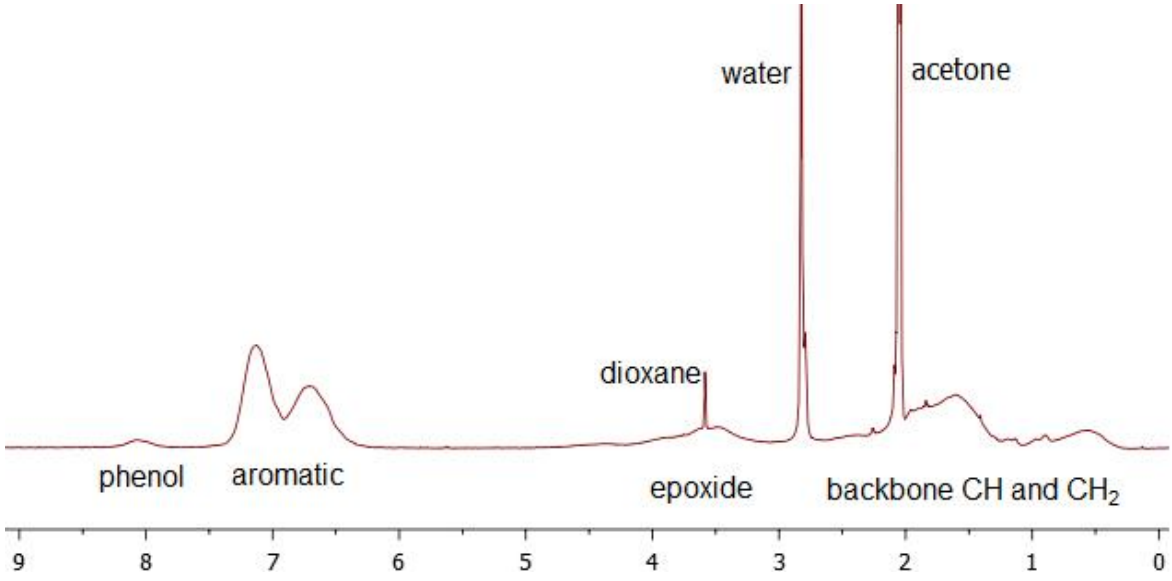

Figure A.4 [1]H-NMR spectrum of PS-r-PHOST-r-PGMA in Acetone-d.

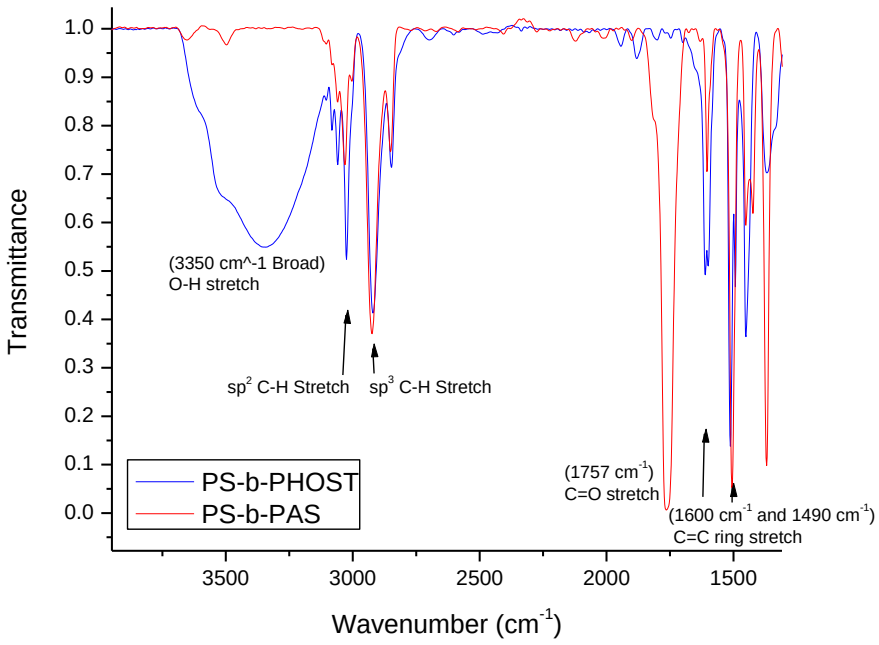

Figure A.5 FTIR spectra of the deprotection of PS-b-PAS (red) providing PS-b-PHOST (blue).

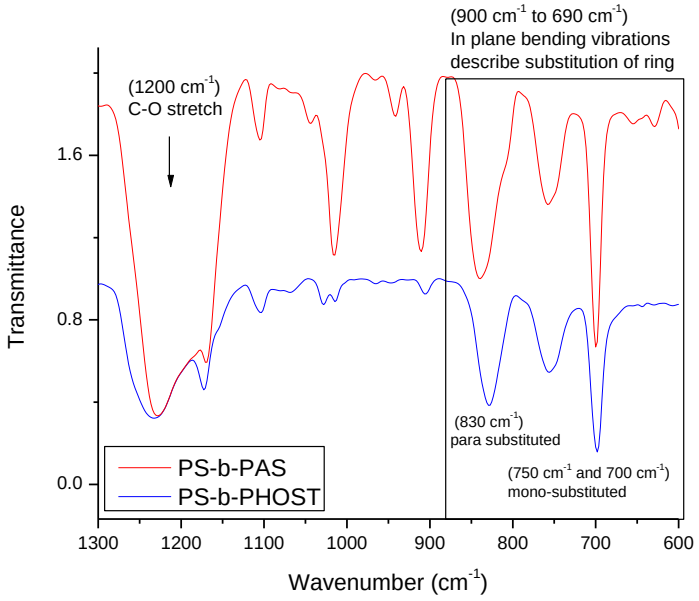

Figure A.6 FTIR spectra of the deprotection of PS-b-PAS (red) providing PS-b-PHOST (blue).

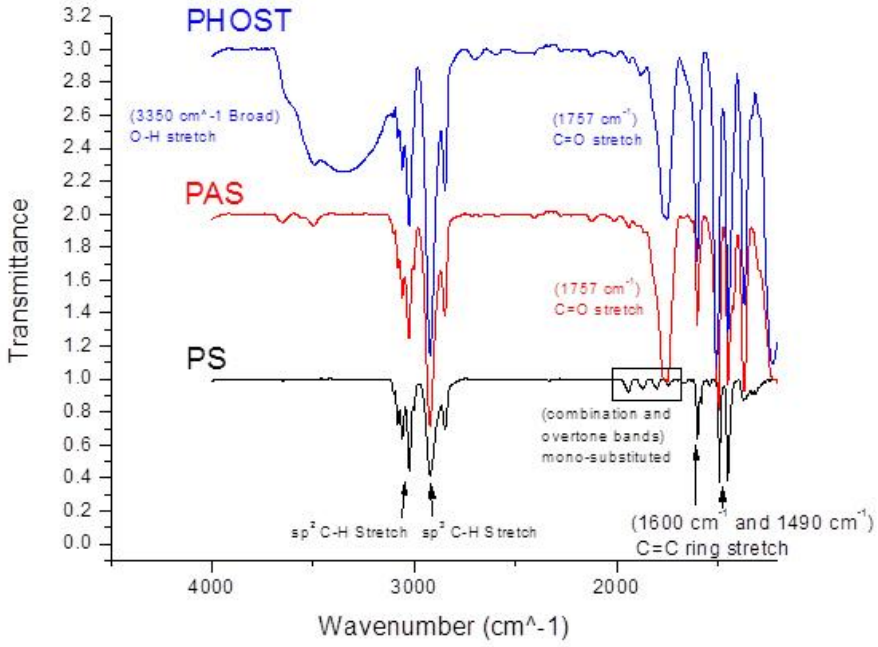

Figure A.7 FTIR spectra of the PHOST (commercial product provided by Triquest), PAS, and PS. Signal at 1757cm^{-1} representing C=O stretch indicates oxidation of the commercial PHOST material.

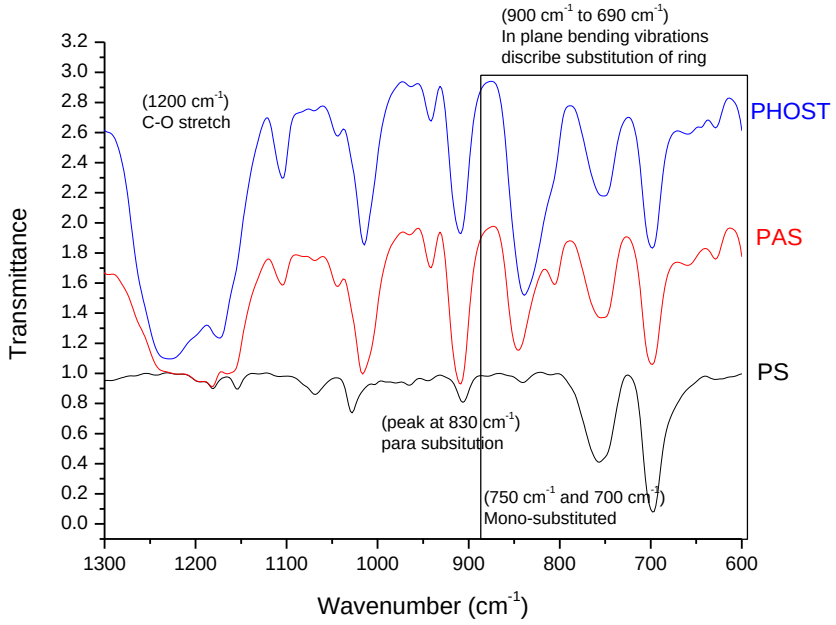

Figure A.8 FTIR spectra of the PHOST (provided by Triquest), PAS, and PS.

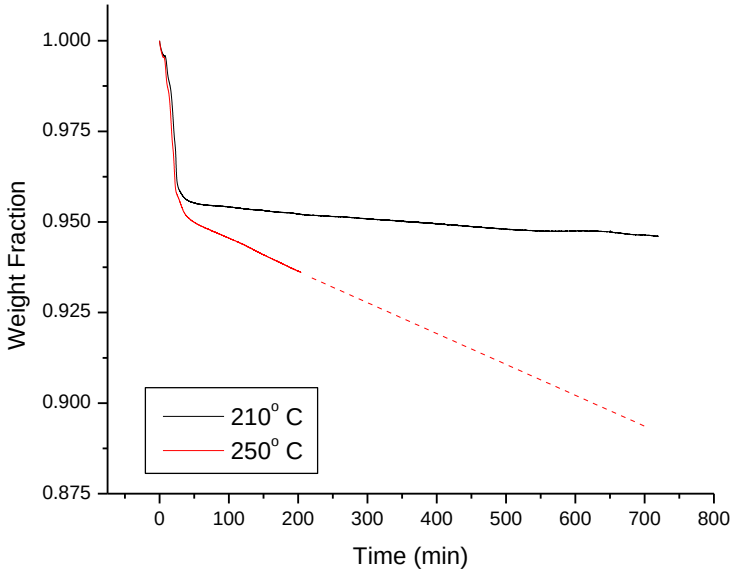

Figure A.9 Thermogravimetric analysis of PS-b-PHOST under isothermal conditions at 210 ˚C and 250 ˚C.

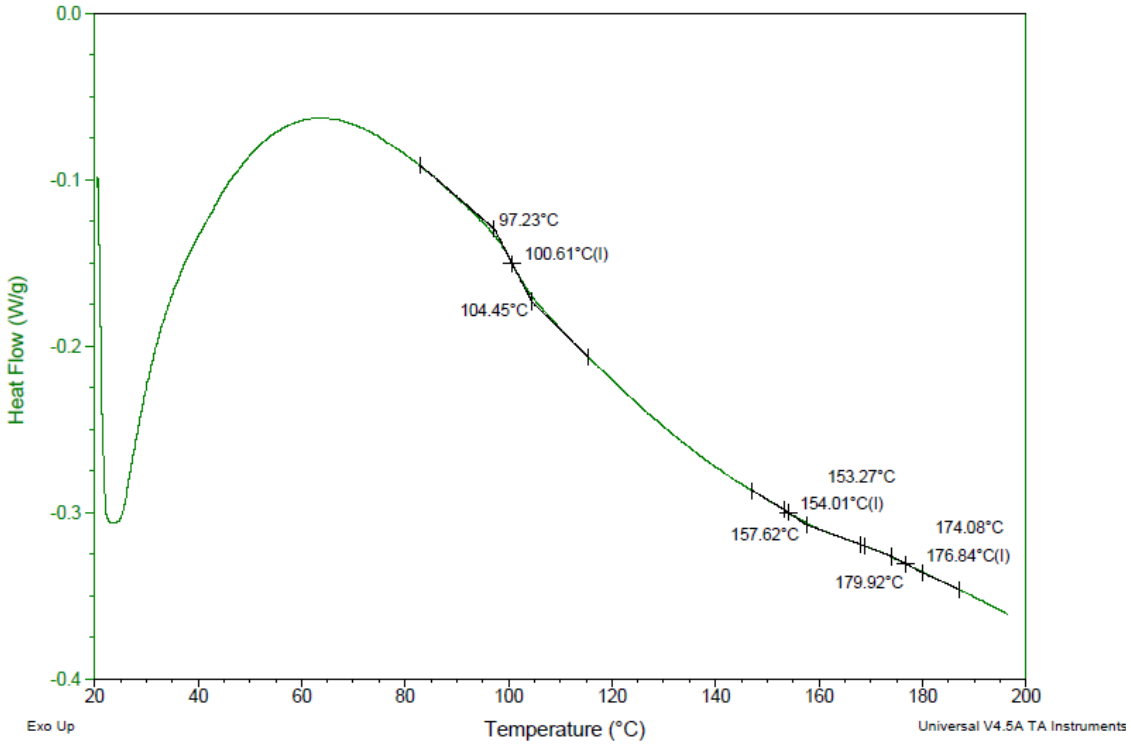

Figure A.10 Standard differential scanning calorimetry (DSC) of PS-b-PHOST from 20 ˚C to 200 ˚C with heating rate of 10 ˚C/min.

The glass transition temperature of PS-b-PHOST was determined by standard differential scanning calorimetry (DSC, TA Instruments, Model Q2000). Here, a sample of about 3 mg was hermetically sealed in an aluminum pan and placed in the DSC cell under nitrogen purge. The sample was equilibrated at 20 ˚C, and heated at the rate of 10 ˚C/min to 200 ˚C. Figure A.10 shows the DSC measurement result for PS-b-PHOST. A distinct second order transition is observed at approximately 100 ˚C, which corresponds to the glass transition temperature of PS. The transition at 177 ˚C could represent to the glass transition temperature of PHOST.

APPENDIX B

CHARACTERIZATION OF MATERIALS ASSOCIATED WITH POLY(TRIMETHYLSILYLSTRENE)-b-POLY(HYDROXYSTYRENE)

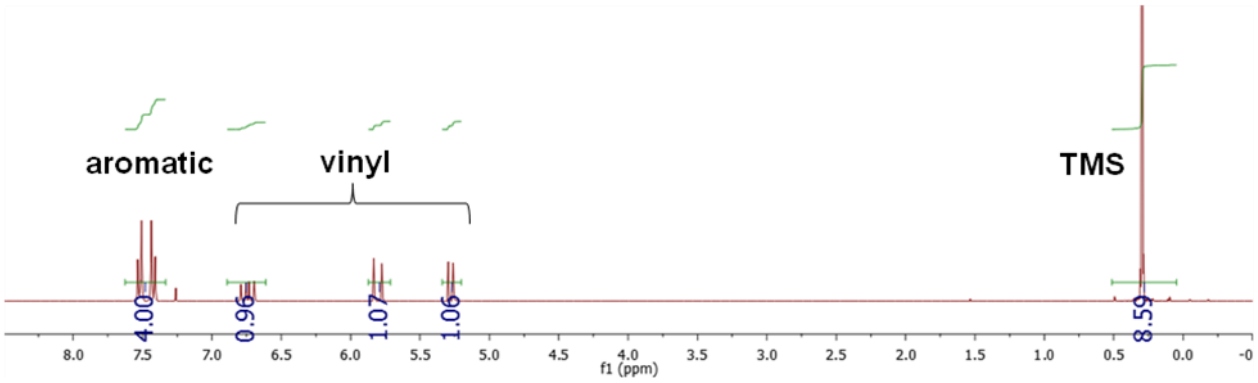

Figure B.1 ^{1}H-NMR spectrum of TMSS in Chloroform-d (with residual Chloroform peak at 7.26 ppm).

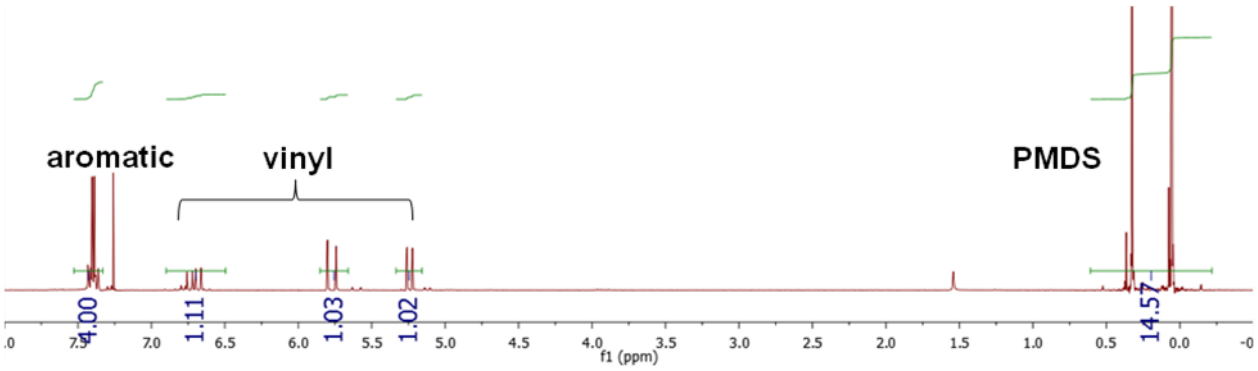

Figure B.2 ^{1}H-NMR spectrum of PMDSS in Chloroform-d (with residual Chloroform peak at 7.26 ppm).

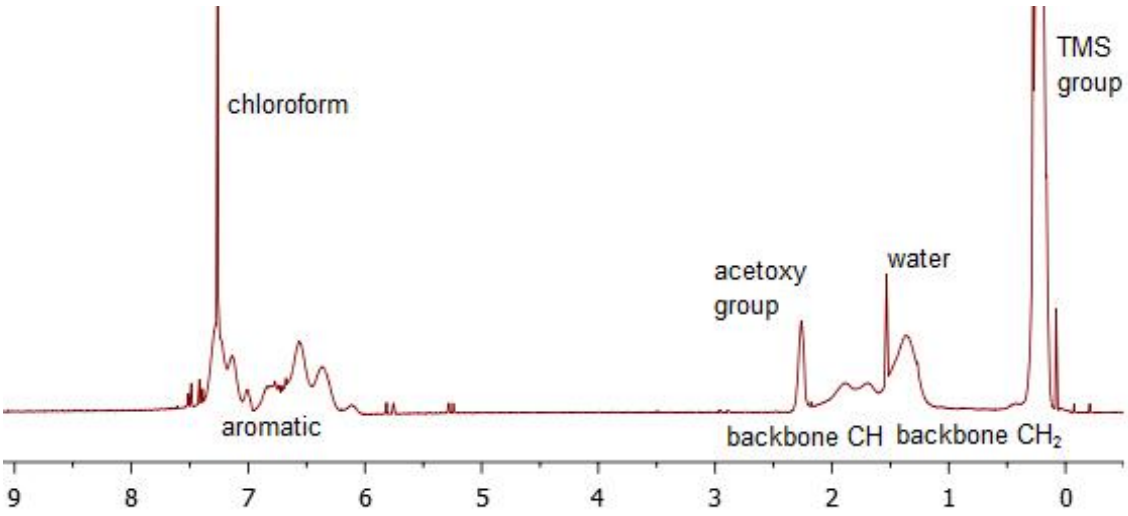

Figure B.3 [1]H-NMR spectrum of PTMSS-b-PAS in Chloroform-d.

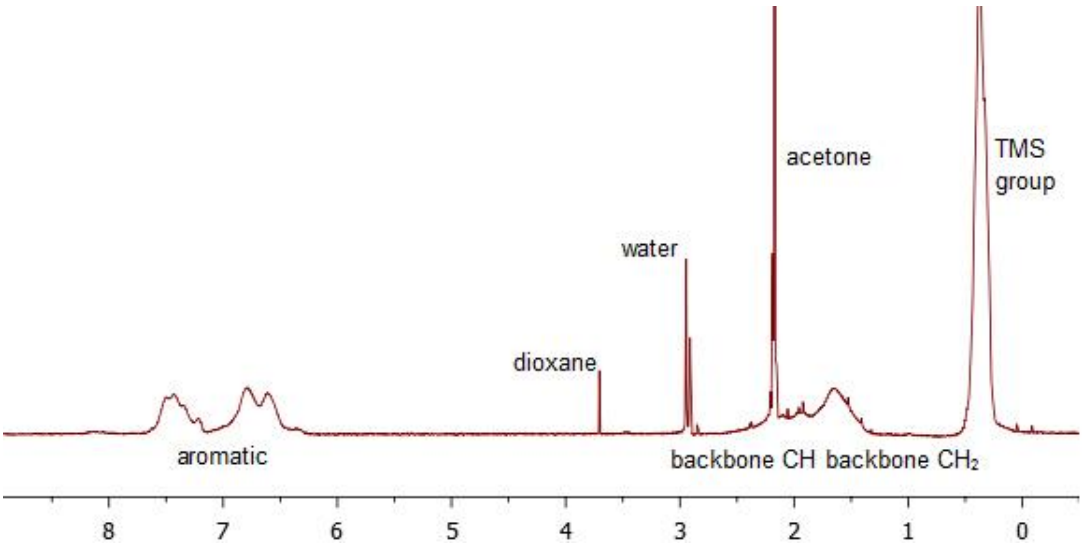

Figure B.4 [1]H-NMR spectrum of PTMSS-b-PHOST in Acetone-d.

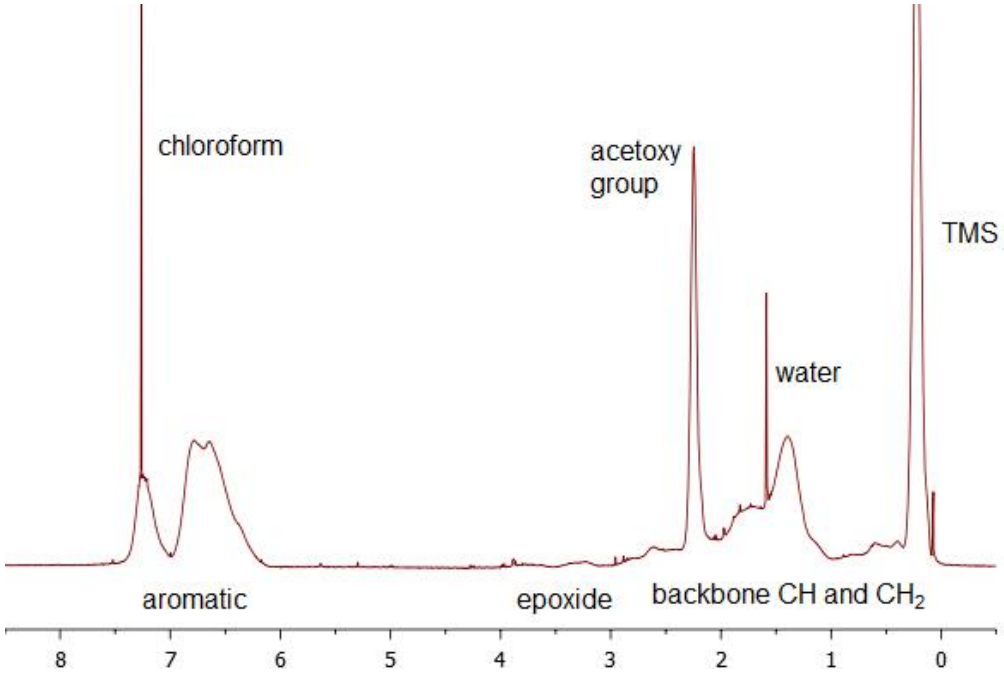

Figure B.5 [1]H-NMR spectrum of PTMSS-r-PAS-r-PGMA in Chloroform-d. [1]*H-NMR data used in calculating molar composition: 1H NMR (300MHz, Acetone-d, ppm) δ 7.25-6.16 (aromatic region), 4.10-3.02 (COO-CH_2 on glycidyl functional group), 2.47-2.10 (acetoxy group).*

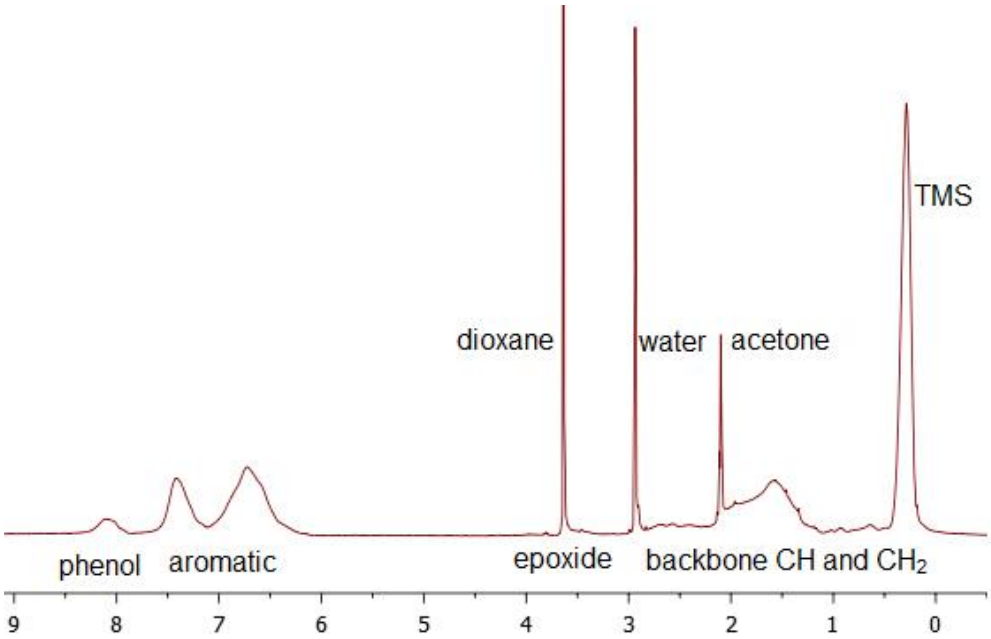

Figure B.6 [1]H-NMR spectrum of PTMSS-r-PHOST-r-PGMA in Acetone-d.

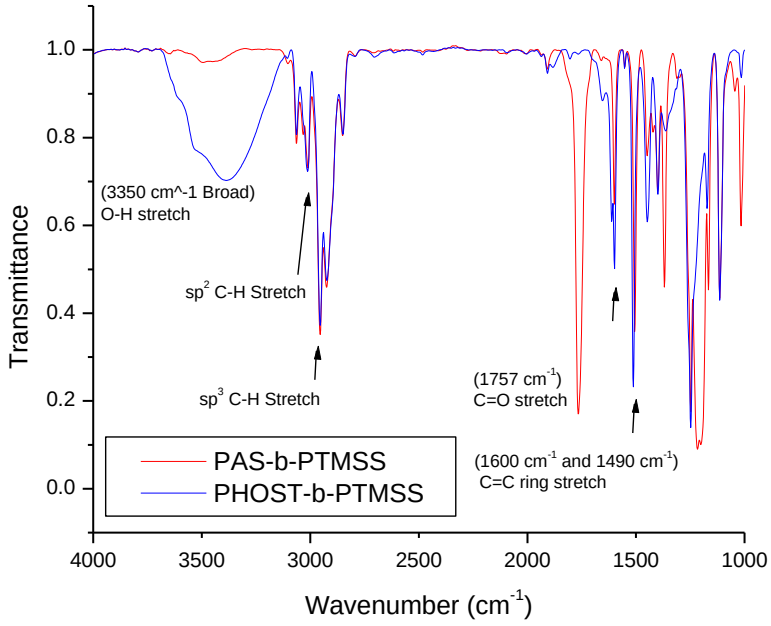

Figure B.7 FTIR spectra of the deprotection of PTMSS-b-PAS (red) providing PTMSS-b-PHOST (blue).

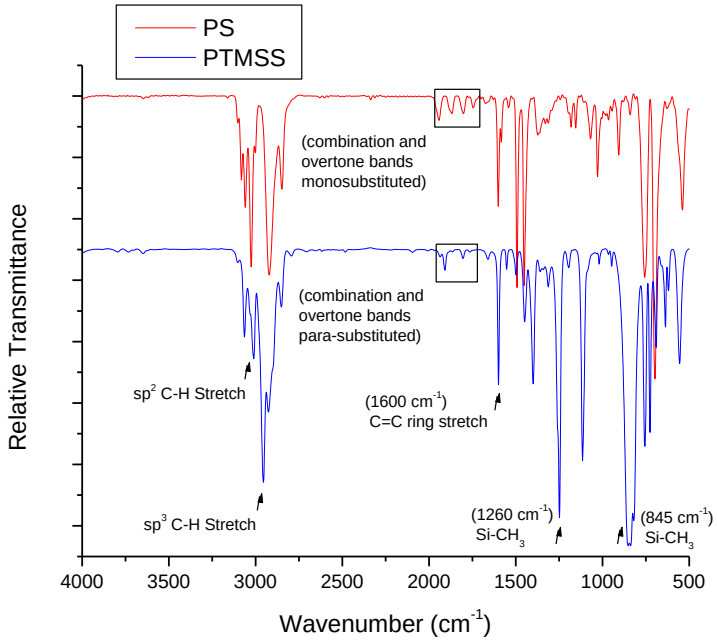

Figure B.8 FTIR spectra of the PS and PTMSS.

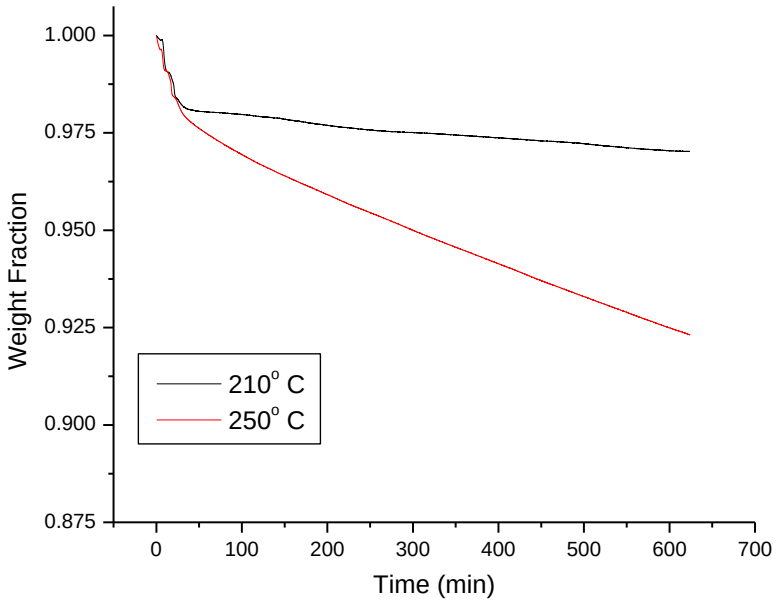

Figure B.9 Thermogravimetric analysis of PTMSSS-b-PHOST under isothermal conditions at 210 ˚C and 250 ˚C.

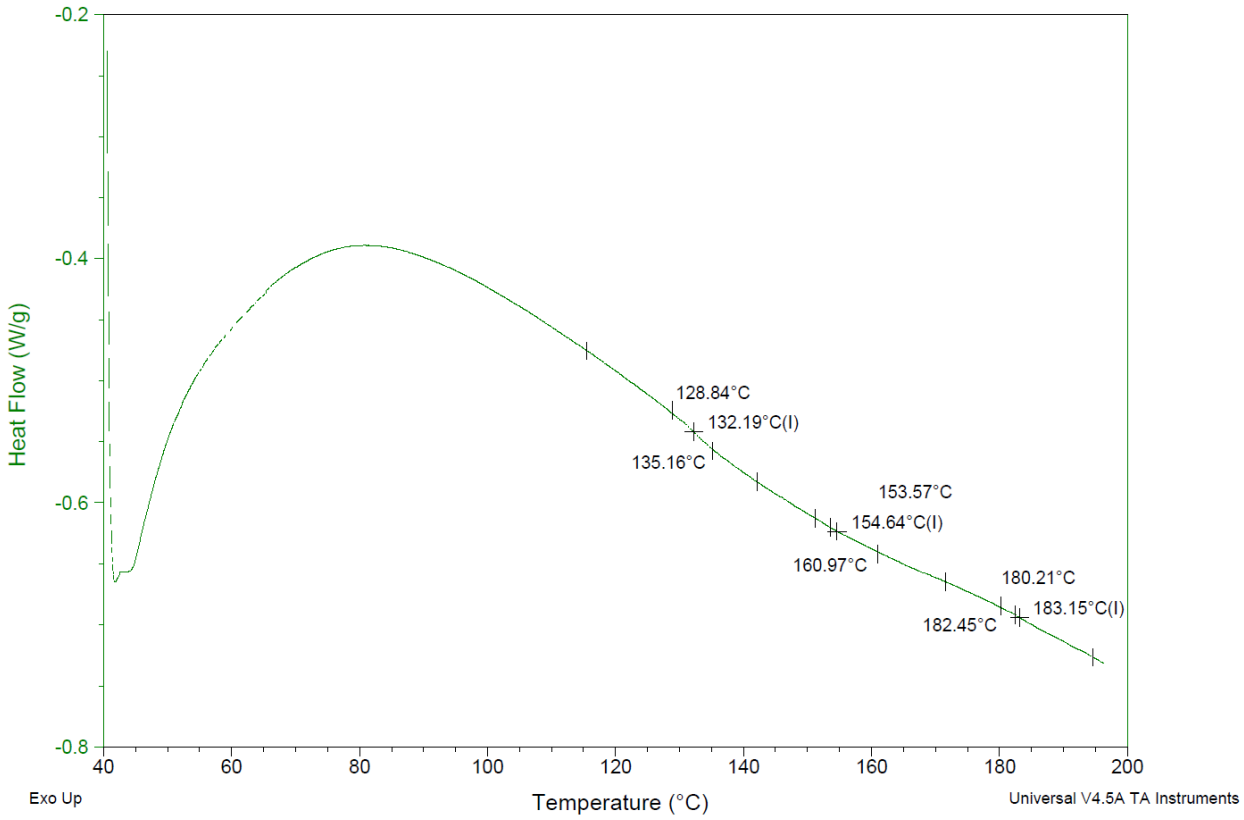

Figure B.10 Standard differential scanning calorimetry (DSC) of PTMSS-b-PHOST from 20 ˚C to 200 ˚C with heating rate of 10 ˚C/min.

The glass transition temperature of PTMSS-b-PHOST was determined by standard differential scanning calorimetry (DSC, TA Instruments, Model Q2000). Here, a sample of about 3 mg was hermetically sealed in an aluminum pan and placed in the DSC cell under nitrogen purge. The sample was equilibrated at 20 ˚C, and heated at the rate of 10 ˚C/min to 200 ˚C. Figure B.10 shows the DSC measurement result for PS-b-PHOST. A distinct second order transition is observed at approximately 132 ˚C, which corresponds to the glass transition temperature of PTMSS. The transition at 182 ˚C could represent to the glass transition temperature of PHOST.